University of Alberta
Department of Civil Engineering

Structural Engineering Report No. 172

THE EFFECTIVE MODULUS OF ELASTICITY OF CONCRETE IN TENSION

by

ATIF F. SHAKER

and

D. J. LAURIE KENNEDY

APRIL, 1991

Abstract

When the concrete slab of a composite beam shrinks, it is restrained by the steel beam to which it is connected. Tensile strains are developed in the restrained concrete and strains, varying from compression at the top to tension at the bottom, are developed in the steel beam. The resulting deflections are of interest to design engineers. An equilibrium model has been proposed by others based on, (i) strain compatibility at the steel-concrete interface, (ii) a linear variation of strains in the steel beam and (iii) the necessary condition that the internal forces arising due to shrinkage must be self-equilibrating. To use this model, the effective modulus of elasticity of concrete in tension is required. This modulus varies with time and reflects the changing characteristics of the concrete as it sets, drys, shrinks, creeps, and is gradually loaded from the green state.

Shrinkage strains were measured on plain and reinforced concrete specimens from 2 normal weight concrete mixes of 28 day compressive strengths of 30 and 40 MPa over periods of 140 and 170 days. A total of 27 specimens with percentages of steel from zero to 4.44% were tested. Specimens were moist cured for 7 days after casting and left to dry under working laboratory conditions where the average temperature was 20° C and the average relative humidity was 38%.

The effective modulus decreases with both time and percentage of steel. Initial values of the modulus obtained from uncracked specimens ranged between 7,500 and 10,000 MPa for

steel percentages of 4.44 to 0.44% respectively. At about 150 days, the values reduced to 2,500 to 4,600 MPa. The initial values are about 30 to 50% of the 28 day modulus in compression while the long term ones are only 10 to 20% of the 28 day modulus.

Cracking of the concrete was observed only in the specimens with a No. 35 bar. Cracks occurred near mid-length of the specimen and generally started at one corner and progressed across adjacent surfaces. As cracking relieves shrinkage stresses in the same manner as does creep of concrete, the apparent effective modulus is also reduced.

TABLE OF CONTENTS

List of Tables

List of Figures

Figure Page

Figure Page

Figure Page

Figure Page

Figure Page

List of Symbols

A = the exposed surface area of a concrete specimen, mm^2

A_c = area of concrete cross-section, mm^2

A_s = area of steel bar, mm^2

$\overline{A}$ = age adjusted area of the transformed section, mm^2

b = a distance related to the dimensions of the specimen, mm; the width of the specimen, mm

c = empirical constant

C_s = axial compression force in the steel bar induced by shrinkage, N

d = depth of the steel beam, mm

e = lever arm between the compressive force C and the tensile force T, mm

E_c = modulus of elasticity of concrete in compression, MPa

$E_c(t_o)$ = modulus of elasticity of concrete in compression at time t_o, MPa

E_e = effective modulus of elasticity of concrete in tension, MPa

E_i = initial value of the effective modulus of elasticity of concrete in tension at the beginning of drying $t = 0$, MPa

E_s = modulus of elasticity of steel reinforcement, MPa

E_∞ = effective modulus of elasticity of concrete in tension after an extended time period $t = \infty$, MPa

E'_c = effective modulus of elasticity of concrete, MPa

$\bar{E}_c(t,t_o)$ = age adjusted modulus of elasticity of concrete, MPa

f = surface factor

f_{ct} = tensile strength of concrete, MPa

f'_c = compressive strength of concrete, MPa

F = empirical constant that depends on mix proportions and curing conditions

F_y = static yield stress of the steel reinforcement, MPa

I_s = moment of inertia of the steel beam, mm^4

I_t = transformed moment of inertia of the composite section, mm^4

k = the coefficient of diffusivity

K = creep factor

M = internal bending moment induced in the composite cross-section by transverse cracking and the resulting eccentricity of forces, N.mm

M_c = bending moment induced in the concrete by bowing of the specimen, N.mm

M_s = bending moment induced in the steel bar by bowing of the specimen, N.mm

r_h = relative humidity in percent

s = empirical constant

S_c = section modulus of the uncracked part of the concrete cross-section mm^3

S_s = section modulus of the steel bar, mm^3

t = time from the end of the curing period, days

t_c = thickness of the cover concrete slab, mm

t' = time from casting over which shrinkage measurements were obtained, days

T_c = tensile force in concrete induced by shrinkage acting at the centroid of the uncracked part of the concrete cross-section, N

T_d = four times the average drying path, mm

T_p = time parameter

v = empirical constant that depends on the member size and curing conditions

V = volume of a concrete specimen, mm^3

W_o = water content by weight

y = distance between the centroid of the cover slab and the centroid of the composite section, mm

α = constant that depends on mix proportions and curing conditions

β = non-dimensional parameter

β_s = coefficient to describe the development of shrinkage with time; the CEB M78 function for the unrestrained shrinkage strain at time t

Δ_{sh} = shrinkage deflection of a composite beam, mm

$\Delta\psi$ = curvature due to uniform shrinkage in a non-symmetrically reinforced concrete section

ε_c = concrete shrinkage strain measured on the surface of the specimen, $\mu\varepsilon$

$\varepsilon_{cc}(t)$ = creep strain at time $t > t_o$, $\mu\varepsilon$

$\varepsilon_{ci}(t_o)$ = the initial concrete strain at loading, $\mu\varepsilon$

$\varepsilon_{cs}(t)$ = shrinkage strain at time $t > t_o$, $\mu\varepsilon$

ε_{cso} = notional shrinkage coefficient, $\mu\varepsilon$

ε_{ct} = average tensile strain in concrete, $\mu\varepsilon$

$\varepsilon_{cT}(t)$ = thermal strain at time $t > t_o$, $\mu\varepsilon$

ε_f = free or unrestrained shrinkage strain of concrete, $\mu\varepsilon$

ε_r = restrained shrinkage strain at any time, $\mu\varepsilon$

ε_s = shrinkage strain measured in the steel bar, $\mu\varepsilon$

ε_u = ultimate concrete shrinkage strain at time $t = \infty$, $\mu\varepsilon$

$\phi(t,t_o)$ = dimensionless coefficient that represents the ratio of creep to the instantaneous strain

γ = empirical constant, function of the concrete mix, curing conditions and percentage of reinforcement

χ = aging coefficient of concrete in compression for the time period considered

ρ = ratio of steel reinforcement

σ_{ct} = average tensile stress in the concrete, MPa

Chapter 1

INTRODUCTION

1.1 General

Drying shrinkage is defined as the time dependent volume reduction of concrete due to the loss of free water from capillary pores and adsorbed water from the molecules of the cement paste at a constant relative humidity and temperature. Shrinkage is affected by all the factors which influence the water content of concrete as well as by environmental conditions that affect the rate of water loss. The concrete member size and shape (volume-to-surface area ratio) affect the amount and rate of drying shrinkage as they change the length of the diffusion path. Shrinkage strains increase with time at a decreasing rate reaching equilibrium after an extended period.

Shrinkage is directly related to the deflection of composite concrete-steel beams and trusses, before dead or live loads are imposed, due to the tensile stresses induced in the concrete. Although when loads are applied the concrete will eventually be stressed in compression, shrinkage will cause excessive deflections regardless of the superimposed stress state.

Two parameters are required in order to determine the shrinkage deflections; the free shrinkage of the concrete and its effective modulus of elasticity in tension. Shrinkage deflections can then be calculated using equilibrium and compatibility conditions. Having determined the shrinkage deflections, elastic

and creep deflections due to the applied loads can be superimposed.

The effective modulus of elasticity of concrete in tension is influenced by all the factors that affect drying shrinkage. Its value depends on the rate of loading, the stress level, the age of concrete at loading, the concrete mix proportions, and the relative humidity and temperature conditions. Due to the effect of creep, it would be expected that the modulus of elasticity of concrete decreases as loads are sustained for longer time periods. Higher tensile stresses in the concrete can be achieved by using different ratios of reinforcement.

1.2 Objectives

The objectives of this investigation are

1. to study the shrinkage of unrestrained and restrained concrete and its development with time and
2. to determine the overall or effective modulus of elasticity of concrete in tension as affected by the different degrees of restraint and as it develops with time.

1.3 Scope

A total of 27 specimens, consisting of square concrete prisms of two different concrete strengths, plain or reinforced with a single bar along the center-line, were tested over periods of 140 to 170 days. Five ratios of reinforcement varying from 0 to 4.44% were investigated. The specimens were moist cured for 7 days

after casting and then left to dry under normal laboratory conditions. During this time the average temperature in the laboratory was 70° F and the average relative humidity was 38%.

Demec points were placed on the concrete surfaces to measure the concrete strains and electrical resistance strain gauges were mounted on the steel bars to measure the steel strains and to compute the restraining force developed in the steel. By placing strain gauges along the length of the bar it was possible to monitor the length from each end required to develop full restraint. Unrestrained or free shrinkage strains were obtained from plain concrete specimens while restrained shrinkage strains were obtained from the reinforced ones. Shrinkage strain measurements were started 3 days after casting and were obtained daily in the first 10 days and 3 times a week thereafter.

Using the free and restrained shrinkage measurements, the effective modulus of elasticity of the concrete in tension while it shrank and crept was determined. The relation between the effective modulus and both the tensile stress level in the concrete and time was studied.

Chapter 2

LITERATURE REVIEW

2.1 Concrete Composition and the Shrinkage Process

Neville (1963) defines shrinkage as the withdrawal of water from concrete stored in unsaturated air. The loss of free water causes little or no shrinkage but the removal of adsorbed water, as drying continues, leads to the change in volume of the unrestrained cement paste. He also stated that it is possible that part of shrinkage is related to the removal of zeolitic water from the calcium silicate hydrate.

Neville (1970) states that concrete is a multi-phase composite material consisting of particles of coarse aggregate embedded in a matrix of mortar. The mortar, in turn, is comprised of particles of fine aggregate embedded in a matrix of cement paste which, in turn, consists of grains of unhydrated cement within a matrix of products of hydration of the cement. The products of hydration are a cement gel with a semi-continuum of water-filled or empty capillary pores. Finally, the cement gel is a mixture of particles, some fibrous or needle-shaped, but mostly crumbled sheets and foils, which form a continuous matrix with a continuous network of water-filled gel pores. Neville states that the hydrated cement paste plays the dominant role in the time-dependent deformation of concrete while the aggregate only affects the ultimate shrinkage.

The chemical reaction between the water and cement leads to the formation of a mass of a very porous cement gel of colloidal size and properties. The cement gel adheres to the unhydrated cement particles and fills some of the space which existed prior to hydration and also forms some crystals. The water in excess of that required for hydration occupies the remainder of the capillary voids.

Keeton (1971) divided the water contained in concrete into four types:

(i) capillary or pore water that evaporates at 40% to 50% relative humidity,

(ii) adsorbed water [also called load bearing water (Powers 1968) or active water (Mills 1969)] that evaporates at 0% to 40% relative humidity,

(iii) water of hydration or non-evaporating water, and

(iv) water vapour which fills the remaining space and affects shrinkage.

Keeton investigated shrinkage under load and concluded that at early stages of loading, stress-induced shrinkage occurs due to the migration of free water from areas of higher pressure to areas of lower pressure and/or relative humidity, or to the surrounding atmosphere. This shrinkage is completely recoverable upon removal of load and saturation of concrete. Capillary and

adsorbed water move very slowly and result in creep deformations which are almost entirely non-recoverable.

Wittmann (1982) distinguished between real and apparent shrinkage mechanisms. He considered real mechanisms to be material properties of the hydrated cement paste, and therefore should be independent of the specimen size and shape. Apparent mechanisms on the other hand are caused by other factors which modify the anticipated strain. For example, differential strains between paste and aggregate can cause localized stresses and therefore microcracking at the interface. Also, moisture gradients develop during the drying of the specimen resulting in differential shrinkage between the inner and outer layers causing microcracking or warping or both.

MacGregor (1988) describes shrinkage as being the shortening of concrete during hardening and drying under constant temperature, and states that shrinkage is primarily due to the loss of water from the surface of the gel and that the loss of free or capillary water has little effect on the magnitude of shrinkage. MacGregor, Neville, and Witmann all state that, due to the development of a moisture gradient, the exterior shrinks more rapidly than the interior. This leads to tensile stresses at the exterior and compressive stresses in the interior of plain concrete members. Thus cracking should always start at the surface of the member. For square prisms, cracking would be expected to start at the corner.

Young (1988) defines shrinkage as the observed strain due to the loss of moisture from concrete under drying conditions. When concrete is resoaked in water, only part of the drying shrinkage is recovered by swelling. Young divided shrinkage into three categories:

(i) hydration or chemical shrinkage that takes place as water is removed internally by chemical combination during hydration in a moisture sealed state. If sufficient water is available, swelling may take place during hydration due to the increased volume of solid hydration products,

(ii) capillary or plastic drying shrinkage that occurs while the concrete is in the plastic state when the capillary water evaporates at the exposed surface. It only occurs in the plastic state, and

(iii) carbonation shrinkage that occurs when concrete is carbonated in a low relative humidity environment, its effect is only significant when high CO_2 levels are encountered between 50% and 75% humidity.

Young also pointed out that the heat of hydration that develops during the chemical reaction can cause thermal strains that are opposite to the shrinkage strains.

2.1 Unrestrained or Free Shrinkage

Unrestrained shrinkage refers to shrinkage strains taking place in a member that is free to change in volume without any external or internal restraint. However, even in an otherwise unrestrained concrete member, shrinkage strains develop more at exposed surfaces. The inner portion of the member, shrinking less, restrains the outer portion and differential shrinkage results. In fact, in large concrete members, differential shrinkage may lead to tensile strains at the exposed surface that exceed the ultimate tensile strain of the concrete causing shrinkage cracks to develop at the surface. To control the number and width of shrinkage cracks, most standards specify a minimum amount of shrinkage reinforcement.

Many methods have been developed to predict the unrestrained shrinkage strain as a function of time. Most of these are based on the estimated unrestrained shrinkage strain at a certain time, often taken as 2 years, but ranging from 6 months to 30 years. This strain is referred to as the ultimate shrinkage strain, ε_u, and is itself a function of many factors including concrete mix proportions, member size and the temperature and relative humidity conditions during drying.

Ross (1937) suggested a hyperbolic formula for unrestrained shrinkage of the form

$$[2.1] \qquad \varepsilon_f = \frac{t^v}{t^v + F}\,\varepsilon_u$$

for the prediction of shrinkage strains in unreinforced concrete members.

Pickett (1946), observing that the rate of shrinkage is controlled by the rate of moisture loss, used the equations for heat flow to determine the shrinkage strain in plain concrete elements that are free to contract. This assumes that the laws for heat transfer are analogous to those for the drying of concrete. He observed, however, that the theory must be modified to take into account the inelastic or creep deformation of concrete.

Pickett found reasonable agreement between the shrinkage strains measured from tests and values calculated using the diffusion equation. If the diffusivity, k, and the surface factor, f, are assumed to be constant for a given material and environment, then the shrinkage process is determined by the non-dimensional parameters β and T_p

$$[2.2] \qquad \beta = \frac{f\,b}{k}, \quad \text{and}$$

$$[2.3] \qquad T_p = \frac{k\,t}{b^2}$$

Pickett gives curves and tables that relate shrinkage to the time parameter T_p for various values of the parameter β.

Troxell (1958) conducted creep and shrinkage tests on plain and reinforced concrete specimens for a period of 30 years, he concluded that 34% of the 20 year shrinkage took place in the first two weeks and 66% to 85% within one year. Unrestrained shrinkage strains in the order of 1400 $\mu\varepsilon$ were recorded at 20 years from plain concrete cylinders. He concluded that shrinkage was not appreciably affected by either the water content, the water-cement ratio, or the aggregate-cement ratio. However, he reported higher shrinkage strains when aggregate with a low modulus of elasticity was used in the concrete mix.

Some of Troxell's conclusions were contradicted by Neville (1981) who stated that the modulus of elasticity and content of aggregate has a great effect on shrinkage by acting as a restraint to shrinkage strains and that the aggregate-cement ratio affects shrinkage quantitatively.

Hansen (1966) reported creep and shrinkage test data on plain concrete specimens of different shapes and sizes. The tests were conducted at 70° F and 50% relative humidity on concrete cylinders of diameters from 4 to 24 in., and of I shaped members of depths from 11.5 to 46 inches. The main objective of the tests was to determine the effectiveness of using the volume to surface area ratio as a parameter to estimate the influence of size and shape of the member on shrinkage and creep. Cylindrical and I shaped specimens were made with the same volume to surface area ratios. The forms were stripped after 2 days and strains were

measured at the surface using a 10 inch demountable mechanical strain gauge. Shrinkage strain readings were taken at 1, 2, 3, 6 and 10 days, and at progressively increasing intervals of time thereafter. A hyperbolic equation similar to Ross' [2.1] but with the constant v = 1 was proposed for both shrinkage and creep. Hansen concluded that shrinkage strains increase with the decrease of the size of specimen and that the measured shrinkage strains of different shapes of specimens but with the same volume to surface area ratios were in reasonable agreement. Keeton (1965) reported similar findings regarding the volume to surface area ratio.

Branson (1971, 1972) modified Ross' equation [2.1] for moist cured concrete to

$$[2.4] \qquad \varepsilon_f = \frac{t}{t+35}\,\varepsilon_u$$

He concluded that the modified equation predicted shrinkage behaviour better than the original equation and was more representative of the full time range. He also suggested a method for predicting creep and shrinkage behaviour from 28 day creep and shrinkage tests with an expected accuracy of $\pm$ 15% for creep prediction and $\pm$ 30% for shrinkage prediction. Branson used creep and shrinkage data from different experiments by other researchers to verify his equations and to calculate the percentage error. Correction factors were used for different mixes and storage conditions.

The ACI method as proposed by the ACI Committee 209 (1971, 1982) is described by Branson (1972), Park and Paulay (1975) and Rush (1983). A hyperbolic equation similar to [2.4] is used to describe the development of unrestrained shrinkage strain with time. A value of 800 με is used for the ultimate unrestrained shrinkage strain if no test data are available. The strain obtained from the hyperbolic equation is then multiplied by correction factors to account for non-standard conditions such as different curing conditions, relative humidity, temperature, volume-to-surface area ratio, and concrete composition. The ACI does not suggest any methods for the prediction of restrained shrinkage strains.

The CEB/FIP (1978) method to predict the unrestrained shrinkage strains at any time, t, requires the prediction of the ultimate shrinkage strain. A value of 450 με for the ultimate shrinkage strain is suggested for moist cured concrete in the absence of test data. A hyperbolic function is used for the development of shrinkage strains with time. The shrinkage strain obtained is then multiplied by a coefficient that depends on relative humidity, concrete composition, and the effective thickness of the specimen as well as the area of longitudinal reinforcement with respect to the cross-sectional area of the member. A modular ratio of 20 was suggested by the CEB to account for the effects of creep. Graphs were provided to obtain the different parameters.

The CEB/FIP method is described in detail by Ghali and Favre (1982) and Rush (1983).

Hobbs (1979) after examining the existing shrinkage data, expressed the unrestrained shrinkage strains, taking into account the effects of water content, relative humidity during drying, and member size, as,

$$[2.5] \qquad \varepsilon_f = \frac{1}{10} W_o \cdot f(r_h) \cdot f_1\left[\left(\frac{A}{V}\right)^2 \cdot t\right]$$

Values for $f(r_h)$ and $f_1[(A/V)^2\, t]$ are obtained from graphs. Hobbs pointed out that shrinkage strains are not greatly affected by curing times of less than one month.

Arnaouti (1984) performed creep and shrinkage tests on lightweight aggregate concrete prisms of different sizes and concrete mixes. Smaller specimens had higher shrinkage strains and a relationship was established between the shrinkage strain at any time t and the surface area to volume ratio, $(A/V)^n$. A method was suggested to predict creep and shrinkage strains in concrete elements from short term shrinkage and creep measurements on small plain concrete prisms.

Bryant (1987) carried out shrinkage and creep tests on concrete specimens of different sizes including 150x150x600 mm square prisms to examine the A.C.I equations for prediction of shrinkage and creep strains. The specimens were kept at a

temperature of 68° F and a relative humidity of 60% after curing them for 8 days.

Bryant concluded that the strains obtained from [2.4] were 15% low for 100 mm thick slabs and that the error increased as the specimen size or slab thickness increased. Bryant modified Ross' [2.1] to

$$[2.6] \qquad \varepsilon_f = \frac{\left[\frac{t}{T_d^2}\right]^v}{\left[\frac{t}{T_d^2}\right]^v + \bar{f}} \varepsilon_u$$

where

$$[2.7] \qquad \bar{f} = \frac{F}{T_d^{2v}} \quad , \text{ and}$$

T_d= 4 times the average drying path.

Test results were used to determine the imperical constants F and v and the ultimate shrinkage strain, ε_u. Equation [2.6] gave very good agreement with shrinkage strains obtained from concrete specimens of different sizes.

Nilson (1987) carried out a series of shrinkage and creep tests on plain concrete specimens of different compressive strengths. The cylindrical specimens, 102 mm in diameter and 203 mm long, were loaded to stress levels of 40% of the 28 day compressive strength. Unloaded companion specimens were used to investigate the drying shrinkage. The specimens were moist

cured for 28 days. Tests were carried out at a constant temperature of 72° F and a relative humidity of 50%.

Typical hyperbolic shrinkage-time relationships were obtained for concretes of different compressive strengths. Nilson concluded that the long term drying shrinkage is greater for low-strength concrete than for medium- and high-strength concretes and that the creep up to 60 days, at stress levels of the same percentages of f'_c , is less for high-strength than for medium- and low-strength concretes.

The CEB/FIP Model Code (1990) gives the total strain, $\varepsilon_c(t)$, at time t for a member loaded at time t_o as follows

$$\varepsilon_c(t) = \varepsilon_{ci}(t_o) + \varepsilon_{cc}(t) + \varepsilon_{cs}(t) + \varepsilon_{cT}(t) \qquad [2.8]$$

The total shrinkage or swelling strains may be calculated from

$$\varepsilon_{cs}(t,t_o) = \varepsilon_{cso}\, \beta_s(t - t_o) \qquad [2.9]$$

where β_s is the CEB hyperbolic function that describes the development of shrinkage with time. It takes into consideration the age of concrete, the age of concrete at the beginning of shrinkage or swelling, and the dimensions of the member.

2.3 Restrained Shrinkage Strains

Glanville (1930) studied shrinkage strains and stresses in symmetrically reinforced 152x152x914 mm concrete prisms with reinforcement ratios ranging from 0.55% to 2.23%. Measured steel strains were used to calculate the compressive force in the steel

and thus the tensile force in the concrete. The tensile strain in the concrete was based on the unrestrained shrinkage strain of companion plain concrete specimens. Glanville then calculated the effective modulus of elasticity of the concrete in tension as a function of time. A modular ratio of concrete, as compared to steel, in the range of 10 to 20 was suggested to take the effect of creep into account. He proposed the shrinkage strain at any time t after curing to be

$$[2.10] \qquad \varepsilon_r = \frac{\varepsilon_f}{1 + \frac{E_s A_s}{E_e A_c}}$$

where

$$[2.11] \qquad E_e = \frac{\sigma_{ct}}{\varepsilon_f - \varepsilon_r}$$

Glanville noted that the effective modulus, E_e, tended to decrease with time. He stated that, in his analysis, the instantaneous modulus of elasticity of the concrete in tension is taken as equal to that in compression and deduced that there is no reason to assume that the creep of concrete in tension is not equal to that in compression. Effective moduli of elasticity in the range of 11,200 to 18,800 MPa were computed.

Carlson (1940) conducted some experiments on concrete columns reinforced by single one-inch diameter steel bars bonded at the ends and coated to prevent bond over their mid-length. He introduced new terms such as the sustained modulus of elasticity

and extensibility of concrete. Assuming that the change in length of steel and concrete was the same in the mid-portion and using the free shrinkage strains obtained from unreinforced companion specimens, he concluded that the sustained modulus of elasticity in tension was about 0.35 times the modulus of elasticity in compression.

In a subsequent discussion, Carlson stated that the tensile stress in the concrete at the surface was at least 50% greater than the calculated average stress. However, no attempt was made to calculate the tensile stress on the surface from the test results.

Troxell (1958) conducted shrinkage and creep tests on spirally reinforced 14.5 MPa concrete columns with reinforcement ratios ranging from 1.9 to 5%. Tensile stresses in the concrete of up to 0.52 MPa and compressive stresses in the steel of up to 10.6 MPa prior to the application of load were calculated. The specimens were then initially stressed to 6.28 MPa compression in the concrete and 65.5 MPa compression in the steel. After 22 years, he observed that the stresses in the concrete decreased by 5.72 MPa and the compressive stresses in the steel increased by 130 MPa. As the change in stress was considerably smaller for the specimens stored underwater, Troxell concluded that the change was due to the combined effect of shrinkage and creep of concrete.

Miller (1958) conducted laboratory tests to measure warping of shallow concrete beams due to the presence of

unsymmetrical reinforcement. He stated that warping was not a function of the concrete strength or the modulus of elasticity of concrete. Instead, he suggested using the ratio between the shrinkage strain induced in the steel and the free shrinkage strain of the concrete which is dependent on the thickness of the concrete cover rather than the ratio of reinforcement to calculate deflections. He concluded that bars of all sizes surrounded by a large amount of concrete will have identical shrinkage strains. Miller's conclusions did not apply to members with small eccentricities.

Ferguson (1958) discussing Miller's paper, stated that using the ratio of the induced strain in the steel to the free shrinkage strain of the concrete suggested by Miller would be an oversimplification of a rather complex situation. Based on Miller's experiments, he calculated values of the modular ratio between steel and concrete in the range of 40 to 100 to accommodate the effects of creep. He suggested using values of the modular ratio in the range of 40 to 60 along with an elastic analysis to calculate beam deflections due to differential shrinkage. Ferguson also pointed out that the member size and shape should be considered when using shrinkage data from specimens of different sizes.

Birkeland (1960), investigating the effect of differential shrinkage in composite beams, used the values of the modular ratio suggested by Ferguson to calculate the deflection of a precast concrete beam which had a concrete slab cast on top. Assuming an ultimate shrinkage strain of 500 $\mu\varepsilon$, and using a modular ratio of

40 for the effective modulus of elasticity of the cast-in-place concrete slab, he calculated the deflection of the precast concrete beam using an equilibrium model similar to that used by Brattland and Kennedy (1986). Birkeland compared the calculated values for test beams with the measured values and found good agreement between the two. He concluded that the method described was also applicable to cast-in-place concrete slabs on steel beams.

Hobbs (1979) proposed an equation for the restrained shrinkage strains in symmetrically reinforced concrete members of the form

$$[2.12] \qquad \varepsilon_r = \frac{\varepsilon_f}{1 + (1 + K)\frac{E_s \rho}{E_c}}$$

An equation similar to [2.12] was also proposed by the CEB/FIP (1970) and Neville (1979). Equation [2.12] reduces to [2.10] if the effective modulus of elasticity, E_e, and the ratio of reinforcement, ρ, are expressed as

$$[2.13] \qquad E_e = \frac{E_c}{1 + K}$$

and

$$[2.14] \qquad \rho = \frac{A_s}{A_c}$$

Hobbs, after fitting [2.12] to experimental results, suggested values of K in the range of 0.6 to 3.0 for 6 months to 10 years shrinkage of reinforced concrete respectively. He also suggested using a simpler form of [2.12] for design with a modular ratio in the range of 15 to 25 for moist cured concrete. Hobbs used [2.5] and [2.12] to produce design charts.

Ghali (1986) presented solved examples for calculating the shrinkage strains and stresses in concrete members. Ghali used the CEB M78 method to calculate the shrinkage strains and the equation

$$[2.15] \qquad \varepsilon_s(t,t_o) = \varepsilon_u [\, \beta_s(t) - \beta_s(t_o) \,]$$

to calculate the shrinkage strains occurring in the time period t_o to t. An age adjusted modulus of elasticity is introduced to take into account the effect of sustained loads and creep of the concrete.

$$[2.16] \qquad \bar{E}_c(t,t_o) = \frac{E_c(t_o)}{1 + \chi\, \phi(t,t_o)}$$

For restrained shrinkage, Ghali suggested that shrinkage stresses due to the presence of restraint be calculated from

$$[2.17] \qquad \sigma_{cs} = \bar{E}_c [\, (\Delta\psi)\, y - \varepsilon_f (1 - \frac{A_c}{\bar{A}}) \,]$$

where

$$[2.18] \qquad \bar{A} = \bar{\alpha} (A_s + A'_s) + A_c$$

and

$$\bar{\alpha} = \frac{E_s}{\bar{E}_c} \qquad [2.19]$$

For a symmetrically reinforced concrete member, the curvature, $\Delta\psi$, is equal to zero and thus [2.17] reduces to

$$\sigma_{cs} = \bar{E}_c \varepsilon_f \left(1 - \frac{A_c}{\bar{\alpha} A_s} \right) \qquad [2.20]$$

Knowing that,

$$\sigma_{cs} = \bar{E}_c (\varepsilon_f - \varepsilon_r) \qquad [2.21]$$

equation [2.20] becomes

$$\varepsilon_r = \varepsilon_f \frac{1}{1 + \frac{A_s E_s}{A_c \bar{E}_c}} \qquad [2.22]$$

which is similar to [2.10]. Graphs are given for estimating the creep coefficient, ϕ, and the aging coefficient, χ , at different times and curing periods for various relative humidity conditions and member sizes.

Kennedy and Brattland (1991) performed tests on two full-scale composite trusses made with two different concretes and investigated the deflections due to shrinkage strains of the concrete slab over a period of 65 and 85 days. The unrestrained shrinkage strains obtained from plain concrete control specimens

ranged from 600 to 900 με. The measured restrained shrinkage strains varied from 0.42 to 0.52 times the free shrinkage strain. They concluded that the restraint to shrinkage of the concrete slab developed within a short distance from each end. Using an equilibrium model of the shrinkage forces that developed and the measured restrained and free shrinkage strains, the effective modulus of elasticity of concrete in tension was found to range from 1070 to 1390 MPa corresponding to modular ratios of 187 and 144 respectively. Thus, the effective modulus of elasticity of concrete in tension was only about 7% of the modulus of elasticity in compression and only about 10% of the age adjusted modulus of elasticity calculated using Bazant's method, (1972). It is possible that the flexibility of the shear connectors in the fluted deck contributed to the low values of the modulus of elasticity.

2.4 Shrinkage Induced Cracking

Cracks develop in reinforced concrete members when the stress induced by the free shrinkage strain on the surface of the member (as may be reduced by creep) exceeds the tensile strength of concrete.

Neville (1981) states that cracking depends on the potential contraction, the extensibility of concrete, the strength of the concrete, and the degree of restraint to the deformation. The presence of reinforcing bars increases the extensibility in that it causes the concrete to creep with time under the induced stresses and thus develop strains well beyond that corresponding to

maximum stress. Neville stated that if cracks due to restrained shrinkage form at an early age, and moisture has access to the crack, many of the cracks will be closed by autogenous healing.

Rush (1983) states that increased ratios of reinforcement will not prevent the development of cracks completely but the reinforcement close to the surface prevents internal stress peaks which develop near the surface and controls the crack width.

Base (1982) conducted research into shrinkage cracking and developed expressions that differ fundamentally from those of other researchers. He described the difference between shrinkage cracking, flexural cracking and cracking in axially loaded prisms. Base concluded that primary shrinkage cracks are initiated at the concrete surface where shrinkage and cooling effects are greatest. The cracks are quite widely spaced because the length required for the stresses to develop on each side of an existing crack is large.

Chapter 3

EXPERIMENTAL PROGRAM

3.1 General

The main objective of the experimental program was to determine the effective modulus of elasticity of concrete in tension as it develops with time and is affected by the stress level in the concrete.

A total of twenty seven specimens of two different concrete strengths were tested. This number included three plain concrete specimens of each concrete strength that were used to determine the free or unrestrained shrinkage strain. By placing the reinforcement symmetrically as a single bar on the longitudinal axis, the effect of bowing was eliminated

3.2 Formwork

The forms used to cast the specimens were standard forms used for the modulus of rupture test specimens. The forms consist of two C sections connected to a removable steel bottom plate and two removable steel end plates.

By providing a 3 mm diameter threaded hole in each end of the reinforcing bar, the reinforcing bars were held in position in the forms with bolts placed in holes drilled through the centers of the end plates.

Before casting, the forms were carefully cleaned and coated with mineral oil to facilitate stripping. The lead wires from the

strain gauges were fastened to the sides of the channels to keep the ends clear during casting.

3.3 Test Specimens

The test specimens consisted of square concrete prisms of 154x154 mm cross section by 910 mm length either unreinforced or reinforced longitudinally by a single bar. These cross sectional dimensions are representative of the average depth of continuous depth deck slabs. The length is comparable to that used in previous experiments by Glanville (1930) to investigate shrinkage and the effective modulus of elasticity of concrete in tension. Different ratios of reinforcement were obtained by using single bars of different sizes.

After casting in a horizontal position and stripping the forms, the specimens were placed vertically so that strain readings could be taken on all four sides. No external loads were applied to the specimens. The strains due to the self weight, of the order of 20 $\mu\varepsilon$ at mid height, were considered negligible. Internal strains therefore reflect only the shrinkage and relaxation of concrete. The average mass of the specimens was 47.8 kgs.

The specimens were placed in close juxtaposition during curing and the strain measurement period. The relative humidity and ambient temperature were recorded each working day. Fig. 3.1 shows the 15 specimens from mix 1 and the 12 specimens from mix 2 in the support frame where they were kept while the

strain readings were taken. Fig. 3.2 shows a group of three reinforced concrete specimens.

3.4 Mix 1

Specimens for mix 1 with a design strength of 30 MPa were cast on 1989 11 20 starting at 10:30 am. Forty-five standard cylinders were also cast for compression and tensile splitting tests. Three of the 15 shrinkage specimens were unreinforced.

Three specimens of each of four different nominal ratios of reinforcement of 0.44, 0.89, 2.22 and 4.44%, corresponding to a single No. 10, 15, 25 and 35 bar respectively, were cast.

3.4.1 Curing

After casting, all specimens were covered with polyethylene sheets for a period of 2 days. The sheets were then removed for 8 hours to strip the forms and the specimens were placed in the support frame where the strain gauge leads were connected, and again covered with polyethylene sheets. On the third day the sheets were removed for 9 hours to attach Demec points to measure concrete strains and to obtain the initial set of readings. The sheets were removed daily for 3 hours to obtain strain measurements, until the 7th day when they were removed permanently. The specimens were then left in position under normal laboratory operating temperature and relative humidity conditions.

3.5 Mix 2

The specimens for mix 2, ordered with a design strength of 20 MPa, were cast on 1989 12 17 starting at 10:00 am. Thirty five standard cylinders for compression and splitting tests were also prepared.

Three specimens of each of three different reinforcement ratios, 0.89, 2.22 and 4.44% corresponding to a single No. 15, 25 and 35 reinforcing bar respectively, as well as 3 unreinforced specimens, were cast.

3.5.1 Curing

The curing procedure for the mix 2 specimens paralleled that of the mix 1.

3.6 Instrumentation

3.6.1 General

For both mixes, one specimen of each reinforcement ratio was strain gauged to measure the variation of both concrete and steel strains along the length of the specimen while the remaining two were gauged to measure average strains in the central portion only.

3.6.2 Concrete Strains

A demountable mechanical Demec gauge with a gauge length of 254 mm was used to obtain the change in length on the concrete

surface between Demec points fastened to the concrete surface with sealing wax. Usually, three readings were taken to obtain an average but more were taken if the repeatability was poor.

Two sets of Demec points were applied on each of the four faces of the specimens for mix 1 and one set on each of the four faces for mix 2 as seen in Fig. 3.3 to obtain the average strains at mid height. One specimen of each ratio of reinforcement had five sets of Demec points on each face as shown in Fig. 3.5 (a) to determine the variation of strains along the length.

Calibration of the Demec gauge gave a calibration factor of 7.99 $\mu\varepsilon$ per dial division. The repeatability of the Demec gauge readings was within 2 dial divisions corresponding to $\pm$ 16 $\mu\varepsilon$.

3.6.3 Steel Strains

Showa electrical resistance strain gauges of 5 mm gauge length, a gauge factor of 2.10 $\pm$ 2% and a nominal resistance of 200 $\mu\Omega$ were used to measure the steel strains. Reinforcing bars were prepared by grinding the surface of the bar smooth at the locations of the strain gauges. After the strain gauges were mounted following the standard procedure, lead wires were then soldered to the strain gauges and waterproofed by means of an epoxy coating.

A minimum of three strain gauges were applied to the reinforcing bars in reinforced specimens from both mixes to measure the average strains at mid length as seen in Fig. 3.4.

Seven strain gauges were applied, as shown in Fig. 3.5 (b), to measure the variation of strains along the length, to the reinforcing bars of the specimens having five Demec readings on each face.

The FLUKE data acquisition system model No. 1250 was used to transform the electrical strain gauge signals into strain readings and record the output automatically.

3.7 Shrinkage Measurements

Shrinkage strains were deduced from the shrinkage measurements on the concrete and shrinkage strains on the steel. From day 3 to day 10, one complete set of shrinkage readings was obtained daily from the Demec points and the strain gauges. Measurements were then obtained 3 times per week for at least 80 days more. Additional readings were obtained for mix 1 specimens at 121, 135 and 169 days, and at 118 and 141 days for mix 2.

To minimize operational errors, Demec readings were obtained and recorded by the same person. The Demec gauge was adjusted twice or three times daily using a standard bar to compensate for slight temperature changes.

3.8 Control Tests

Standard concrete cylinders from both mixes were tested in compression and splitting to obtain f'_c, f_{ct} and E_c at different ages of concrete and one reinforcing bar of each size was tested in

tension to determine the yield stress and the modulus of elasticity. The tests are fully described in sections 4.1 and 4.2.

3.9 Relative Humidity and Temperature

Because humidity and temperature conditions could not be controlled in the laboratory, measurements of temperature and relative humidity were taken where the specimens were stored during the test. An alcohol thermometer was used for measuring temperatures and a sling psychrometer was used for relative humidity readings. Measurements were taken whenever shrinkage strain measurements were taken.

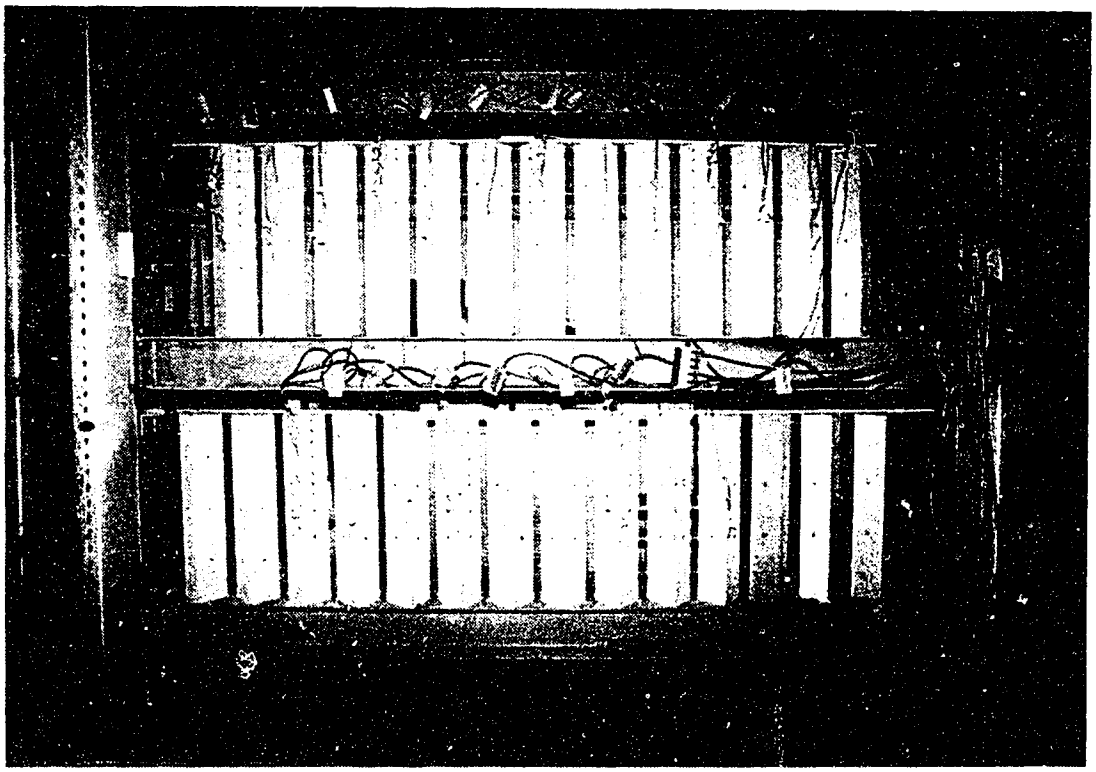

Fig. 3.1 Test Specimens During Shrinkage Measurements

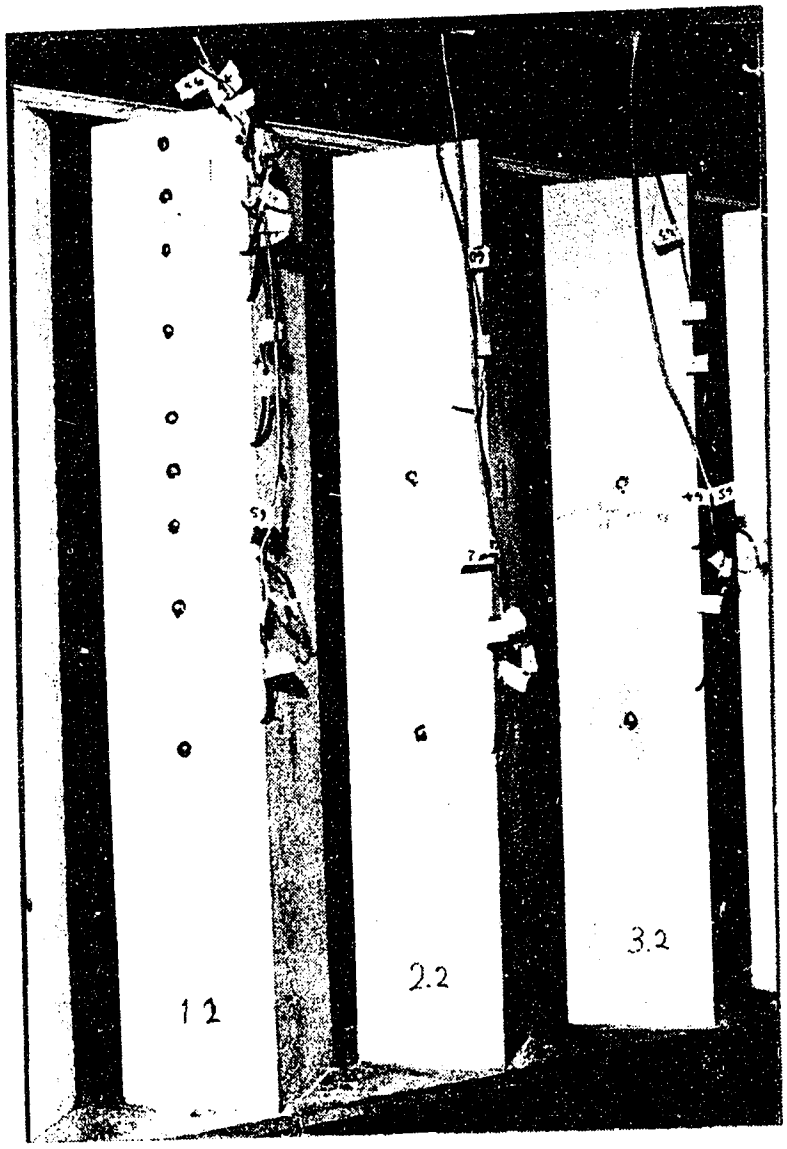

Fig. 3.2 A Group of Three Reinforced Concrete Specimens

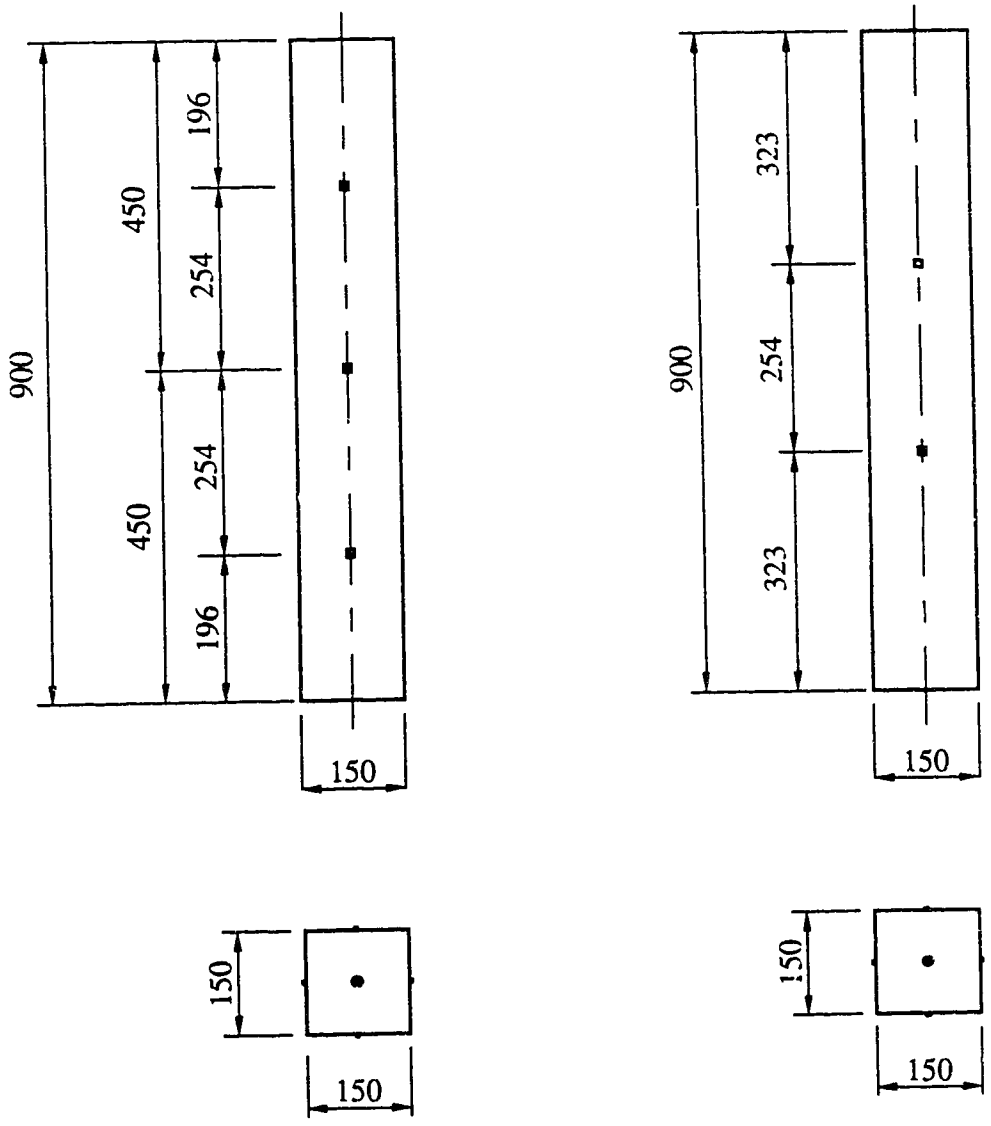

Mix 1

Mix 2

Fig. 3.3 Location of Demec Points on Concrete

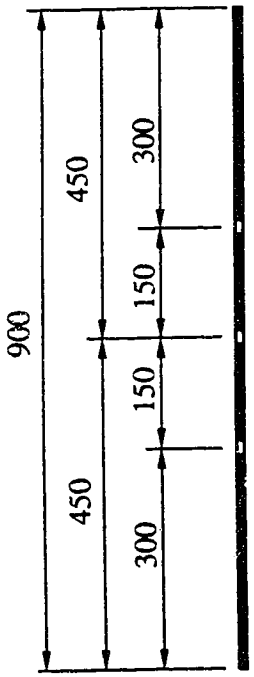

Fig. 3.4 Location of Strain Gauges on Reinforcing Bars, Mixes 1, 2

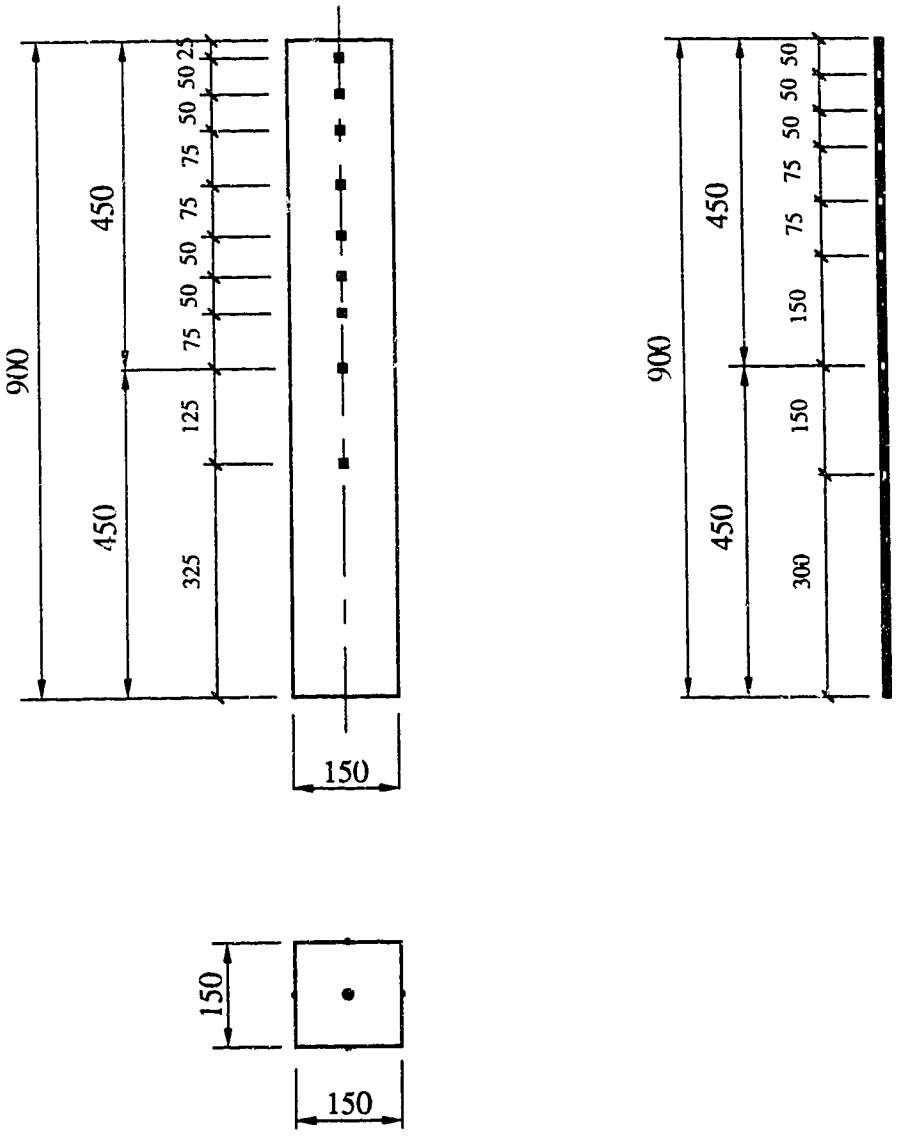

Fig. 3.5 Location of Demec Points and Strain Gauges For Detailed Strain Measurements

Chapter 4

MATERIAL PROPERTIES

4.1 Concrete

4.1.1 General

The concrete mixes selected were within the normal range of strengths and proportions used in practice. Normal weight concretes made with type 10 cement, 15 mm maximum size aggregate, and without fly ash were specified. The mix designs are given in Table 4.1.

Thirty MPa concrete was specified for mix 1. One cubic meter of ready mix concrete was supplied by Alberta Concrete Products. A slump of 55 mm as compared to a specified slump of 75 mm was determined from samples taken from the middle portion of the mix.

Twenty MPa concrete was specified for mix 2 and one cubic meter was delivered by the same supplier. The measured slump of this mix was 35 mm, only about one-half the specified value of 75 mm. At 28 days, cylinder tests gave a strength of 40 MPa, almost double the specified strength.

An electrical hand-held immersion type vibrator was used to consolidate the concrete in the forms which were placed horizontally. The concrete was then screeded and floated and finally trowelled to provide a surface where Demec points could be easily attached. On day 3, the Demec points were mounted and a

reference set of measurements was established. The curing procedure is described in detail in the previous chapter.

Standard concrete cylinders for compression and splitting tests were prepared in accordance with CSA testing procedure A23.2-3C (CSA, 1990) to determine the material characteristics for each mix of concrete at different ages. These specimens were cured for 7 days under polyethylene sheets and stored in the same place as the shrinkage specimens to ensure similar curing conditions.

4.1.2 Ancillary Tests

Three concrete cylinders were tested, in accordance with CSA A23.2-9C, at intervals to determine the variation in the modulus of elasticity and the compressive strength of each mix of concrete with time. A total of 21 cylinders were tested for mix 1 at 3, 7, 15, 29, 43, 56 and 80 days, and 18 cylinders for mix 2 at 3, 7, 15, 28, 42 and 60 days.

Two split cylinder tests were conducted in accordance with CSA A23.2-13C, with each set of 3 compression tests, to determine the splitting tensile strength of concrete and to compare it with the tensile stress at cracking.

4.1.3 Compressive Strength

The average strength from 3 compression cylinders was taken as the compressive strength at a given time. The results of the compression tests at different times are given in Table 4.2 for

mix 1 and in Table 4.3 for mix 2. Fig 4.1 shows the variation of compressive strength with time for both mixes. The 29 day strength of mix 1 of 30.5 MPa was 1.02 times the specified value while for mix 2, for no obvious reason, the 28 day strength of 38.7 MPa was 1.94 times the specified value. The supplier was unable to explain this discrepancy.

The curves in Fig. 4.1 show that the gain in strength beyond 28 days was relatively small.

4.1.4 Modulus of Elasticity in Compression

The modulus of elasticity was determined by dividing the difference between the stress at 40% of the maximum load and the stress at 0.0005 strain by the difference in the corresponding strains.

Values of the modulus of elasticity in compression at different times are given in Table 4.2 for mix 1 and in Table 4.3 for mix 2. The variation of the modulus of elasticity in compression with time is given in Fig. 4.2 for both mixes. For mix 1, at 28 days, the modulus of elasticity was only 79% of the value of $5000\sqrt{f'_c}$ given in the CSA Standard A23.3 1984. For mix 2, the corresponding figure was 76%.

Typical stress strain curves (at 80 days for mix 1 and at 60 days for mix 2) are given in Figs. 4.3 and 4.4.

4.1.5 Tensile Strength

Tensile strength was determined from standard concrete cylinders using the split-cylinder or Brazilian test. The results of the splitting tests at different times and the ratios of the tensile strengths to the specified value of $0.5\sqrt{f'_c}$, ACI (1983) Sec. 11.4.2.1, are given in Table 4.2 for mix 1 and Table 4.3 for mix 2. The average tensile strength was 0.956 times the specified value of $0.5\sqrt{f'_c}$ with a standard deviation of 0.082 for mix 1 concrete, and 0.970 times $0.5\sqrt{f'_c}$ with a standard deviation of 0.112 for mix 2 concrete.

Fig. 4.5 shows the variation of the measured tensile strength with time for both mixes.

4.2 Steel Reinforcement

4.2.1 General

One steel bar of each size was tested in tension to determine its stress-strain characteristics and a piece cut from the middle portion of each steel bar size was used to measure its cross-sectional area.

4.2.2 Cross Sectional Area

The average area of the cross section was determined both by weighing the bar and by measuring its volume. In the weighing procedure, the cross sectional area was determined by dividing the weight of a measured length of bar by the nominal

density of steel of 7850 kg/m^3 and the measured length. In the volumetric procedure, the volume was obtained by immersing it in distilled water and measuring the volume of the displaced water, this value was then divided by the length to determine the average cross sectional area.

Table 4.4 shows the nominal and measured areas. The two procedures gave results within 0.5% of each other. The areas obtained by the weighing procedure were used in the analysis. The mean measured area was 0.97 of the nominal value with a standard deviation of 0.01%.

4.2.3 Tensile Tests

Tensile tests were carried out in the Morrison Structural Laboratory in accordance with ASTM Standard A370-77 (1977) using the MTS 1000 testing machine for the No. 10, 15, and 25 bars and the MTS 6000 for the No. 35 bar. Strains were obtained from two electrical resistance strain gauges mounted on the mid-length of the bar in addition to an electrical extensometer.

Because the actual stresses during the shrinkage tests would be much less than the yield value, the specimens were only loaded into the yield or strain hardening range. Typical stress strain curves for the bars are shown in Figs. 4.6 to 4.9.

Mechanical properties of the bars given in Table 4.4 show that the yield strength varied from 408 to 465 MPa as compared to a nominal value of 400 MPa for CSA G30-12M Grade 400 steel.

The modulus of elasticity had a mean value of 0.993 times the nominal value of 200 000 MPa with a standard deviation of 0.013.

Table 4.1 Concrete Mix Designs

Item	Mix 1	Mix 2
Inland Type 10 Cement, kg/m^3	302	274
Fine Aggregate, kg/m^3	910	980
Coarse Aggregate 5 mm to 15 mm, kg/m^3	1080	940
Water, kg/m3	138	146
Admixture PDA 304, kg/m^3	21	19
Design Slump, mm	75	75
Measured Slump At Delivery, mm	55	35

Table 4.2 Ancillary Tests Results, Mix 1

TIME FROM CASTING, Days	COMPRESSION TEST: CONCRETE COMPRESSIVE STRENGTH, MPa	COMPRESSION TEST: SECANT MODULUS of ELASTICITY, MPa	SPLITTING TEST: CONCRETE TENSILE STRENGTH, MPa	$f_{ct} / 0.5\sqrt{f_c}$
3	20.3 21.8 20.7 μ =20.9	 16 900 18 600 μ =17 800	2.35 1.82 μ =2.08	0.910
7	23.3 24.9 23.8 μ =24.0	21 000 21 500 21 000 μ =21 200	2.10 2.07 μ =2.08	0.850
15	29.4 28.6 27.7 μ =28.6	22 100 21 800 20 000 μ =21 300	2.76 2.69 μ =2.73	1.021
29	30.0 30.8 30.6 μ =30.5	22 800 20 600 22 200 μ =21 800	2.26 2.46 μ =2.36	0.855
43	33.1 30.7 32.4 μ =32.1	22 300 20 900 24 200 μ =22 400	2.69 3.04 μ =2.86	1.010
56	31.9 33.4 30.8 μ =32.0	20 900 22 700 22 400 μ =22 000	2.97 2.90 μ =2.94	1.039
80	33.1 31.1 30.0 μ =31.4	23 600 23 100 22 400 μ =23 000	2.90 2.75 μ =2.83	1.010
				μ = 0.956 σ = 0.082

Table 4.3 Ancillary Tests Results, Mix 2

TIME FROM CASTING, Days	COMPRESSION TEST: CONCRETE COMPRESSIVE STRENGTH, MPa	COMPRESSION TEST: SECANT MODULUS of ELASTICITY, MPa	SPLITTING TEST: CONCRETE TENSILE STRENGTH, MPa	$f_{ct} / 0.5\sqrt{f_c}$
3	23.5 24.6 25.6 μ =24.6	 20 200 20 500 μ =20 400	1.70 2.10 μ =1.90	0.766
7	29.1 22.4 30.0 μ =27.2	22 800 21 000 22 300 μ =22 000	2.68 2.76 μ =2.72	1.043
15	36.5 35.9 35.9 μ =36.1	24 300 23 700 23 300 μ =23 800	2.69 2.97 μ =2.83	0.942
28	38.2 38.5 39.3 μ =38.7	23 300 22 900 24 500 μ =23 600	2.97 2.97 μ =2.97	0.955
42	38.7 38.5 39.1 μ =38.8	23 600 24 100 24 000 μ =23 900	3.47 3.04 μ =3.26	1.047
60	37.6 39.6 39.9 μ =39.0	23 700 23 100 23 900 μ =23 600	3.47 3.18 μ =3.33	1.066
				μ = 0.970 σ = 0.112

Table 4.4 Mechanical Properties of Steel Reinforcement

Rebar Size	Nominal Area, mm^2	Area By Weight, mm^2	Area By Volume, mm^2	E MPa	F_y MPa
10	100	97.0	97.4	201.4×10^3	465
15	200	194.0	195.0	196.5×10^3	448
25	500	485.1	____	200.2×10^3	416
35	1000	970.2	____	196.5×10^3	408

Fig. 4.1 Development of Compressive Strength With Time

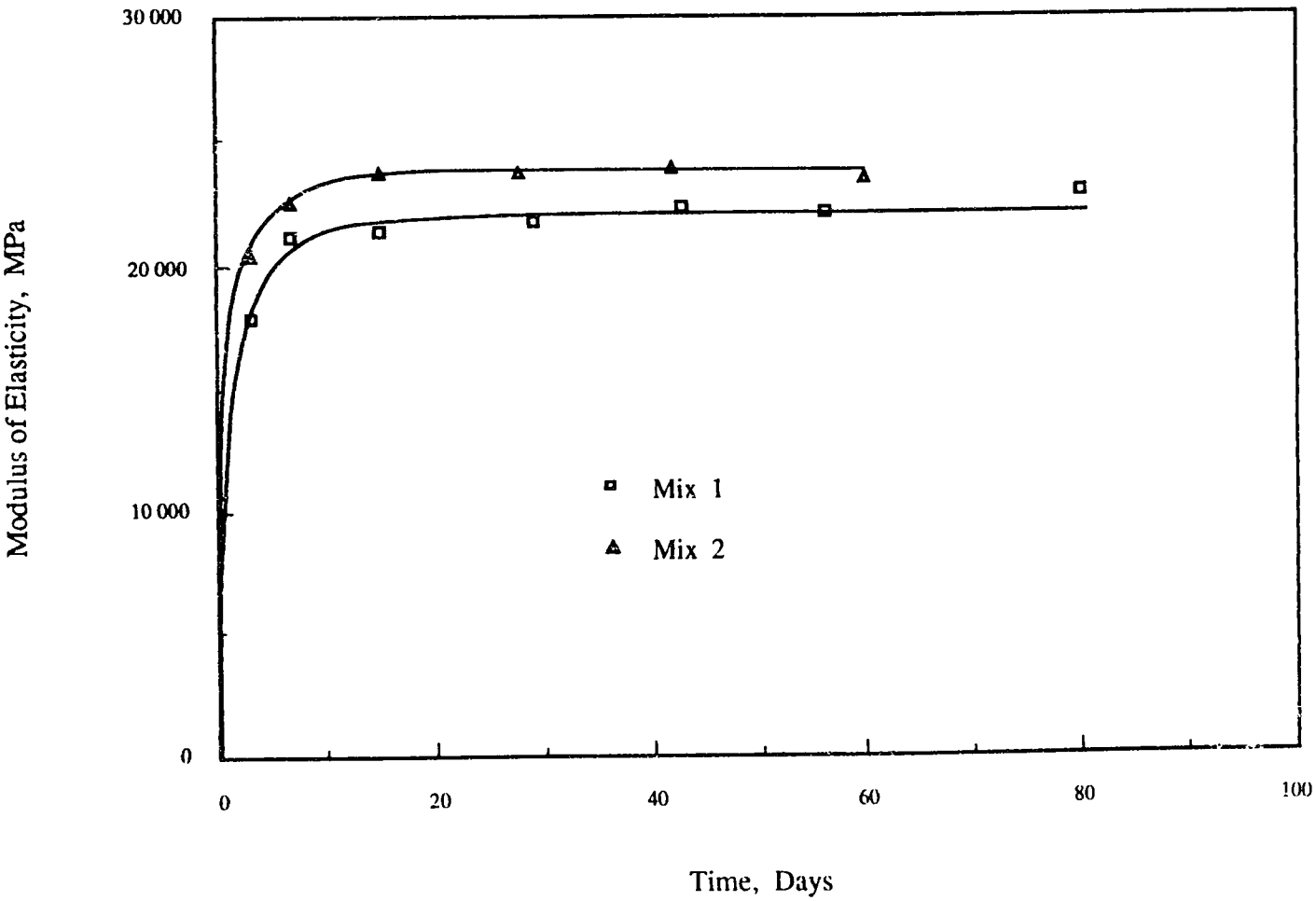

Fig. 4.2 Development of Modulus of Elasticity in Compression With Time

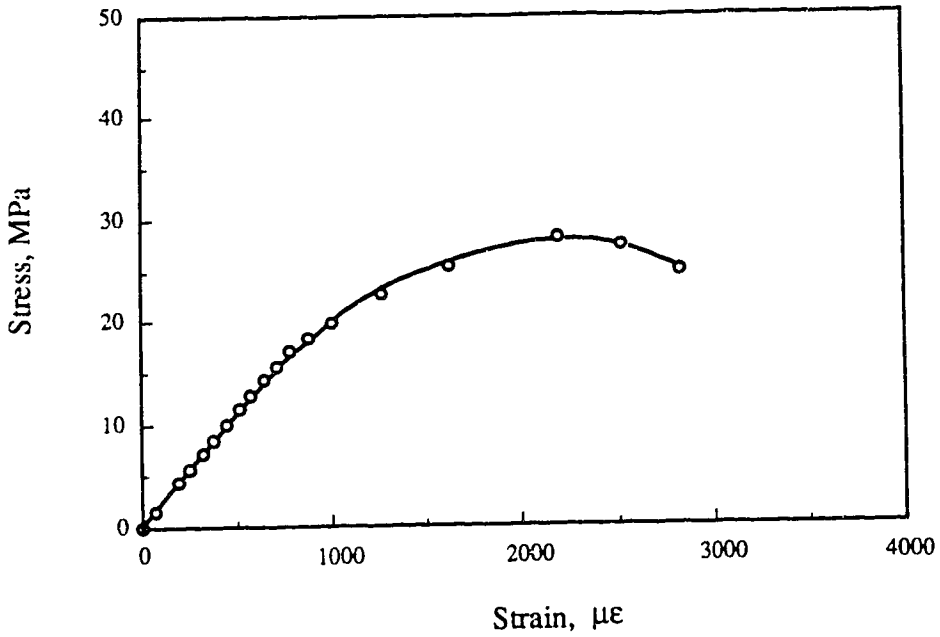

Fig. 4.3 Typical Stress-Strain Curve for Mix 1 Concrete at 80 Days

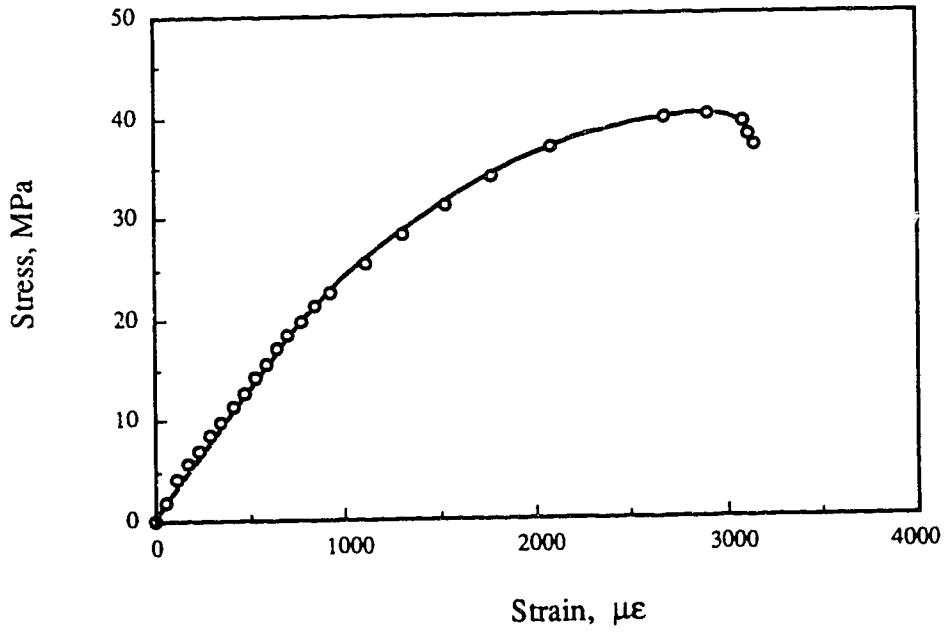

Fig. 4.4 Typical Stress-Strain Curve for Mix 2 Concrete at 60 Days

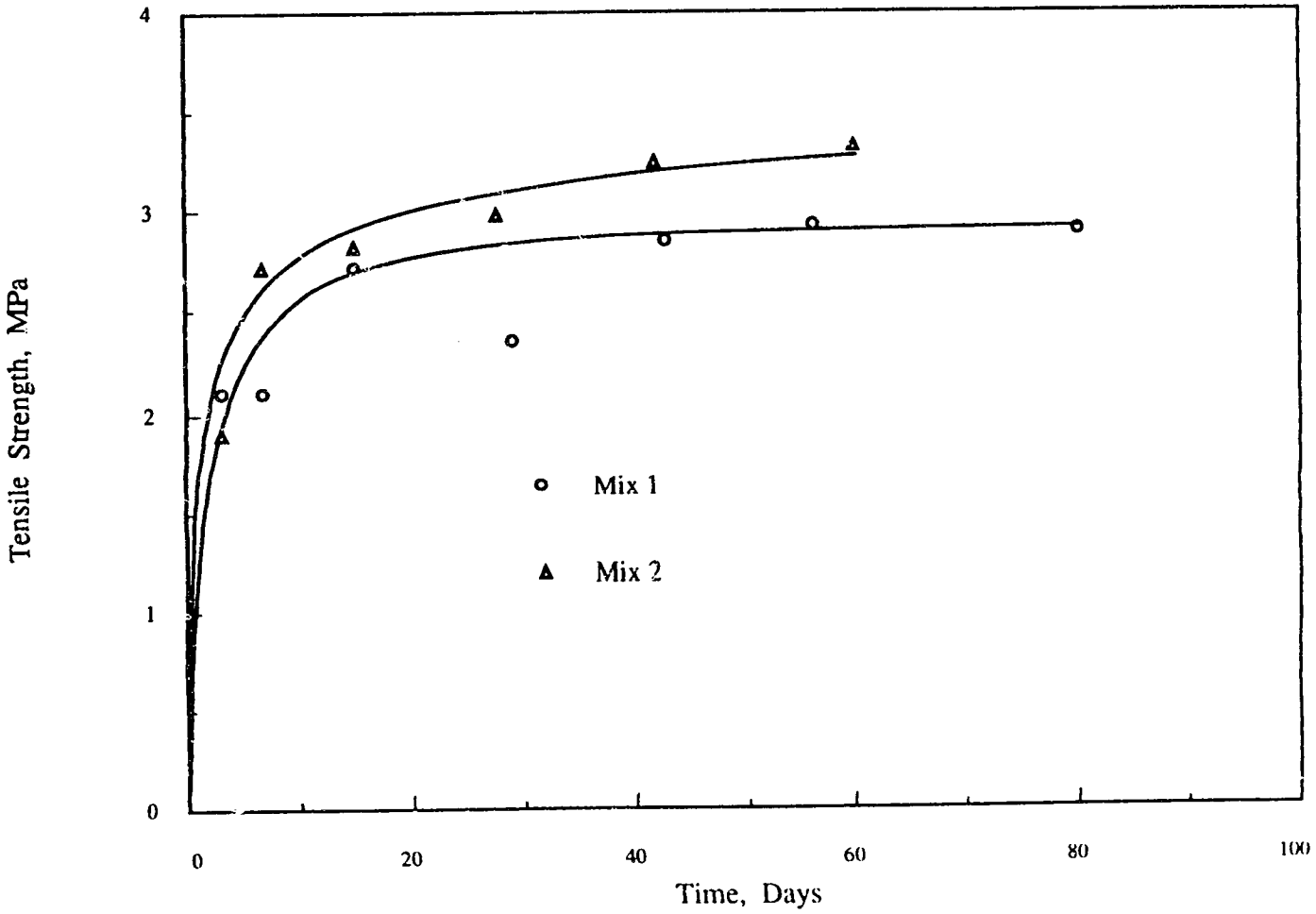

Fig. 4.5 Development of Tensile Strength With Time

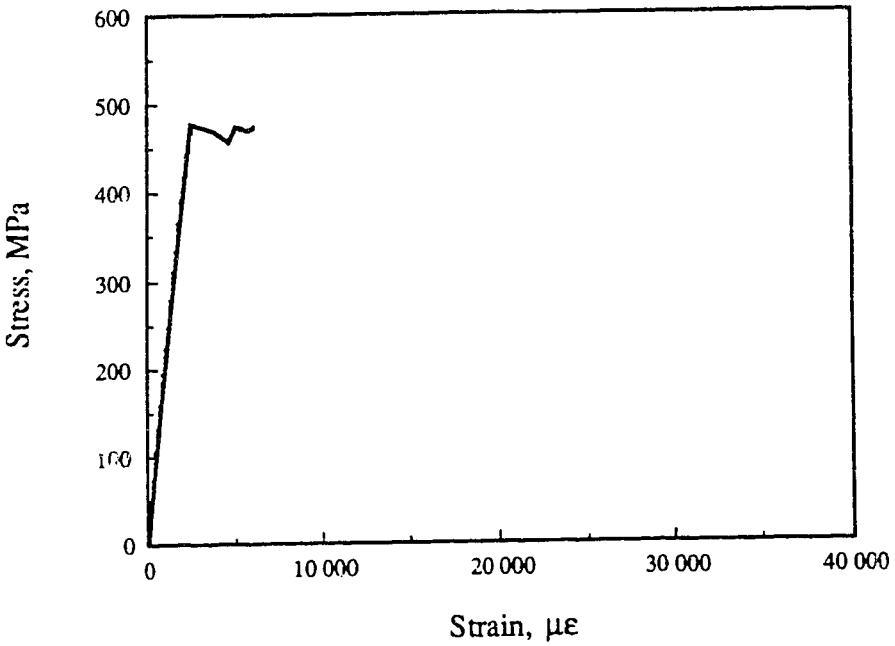

Fig. 4.6 Stress-Strain Curve for No. 10 Bar

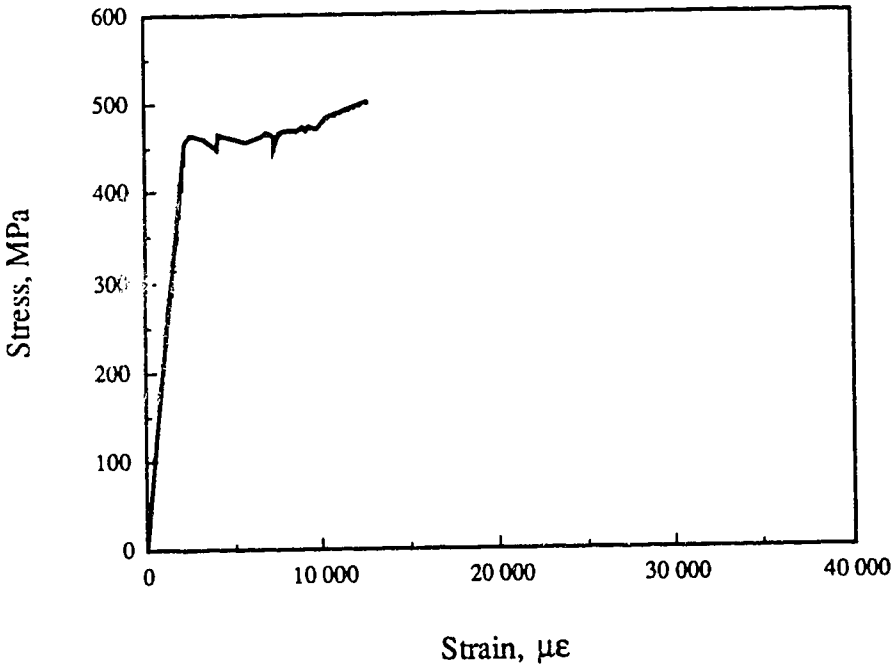

Fig. 4.7 Stress-Strain Curve for No. 15 Bar

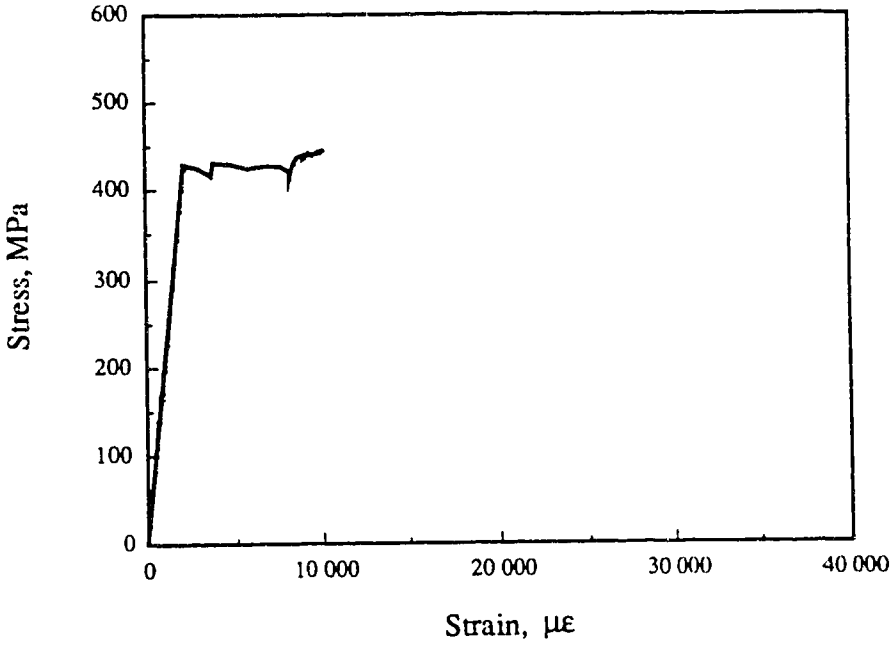

Fig. 4.8 Stress-Strain Curve for No. 25 Bar

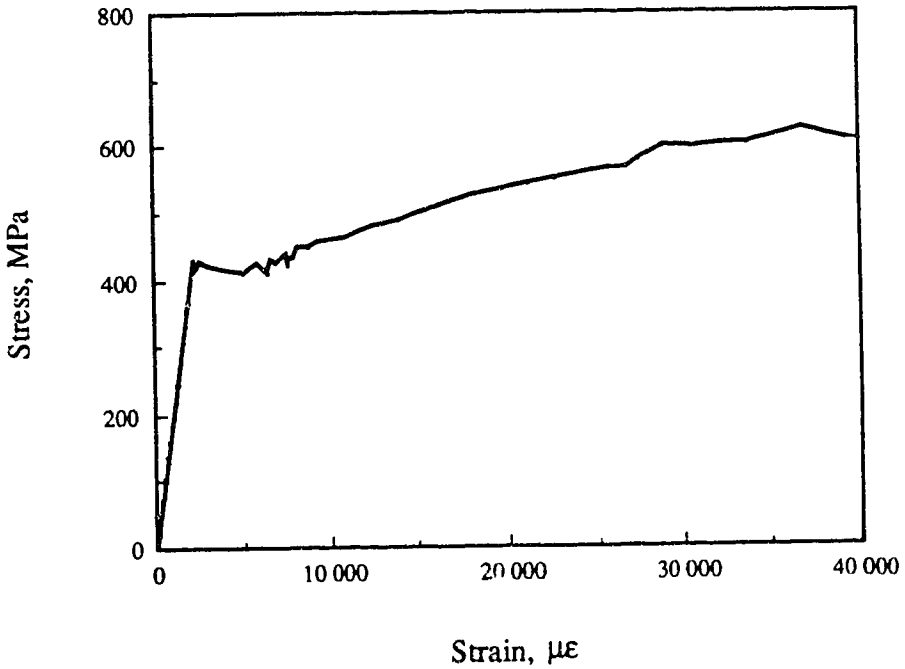

Fig. 4.9 Stress-Strain Curve for No. 35 Bar

Chapter 5

TEST RESULTS

5.1 General

Strain measurements were taken for a period of 169 days on the specimens of mix 1 and for a period of 141 days on the specimens of mix 2.

Concrete strains, obtained from Demec points on the four faces at the same cross section, were averaged to get one value of the strain at that section. The average strain at a certain cross section from each specimen was then averaged with the corresponding strains from specimens of the same mix and ratio of reinforcement to obtain the overall average strain and the standard deviation. Outliers of the average strain at any one cross-section were then rejected using Chauvenet's criterion and the remaining averages were used in plotting the graphs.

The same procedure was followed with the steel strains obtained from the strain gauges except that Chauvenet's criterion was applied to the individual strain gauge readings on the reinforcing bars.

A numbering system consisting of 4 digits was used to identify the specimens of both mixes. The first digit refers to the concrete mix, the second and third digits refer to the reinforcing bar size, and the last digit refers to the specimen number within the group of three. For example, specimen 1152 is from mix 1,

reinforced with a No. 15 bar and it is the second specimen. For the unreinforced specimens, the second and third digits are both zeros. The first specimen in each group of three reinforced concrete specimens was the one used for the measurements of strain development with length.

5.2 Mix 1

5.2.1 Unrestrained Shrinkage Strains

The free or unrestrained shrinkage strains from the unreinforced shrinkage control specimens, were obtained from Demec points mounted on the surface of the concrete. Fig. 5.1 shows the free shrinkage strains at mid-length plotted versus time for the 3 free shrinkage specimens of mix 1. For each specimen, with 3 Demec points on each face, 2 average strains termed upper and lower were obtained. The equation in Fig. 5.1 is discussed in Section 6.1.

Shrinkage strains developed at a gradually decreasing rate to finally approach an asymptotic value. The average shrinkage strain increased from 737 $\mu\varepsilon$ at 90 days to 806 $\mu\varepsilon$ at 121 days, 819 $\mu\varepsilon$ at 137 days and 844 $\mu\varepsilon$ at 169 days. The rate of increase was 2.23 $\mu\varepsilon$ per day from 90 to 121 days and decreased to 0.8 $\mu\varepsilon$ per day for the period from 137 to 169 days.

The scatter in the data at any day from the mean, as discussed subsequently, is attributed to the variation in the temperature and relative humidity in the laboratory. The scatter

on a given day is about $\pm$ 16 $\mu\varepsilon$ which corresponds to the repeatability of the Demec readings of 2 dial divisions.

The temperature, plotted versus time in Fig. 5.2, ranged from 20 to 26° C, while the relative humidity, plotted in Fig. 5.3, ranged from 21 to 48% with the exception of days 66 and 67 when it plunged to about 7%.

5.2.2 Restrained Shrinkage Strains at Mid Length

Figs. 5.4 to 5.15 show the development of the restrained shrinkage strains near mid length with time for the reinforced specimens 1101 to 1253 of mix 1 with No. 10, 15 and 25 bars. The concrete of the specimens with No. 35 bars cracked during the test period and their data are presented separately.

The measured strains in the concrete are the restrained shrinkage strains that result when the concrete attempts to shrink but is restrained by the steel embedded in it. The strains in the steel are the compressive strains induced in the steel as it restrains the shrinkage of the concrete. Both strains therefore can be classified as restraint induced shrinkage strains. The concrete strains are restrained shrinkage strains and the steel strains are restraining shrinkage strains. The steel is in compression and for equilibrium the concrete is in tension though undergoing negative strains (contraction).

The data for the specimens of mix 1 reinforced with a No. 10 bar, specimens 1101 to 1103, is plotted versus time in

Figs. 5.4 to 5.6 and the average data for the 3 specimens is plotted in Fig. 5.7.

For the individual specimens the data for 2 concrete strains obtained from the Demec points and 3 steel strains obtained from the electrical resistance strain gauges were plotted. The steel strains and concrete strains lie close together with the steel strains being generally slightly lower than the concrete strains, the difference is attributed to the greater rate of moisture loss at the surface of the specimen than in the middle. From Fig. 5.7 where the average data are plotted, the mean restrained strain at 169 days, for example, is 701 $\mu\varepsilon$ with a coefficient of variation of 0.049 and the average concrete strain is 1.06 times the average steel strain.

Figs. 5.8 to 5.10 give the strains near mid length for specimens 1151 to 1153 respectively with a No. 15 bar and Fig. 5.11 gives the average strains for the 3 specimens plotted versus time.

It is observed that the steel and concrete strain variation with time have the same pattern as for the specimens with the No. 10 bars with the concrete strains being relatively greater than the steel strains. At 169 days, for example, the mean restrained strain is 603 $\mu\varepsilon$, with a coefficient of variation of 0.087, and the average concrete strain is about 1.14 times the average steel strain.

The same pattern of strain development with time is repeated for the specimens 1251 to 1253 with No. 25 bars plotted in Figs. 5.12 to 5.14 respectively. The average strains for the 3 specimens are plotted in Fig. 5.15.

At 169 days the mean restrained shrinkage strain is 348 με, with a coefficient of variation of 0.19, and the average concrete strain is 1.27 times the average steel strain.

Thus, for the specimens with No. 10, 15 and 25 bars, the steel and concrete shrinkage strains near mid length exhibited similar behaviour with 2 distinct attributes. That the strains on the surface of the concrete are in all cases higher than those of the steel which is attributed to the greater moisture loss at the surface than at the interior of the concrete. The steel strain decreases significantly with increased bar size due to the greater restraint to shrinkage provided by the larger bars.

5.3 Mix 2

5.3.1 Unrestrained Shrinkage Strains

For mix 2, only one average strain was obtained at mid length from one set of Demec points on each face.

The shrinkage strains plotted in Fig. 5.16 for mix 2 developed with time in a similar manner to those from mix 1. The average unrestrained shrinkage strain increased from 702 με at 91 days to 720 με at 114 days and 742 με at 141 days. The rate of

increase was 0.82 με per day from 90 to 121 days and decreased very slightly to 0.80 με per day afterwards.

Again, the scatter in the data from day to day is attributed to the variation in humidity and temperature conditions in the laboratory. The temperature in the laboratory, plotted versus time in Fig. 5.17, ranged between 20 to 26° C, while the relative humidity, plotted in Fig. 5.18, ranged from 21 to 48% with the exception of days 42 and 43 when it went down to 7%.

5.3.2 Restrained Shrinkage Strains at Mid Length

Concrete and steel strains for mix 2 specimens were obtained in a manner similar to those for mix 1 except that only one average concrete strain was obtained at mid length from one set of Demec points on each face. Only specimens with No. 15, 25 and 35 bars were tested.

The development of restrained shrinkage strains at mid length for specimens 2151 to 2153 and 2251 to 2253 with time is similar to that for the corresponding specimens of mix 1. The concrete of specimens with a No. 35 bar cracked during the test period and the strain data for these specimens are presented separately.

Figs. 5.19 to 5.21 give the development of restrained shrinkage strains with time for specimens 2151 to 2153 with a No. 15 bar and the average data are plotted in Fig. 5.22.

At 141 days, for example, the mean restrained strain is 501 $\mu\varepsilon$, with a coefficient of variation of 0.112, and the average concrete strain is 1.16 times the average steel strain. The difference is attributed to the phenomenon of differential drying as described previously.

The development of shrinkage strains with time is plotted for specimens 2251 to 2253 with a No. 25 bar in Figs. 5.23 to 5.25 with the average strains for the 3 specimens plotted in Fig. 5.26.

At 141 days, the mean restrained shrinkage strain is 300 $\mu\varepsilon$, with a coefficient of variation of 0.21, and the average concrete strain is 1.50 times the average steel strain. Again the two distinct attributes of the restrained steel and concrete strains are evident. The concrete surface strains exceed the steel strains and the restrained shrinkage strain decreases with increased percentages of steel.

5.4 Specimens Reinforced With a No. 35 Bar

The behaviour of specimens 1351 to 1353 of mix 1 and specimens 2351 to 2352 of mix 2 all reinforced with a No. 35 bar was similar to each other but significantly different from that of the rest of the shrinkage specimens with smaller bars. Each of the former specimens developed cracks visible on the surface of the concrete. It is possible that a micro crack could be formed before it was observed on the concrete surface.

Figs. 5.27 to 5.29 give the development of shrinkage strains with time for specimens 1351 to 1353 of mix 1 and Figs. 5.31 to 5.33 give the same data for specimens 2351 to 2353 of mix 2. Figs. 5.30 and 5.34 give the average concrete and steel strains for the 3 specimens of mix 1 and mix 2 respectively. The times or intervals when cracking was first observed are noted on the figures.

Figs. 5.35 to 5.37 of the developed surfaces of specimens 1351 to 1353 and Figs. 5.38 to 5.40 of specimens 2351 to 2353 show the positions of the transverse cracks which are generally indicated by horizontal lines. The figures above the short transverse lines give the number of days at which the crack had reached the position indicated. The least figure on any crack line, for example on the crack of specimen 1351 (Fig. 5.35), is the first day on which the crack was observed. Cracks started at the corners and propagated on the two adjacent faces with time. The origins are indicated by open circles. The figures also show the positions of the Demec points and the vertical bars adjacent to them indicate the lengths over which the strain measurements were made. Thus it is readily apparent when a crack lies between two points and therefore affects the apparent strain between them.

Considering the behaviour of specimen 1351 as given in Fig. 5.27, for example, it is seen that with cracking, there is a sharp decrease in the concrete strains within the gauge length where the

crack occurred while on the adjacent gauge length, if no cracking occurred, the restrained concrete strains continued to increase. The development of a crack relieves the tensile force developed in the concrete by the presence of restraint. With this release, the compressive force in the steel bar is also reduced as evident by the reduced steel strain. Cracking is discussed subsequently in the following chapter and a model is suggested.

5.5 Strain Variation Along Length

The data for the strain variation along length was obtained from Demec points and strain gauges for one specimen of each ratio of reinforcement for both mixes.

Figs. 5.41 to 5.44 give the steel and concrete strains plotted over a half length from the end of the specimen for specimens 1101, 1151, 1251 and 1351 respectively, and Figs. 5.45 to 5.47 give them for specimens 2151, 2251 and 2351 respectively. For mix 1 specimens, the graphs for strain development were plotted at 30 and 169 days for all the specimens except for specimen 1351 where the figures were plotted, before cracking, at 9 and 23 days. For mix 2, the figures were plotted at 30 and 141 days for all the specimens except for specimen 2351 where the it was plotted at 9 and 35 days (before cracking).

The measured restrained concrete strains decreased gradually from the free shrinkage strains at the end of the specimen, (measured from the unreinforced concrete specimens), to an almost constant strain over a portion of the specimen at mid

length while the measured steel strains increased from zero at the end of the specimen to a constant strain at mid length. The distance over which the strains are varying represents the development length required to transfer the force developed by shrinkage of concrete to the steel bar. The constant strain region indicates constant forces in the concrete and the steel bar.

The difference between the steel and concrete strains at mid length is due to differential shrinkage from the inside of the specimen to the surface. The development length required to develop complete force transfer from the concrete to the steel increases with increased bar size. The difference in the concrete and steel strains at the free end of the specimen is primarily due to the shear deformation of the concrete, that is, the phenomenon of shear lag.

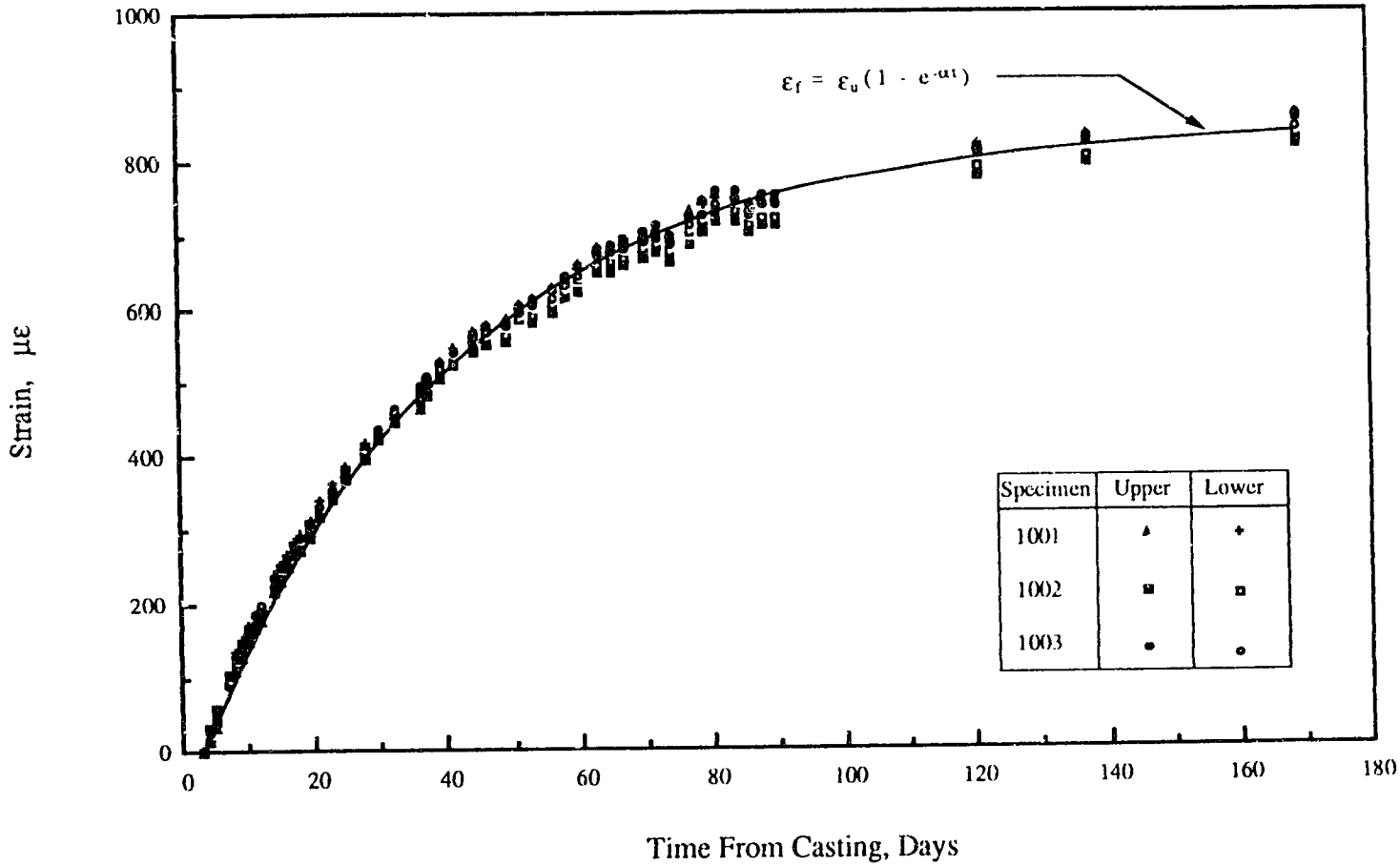

Fig. 5.1 Development of Unrestrained Shrinkage Strains with Time, Specimens 1001 to 1003

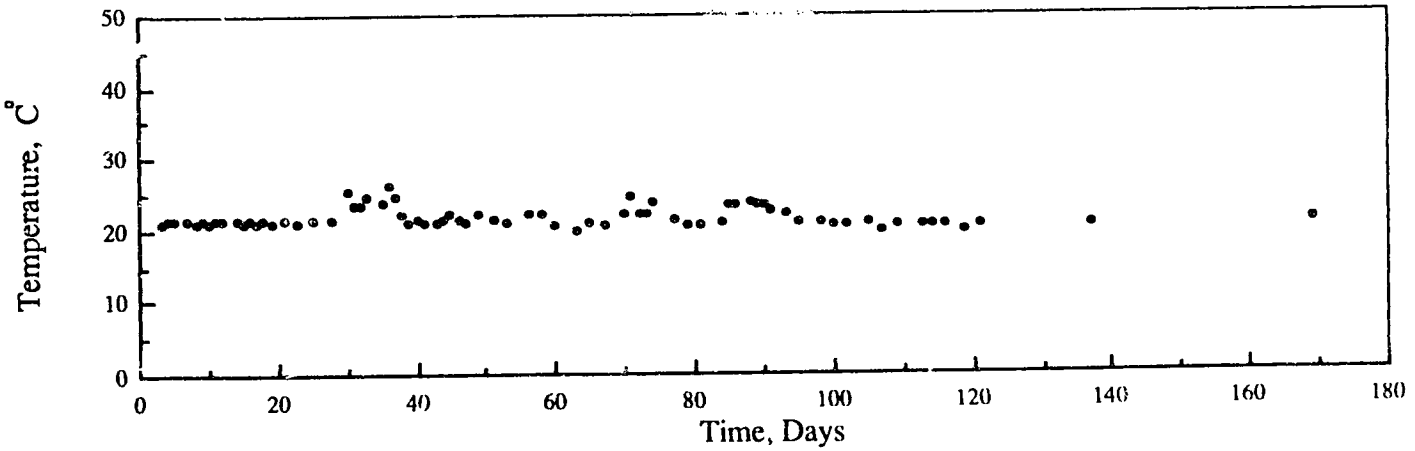

Fig. 5.2 Ambient Temperature vs. Time, Mix 1

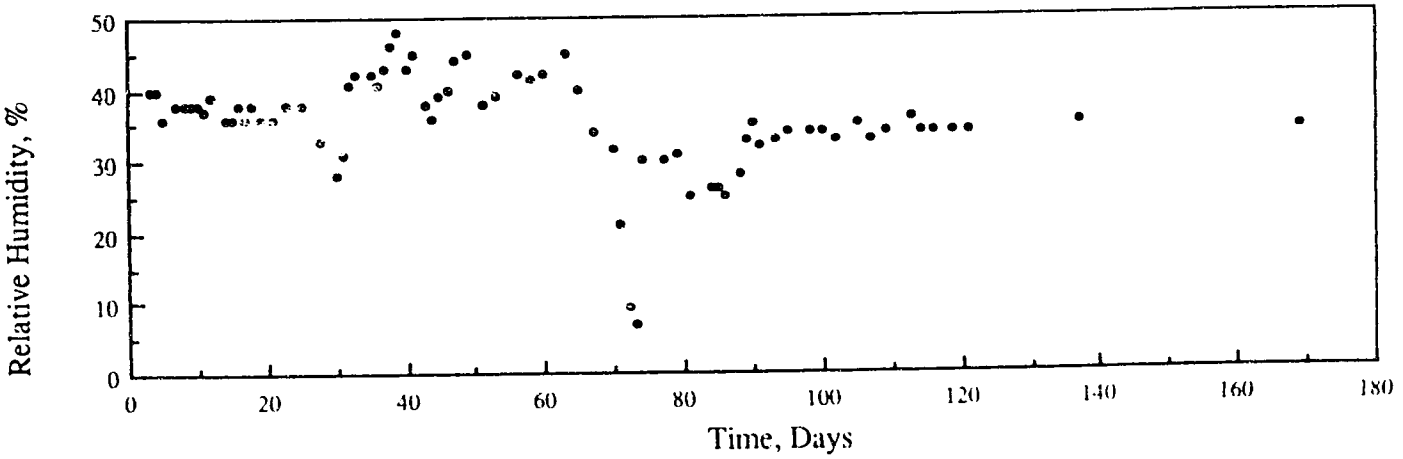

Fig. 5.3 Relative Humidity Conditions vs. Time, Mix 1

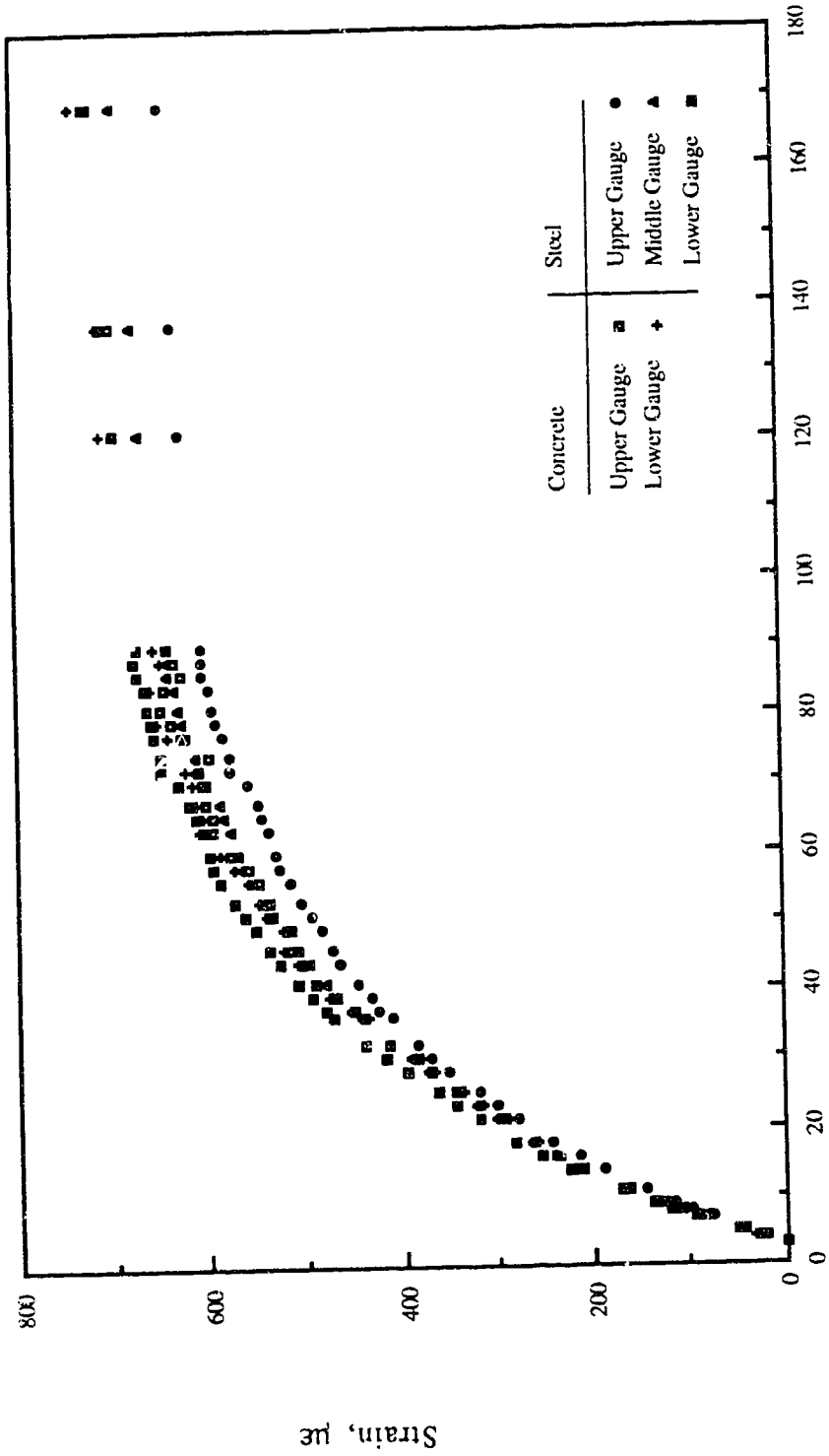

Fig. 5.4 Development of Shrinkage Strains at Mid Length with Time, Specimen 1101

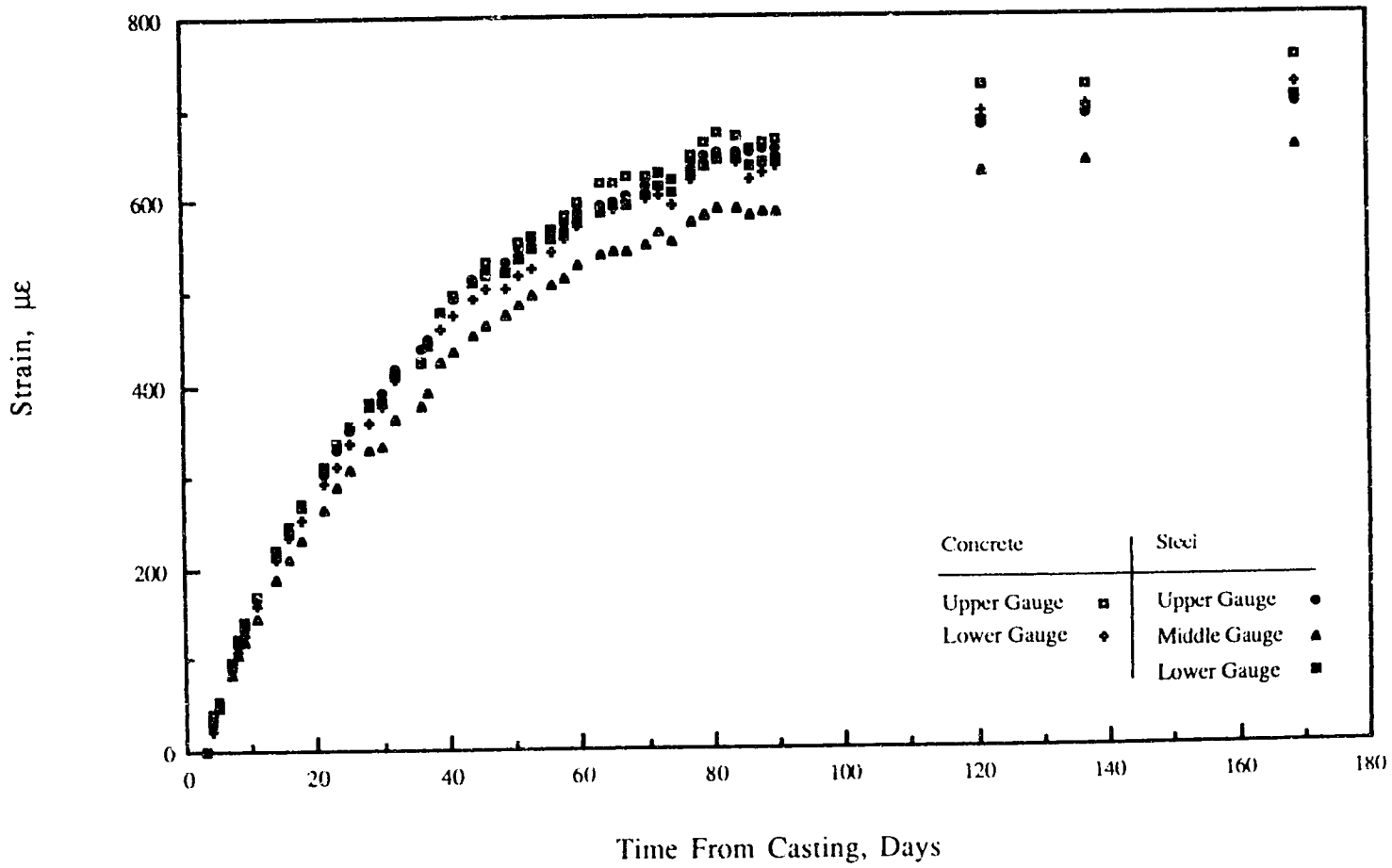

Fig. 5.5 Development of Shrinkage Strains at Mid Length with Time, Specimen 1102

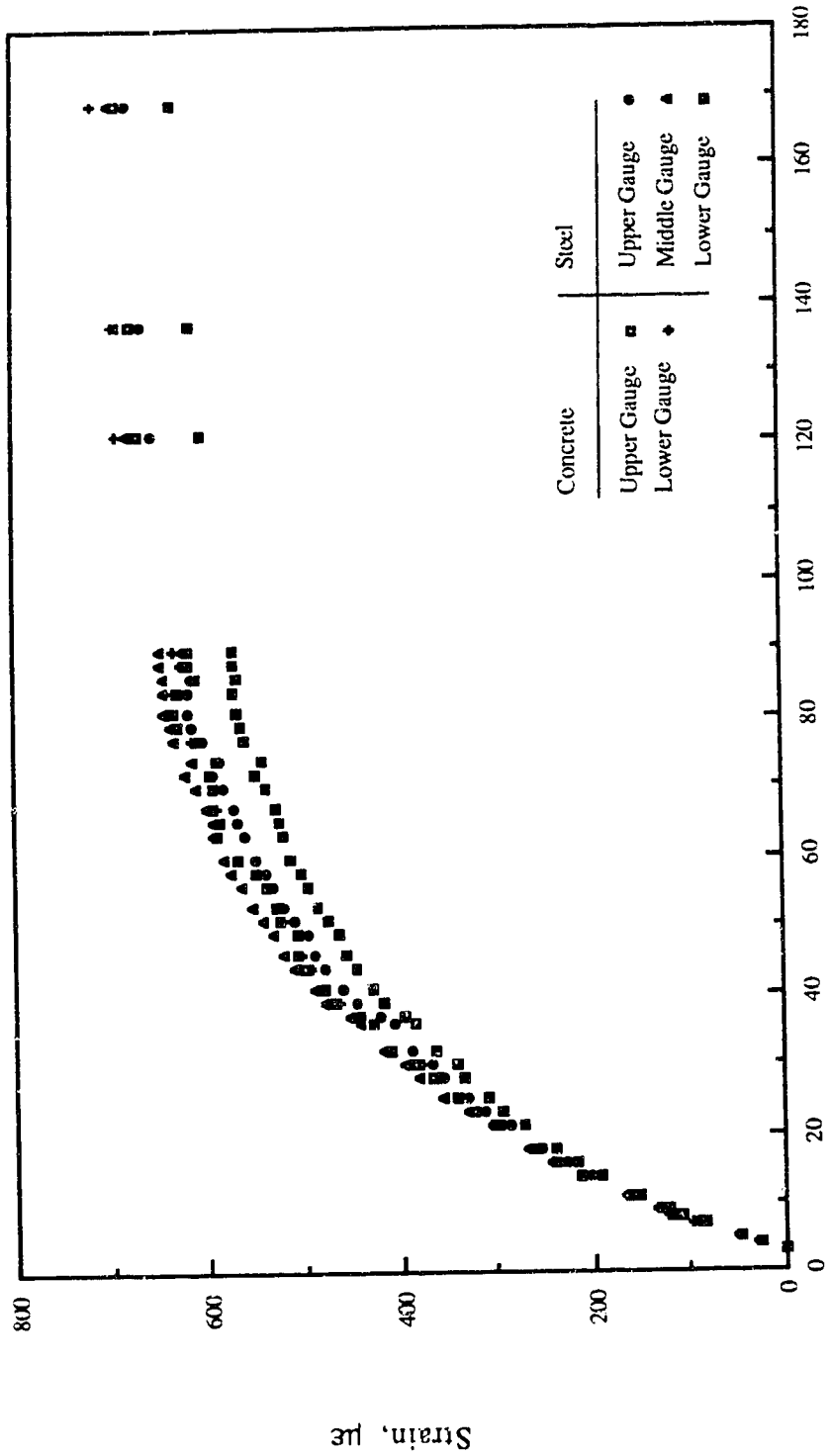

Fig. 5.6 Development of Shrinkage Strains at Mid Length with Time, Specimen 1103

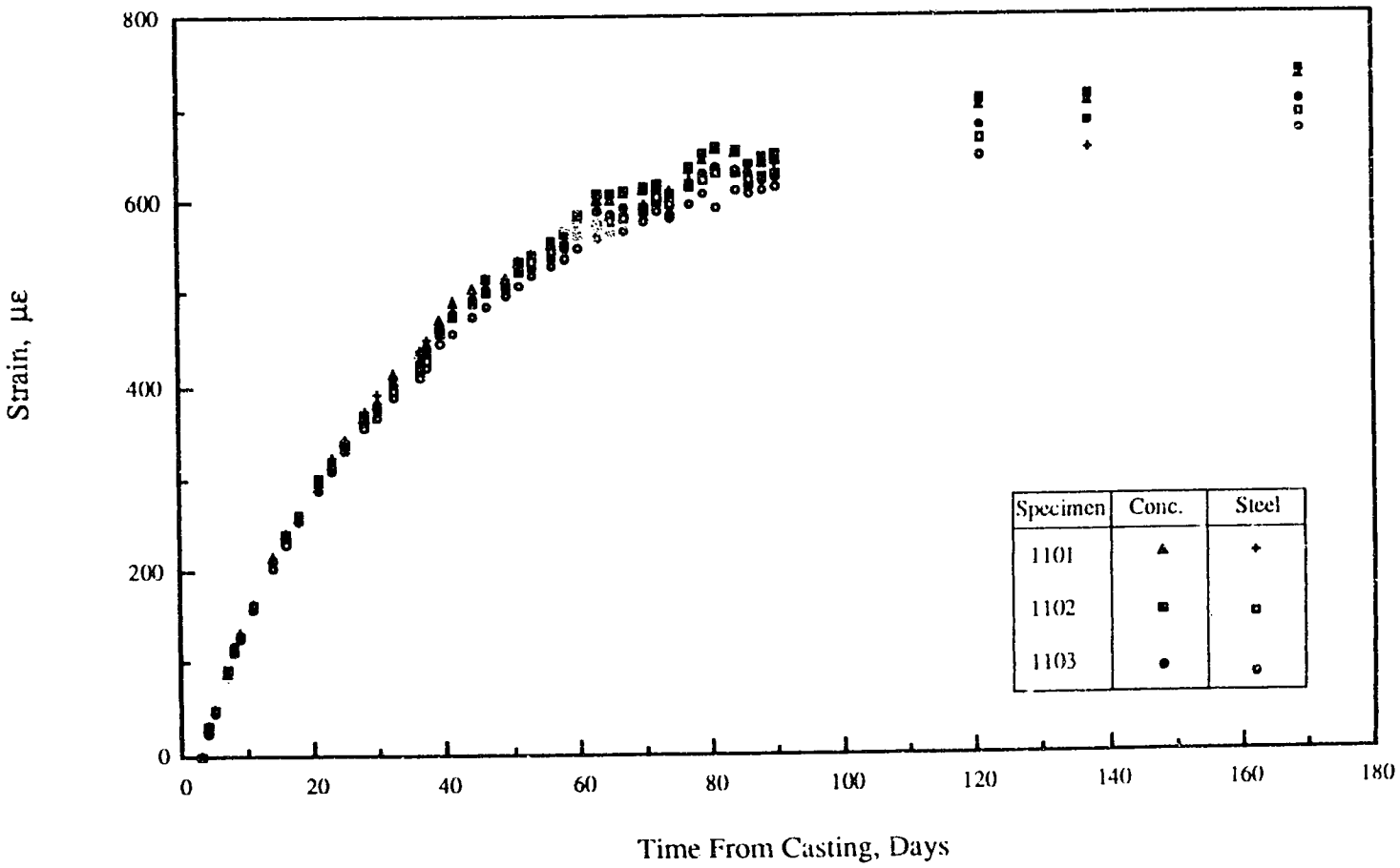

Fig. 5.7 Development of Average Shrinkage Strains at Mid Length with Time, Specimens 1101 to 1103

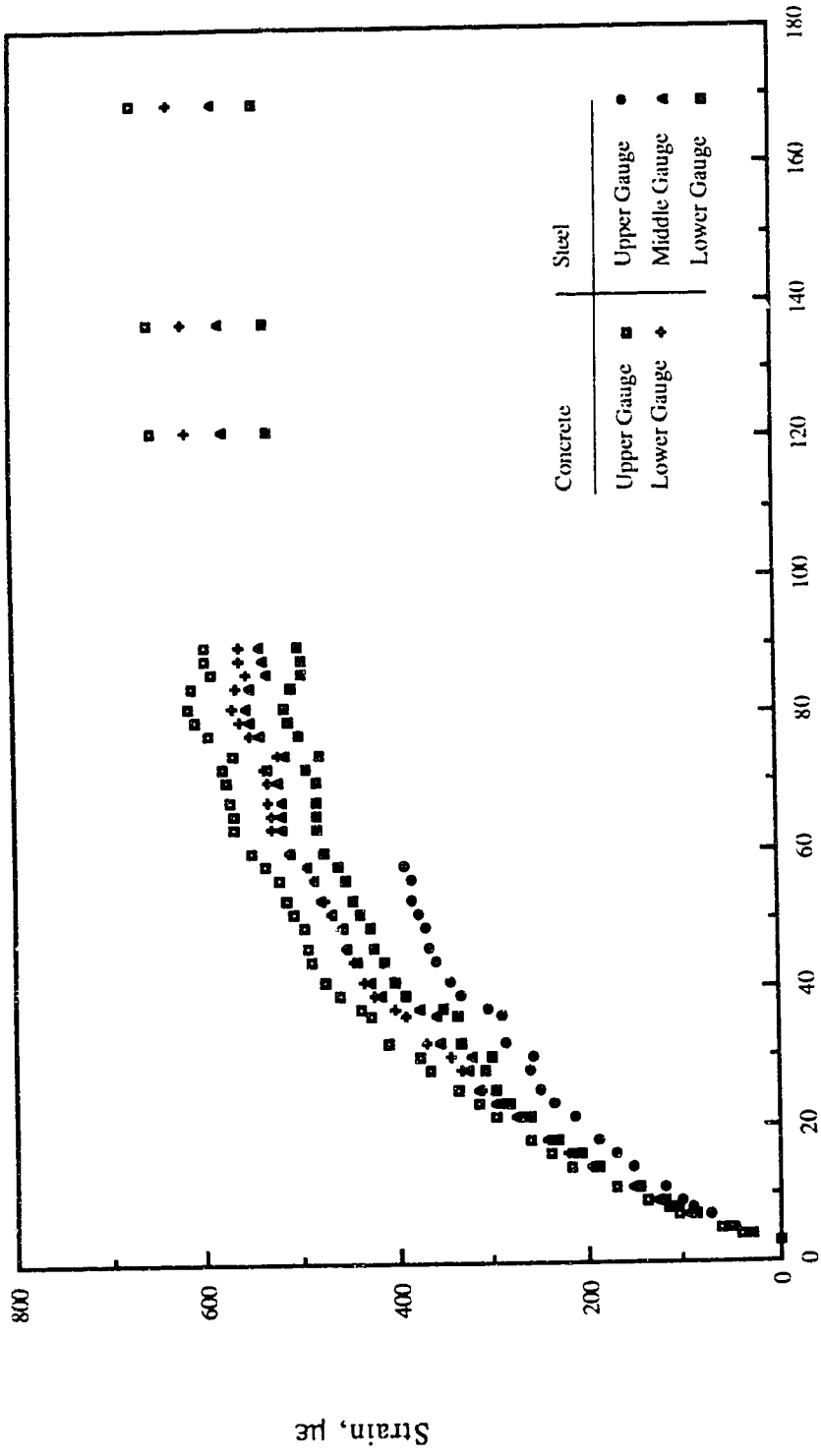

Fig. 5.8 Development of Shrinkage Strains at Mid Length with Time, Specimen 1151

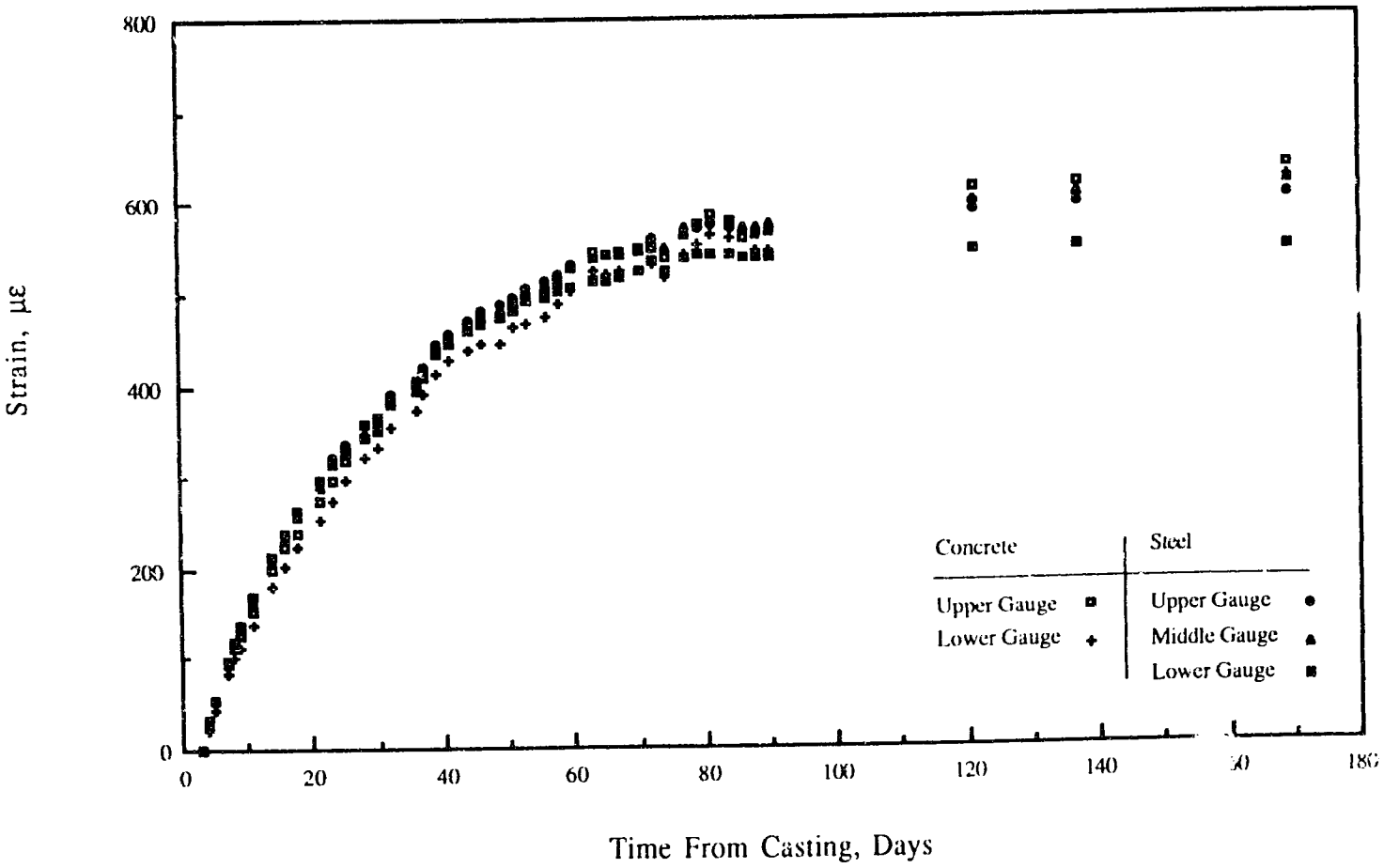

Fig. 5.9 Development of Shrinkage Strains at Mid Length with Time, Specimen 1152

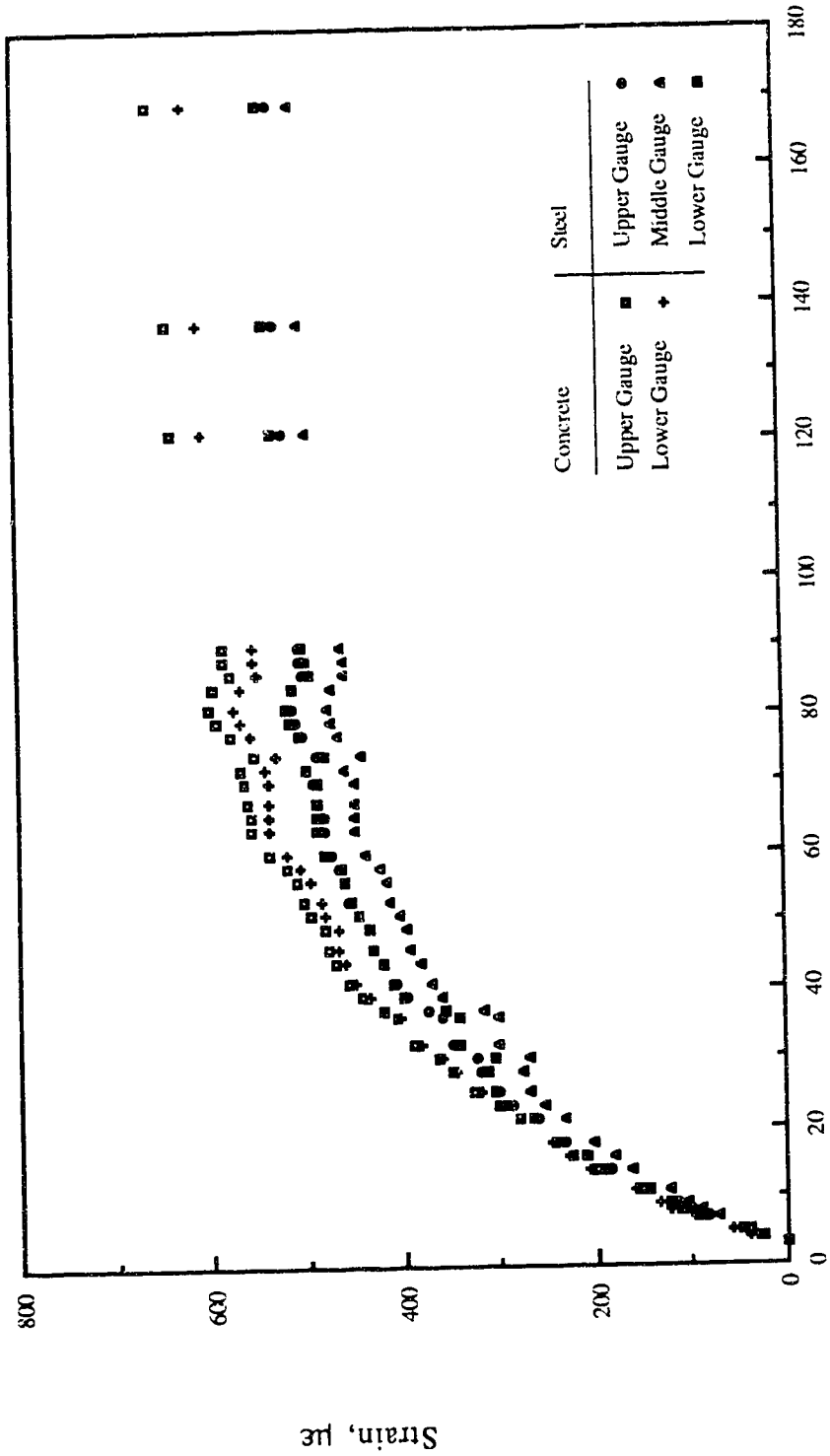

Fig. 5.10 Development of Shrinkage Strains at Mid Length with Time, Specimen 1153

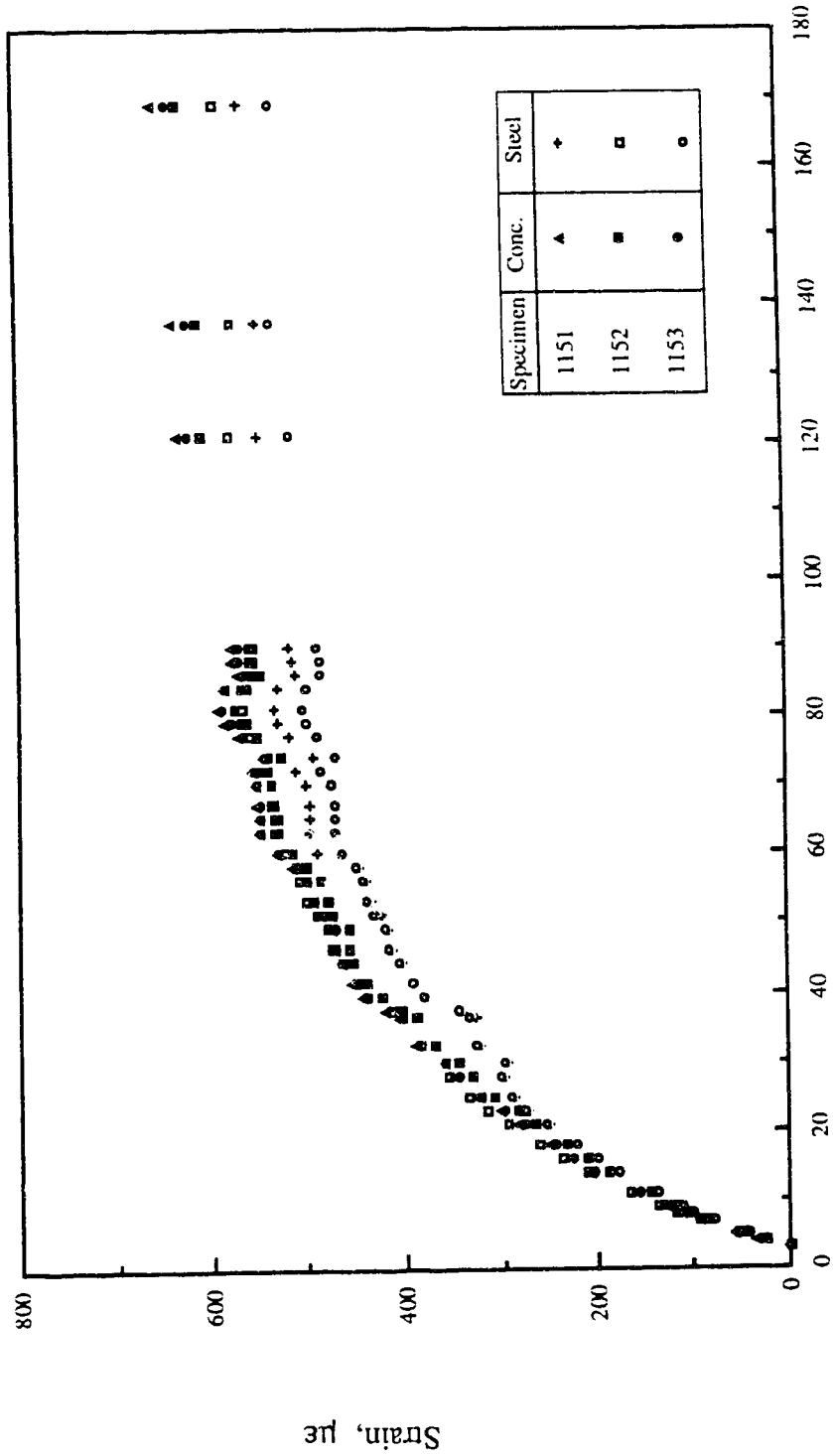

Fig. 5.11 Development of Average Shrinkage Strains at Mid Length with Time, Specimens 1151 to 1153

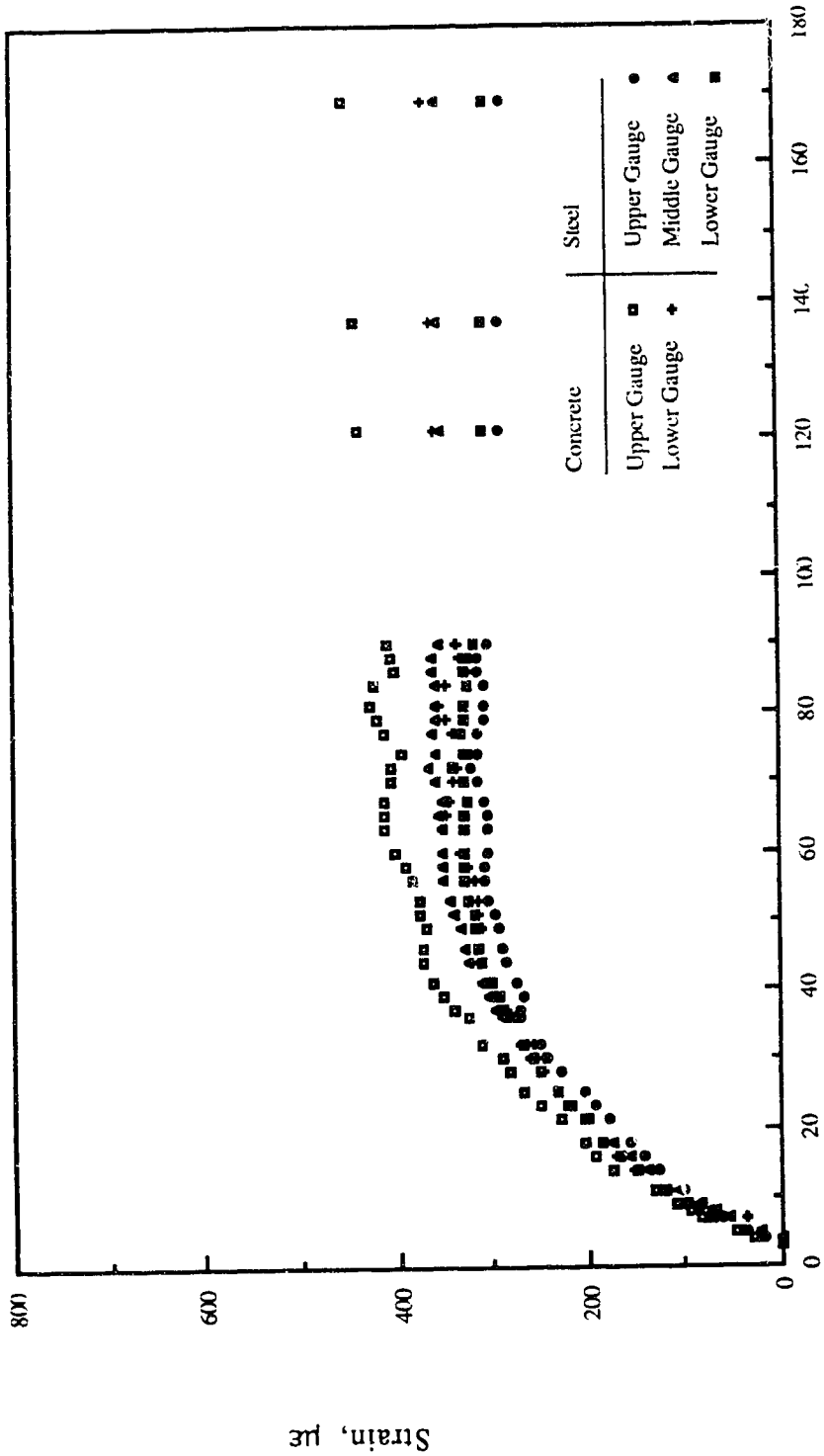

Fig. 5.12 Development of Shrinkage Strains at Mid Length with Time, Specimen 1251

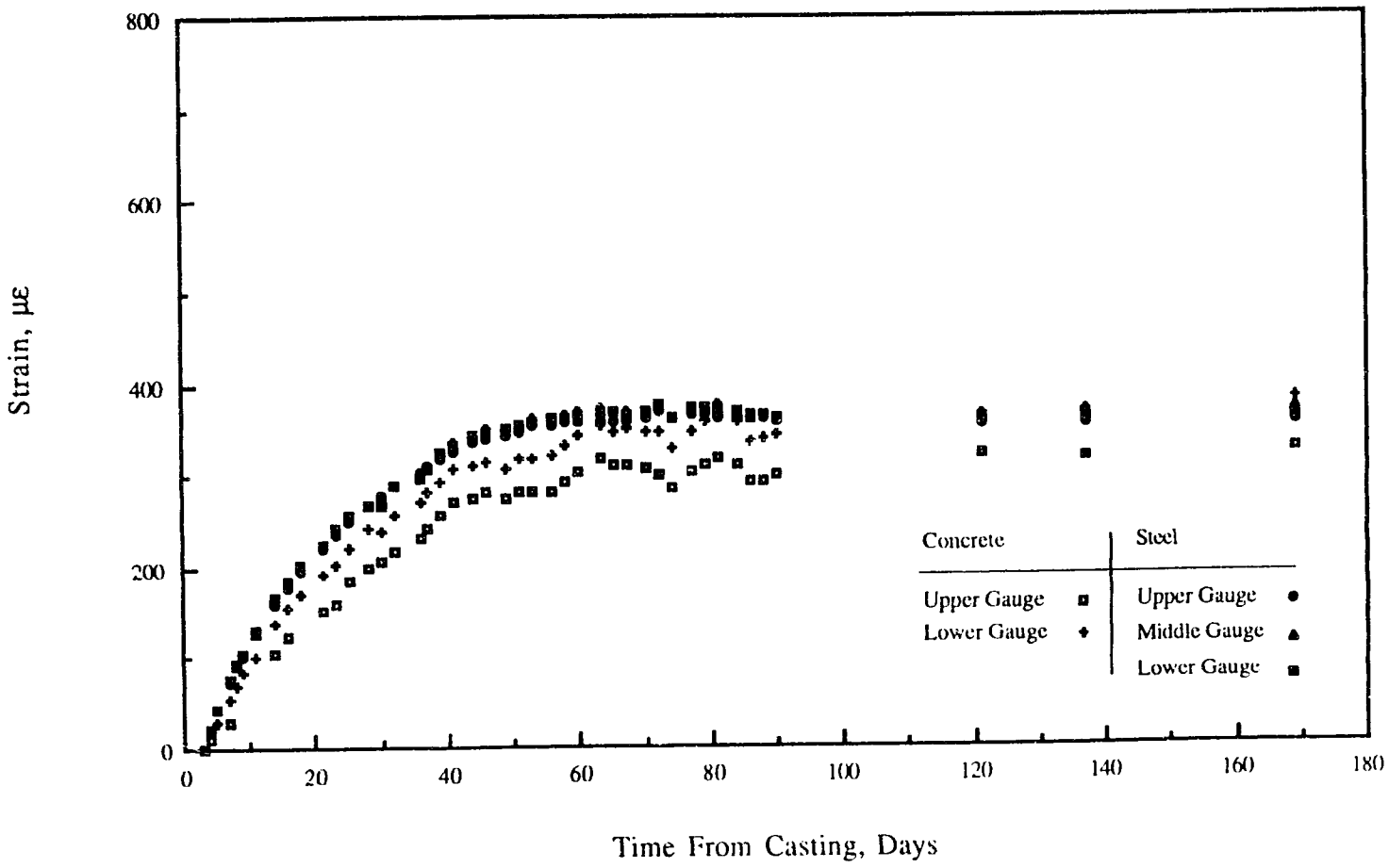

Fig. 5.13 Development of Shrinkage Strains at Mid Length with Time, Specimen 1252

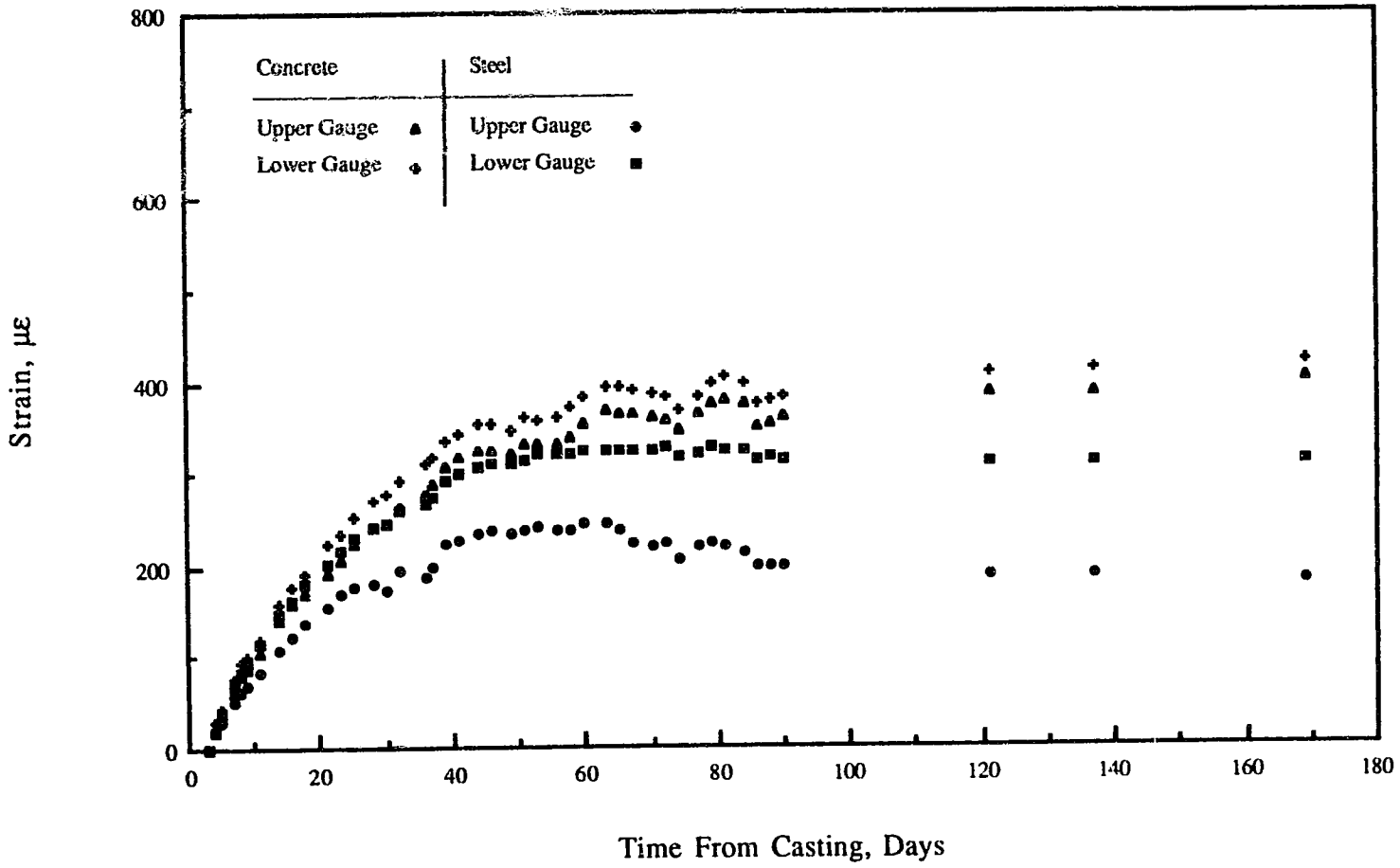

Fig. 5.14 Development of Shrinkage Strains at Mid Length with Time, Specimen 1253

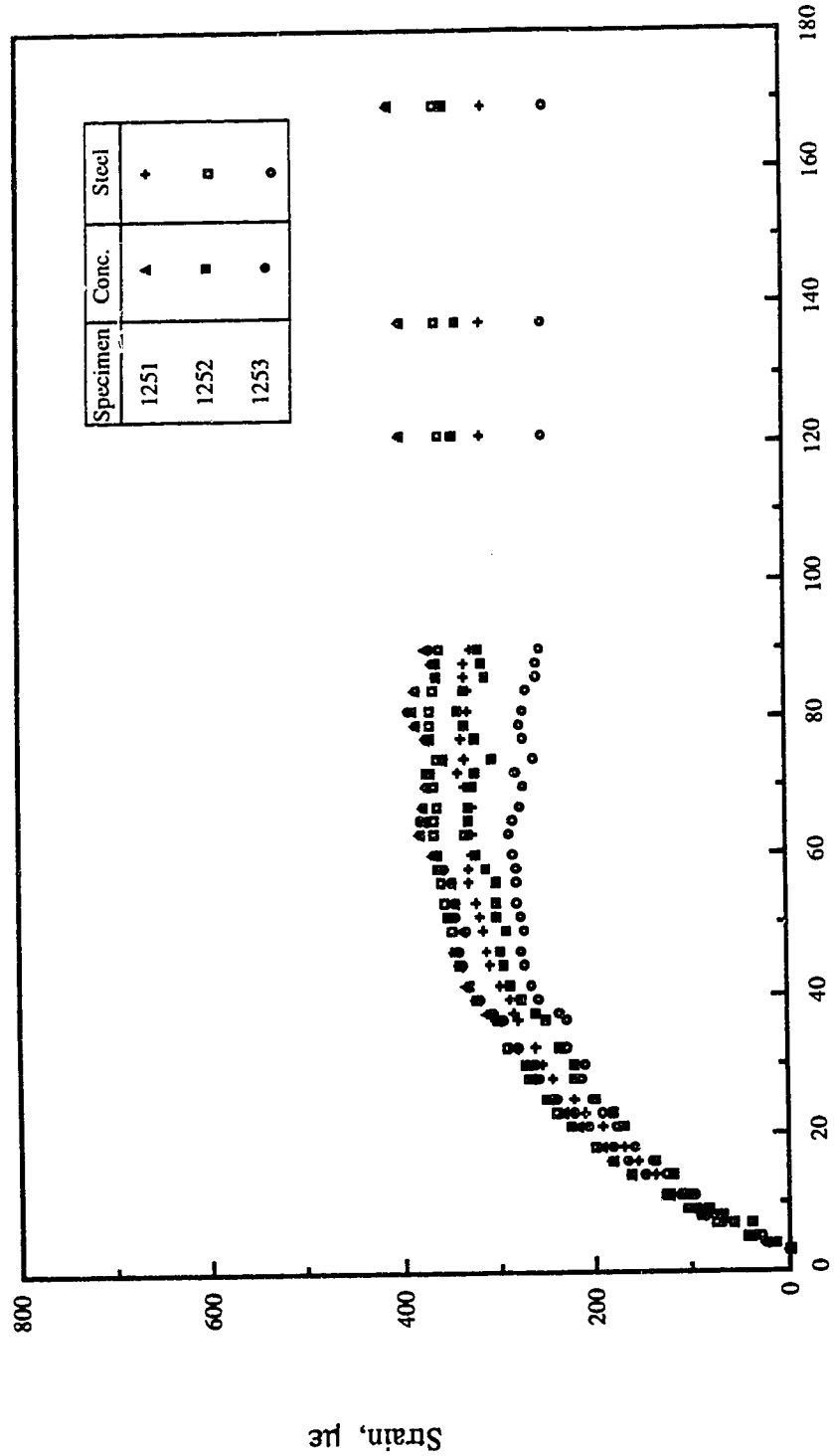

Fig. 5.15 Development of Average Shrinkage Strains at Mid Length with Time, Specimens 1251 to 1253

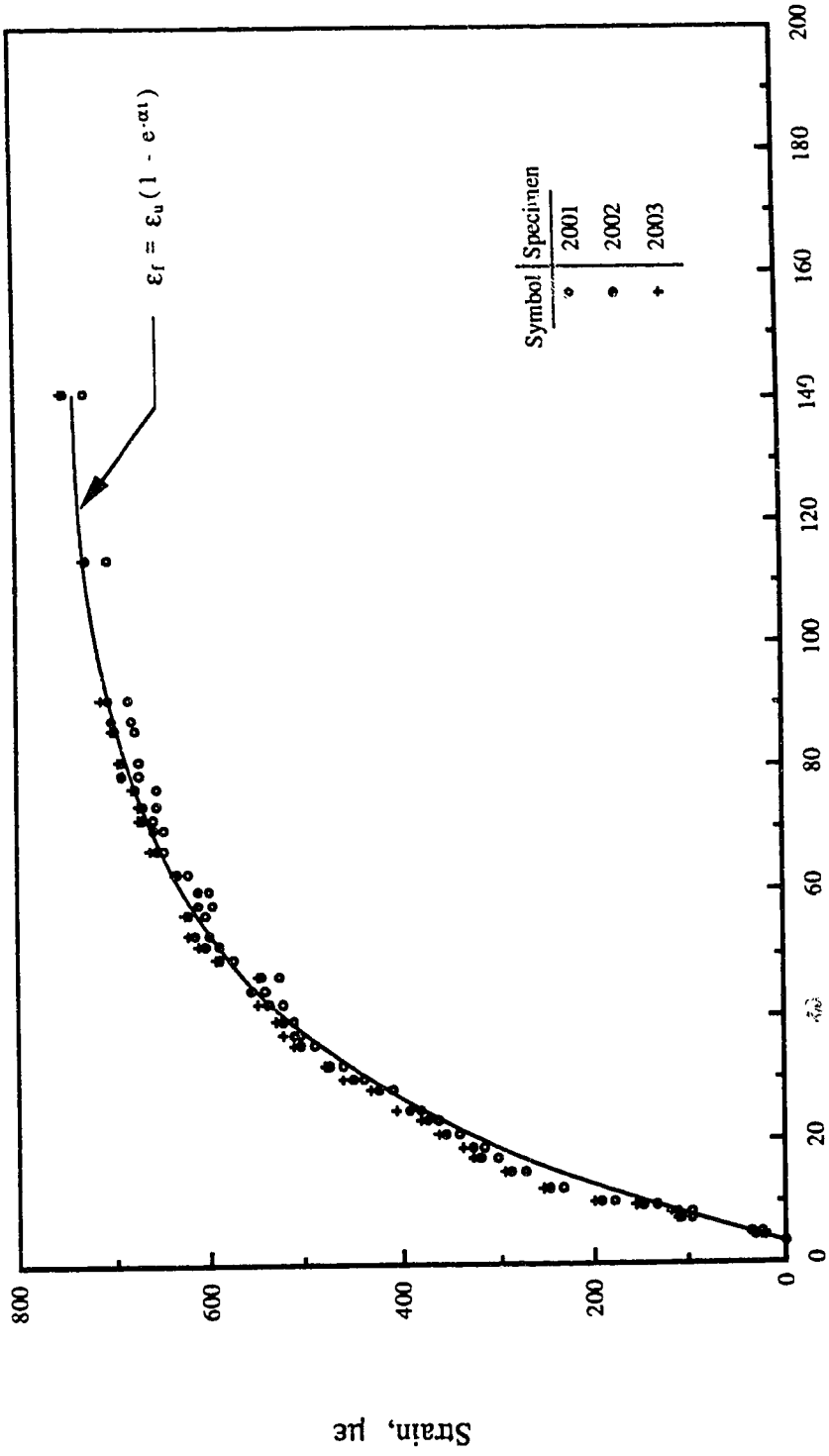

Fig. 5.16 Development of Unrestrained Shrinkage Strains with Time, Specimens 2001 to 2003

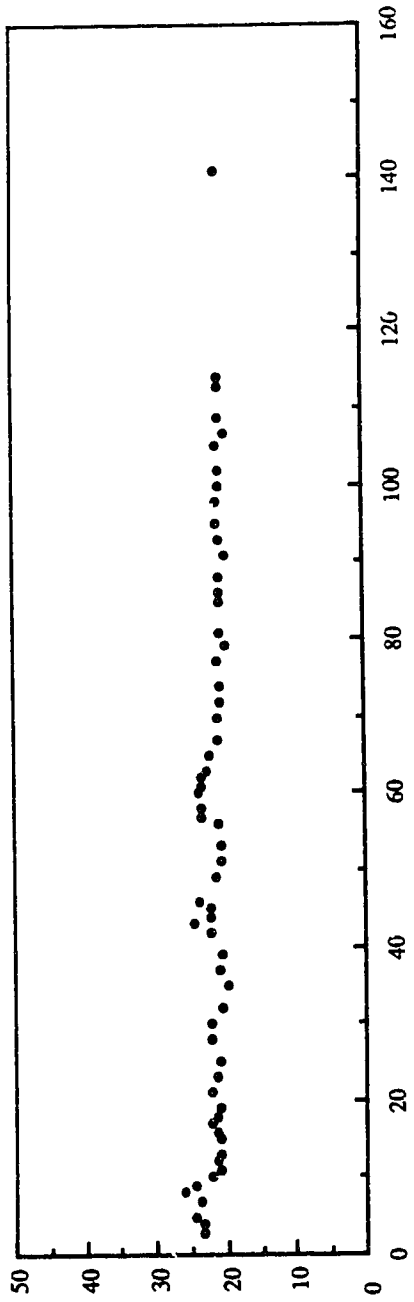

Fig. 5.17 Ambient Temperature vs. Time, Mix 2

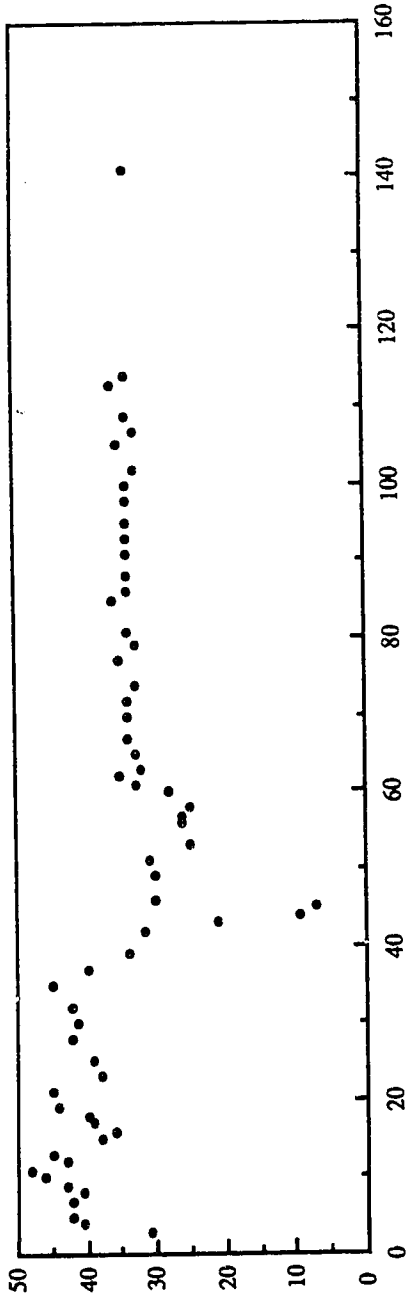

Fig. 5.18 Relative Humidity Conditions vs. Time, Mix 2

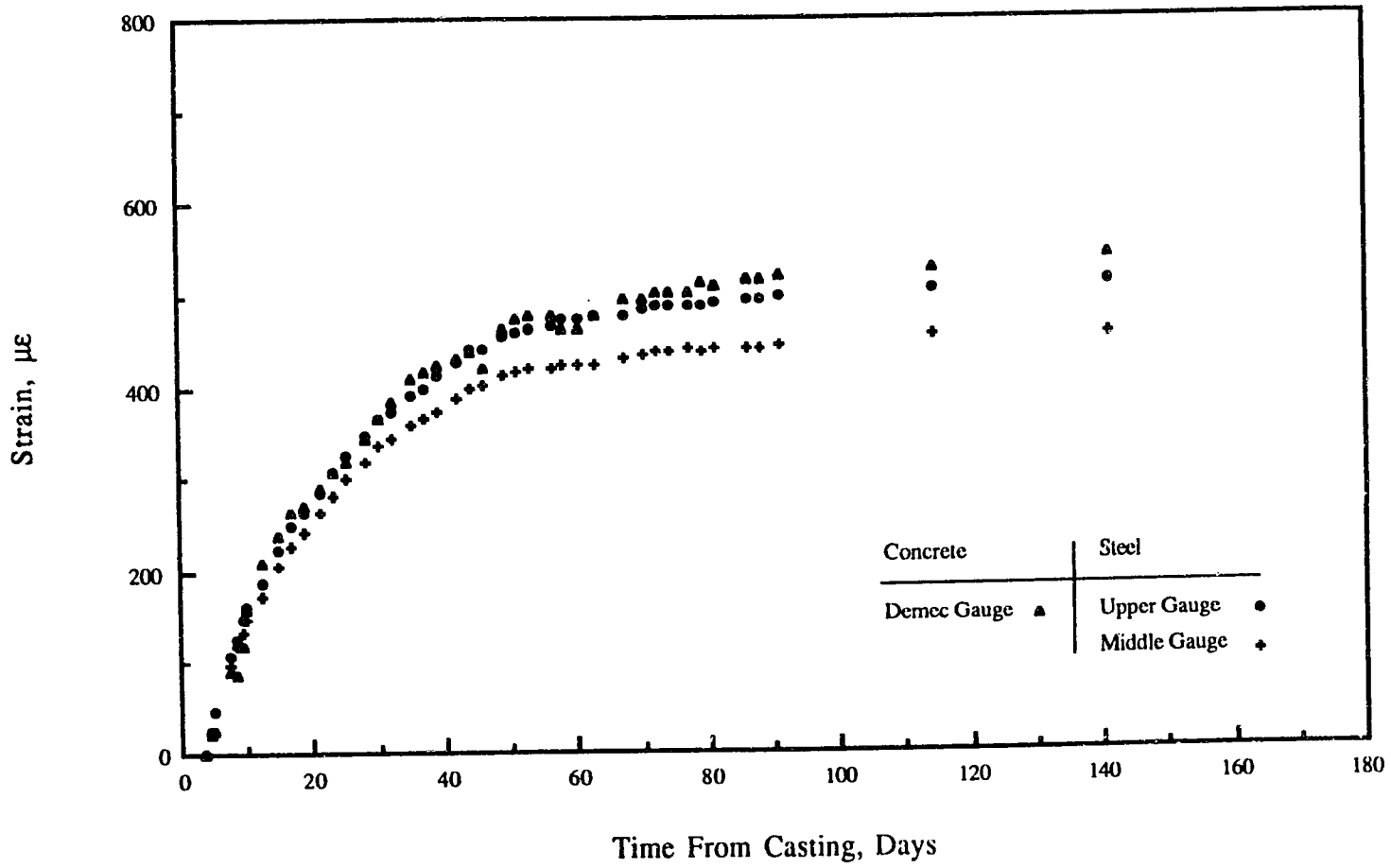

Fig. 5.19 Development of Shrinkage Strains at Mid Length with Time, Specimen 2151

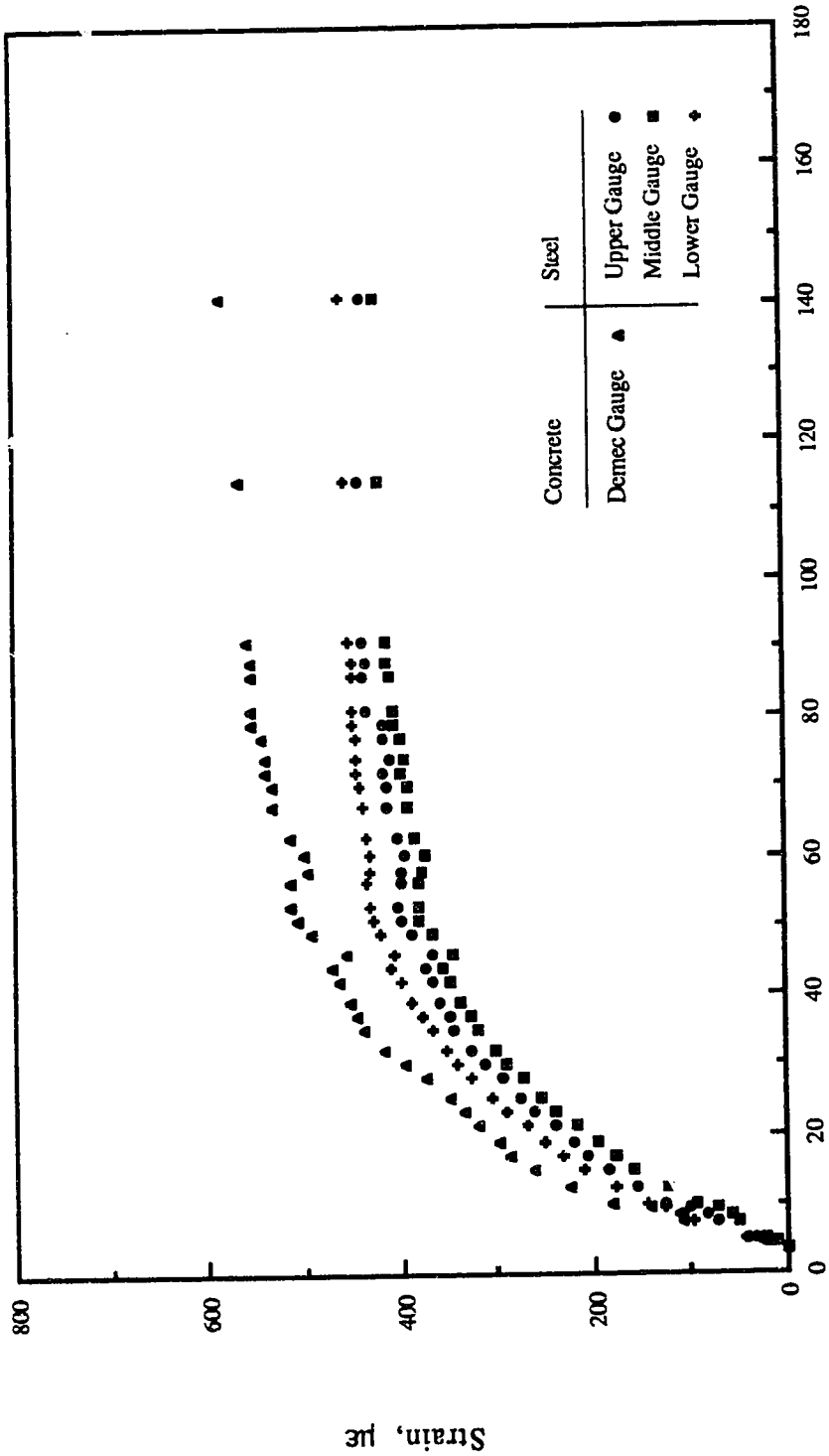

Fig. 5.20 Development of Shrinkage Strains at Mid Length with Time, Specimen 2152

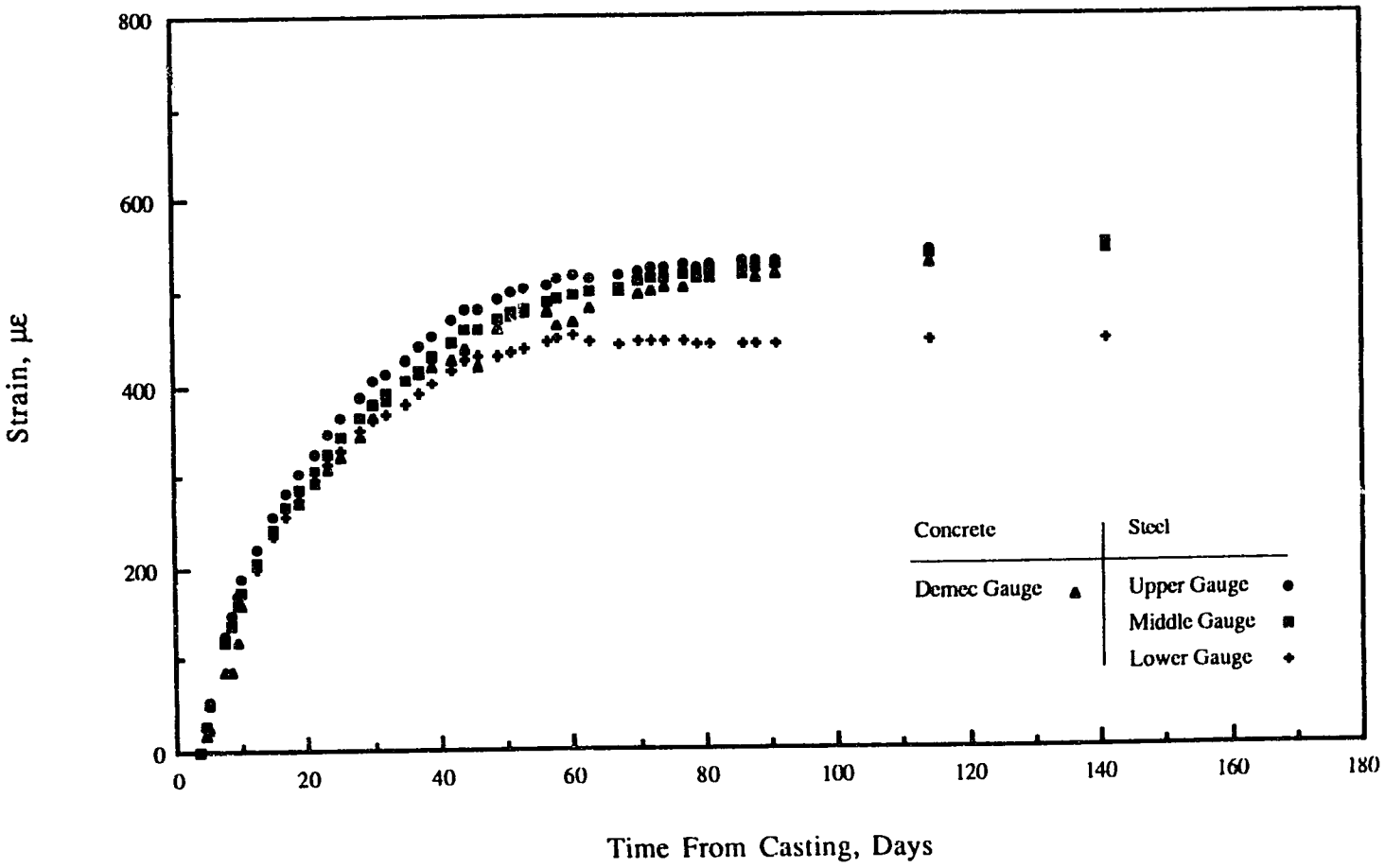

Fig. 5.21 Development of Shrinkage Strains at Mid Length with Time, Specimen 2153

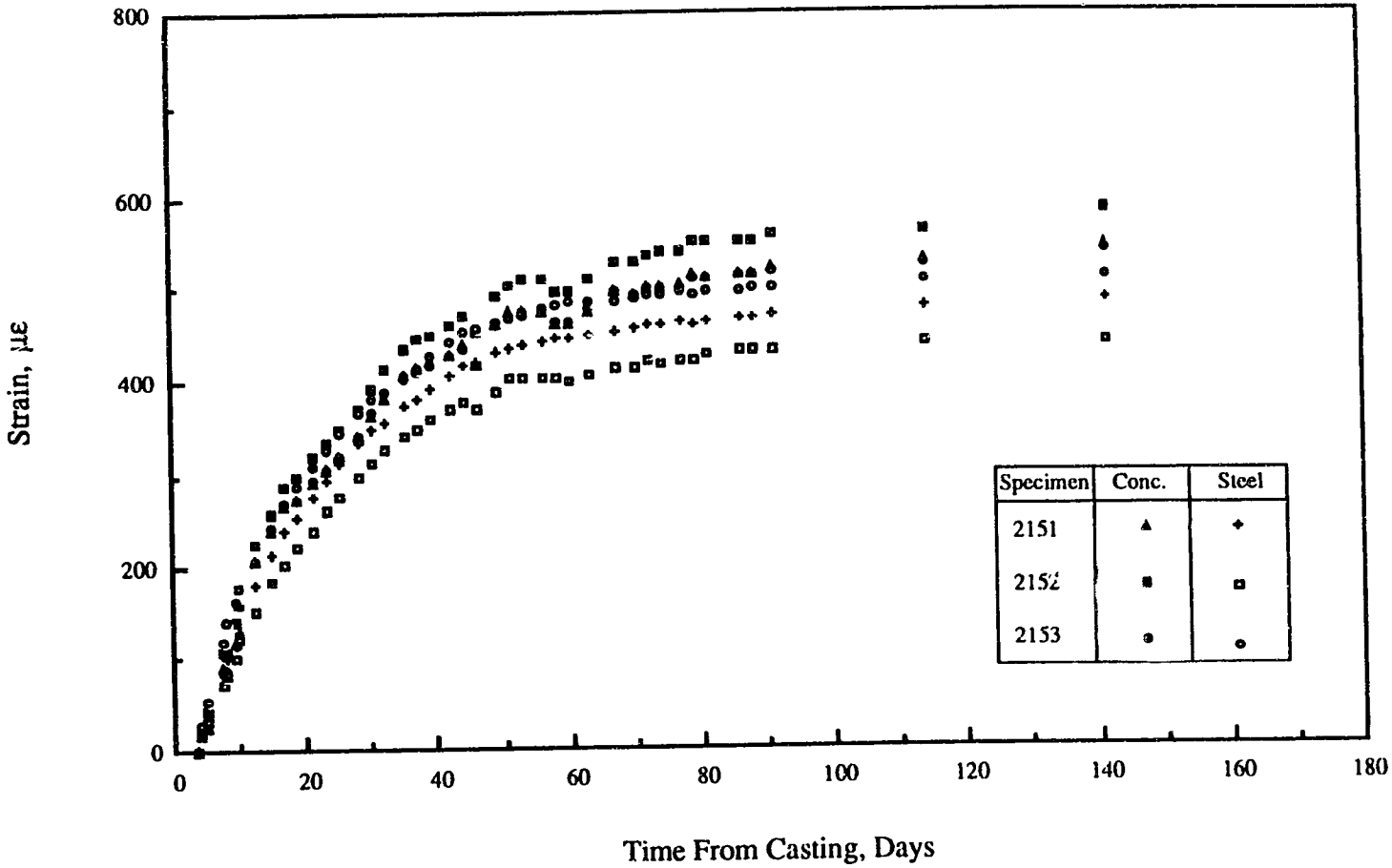

Fig. 5.22 Development of Average Shrinkage Strains at Mid Length with Time, Specimens 2151 to 2153

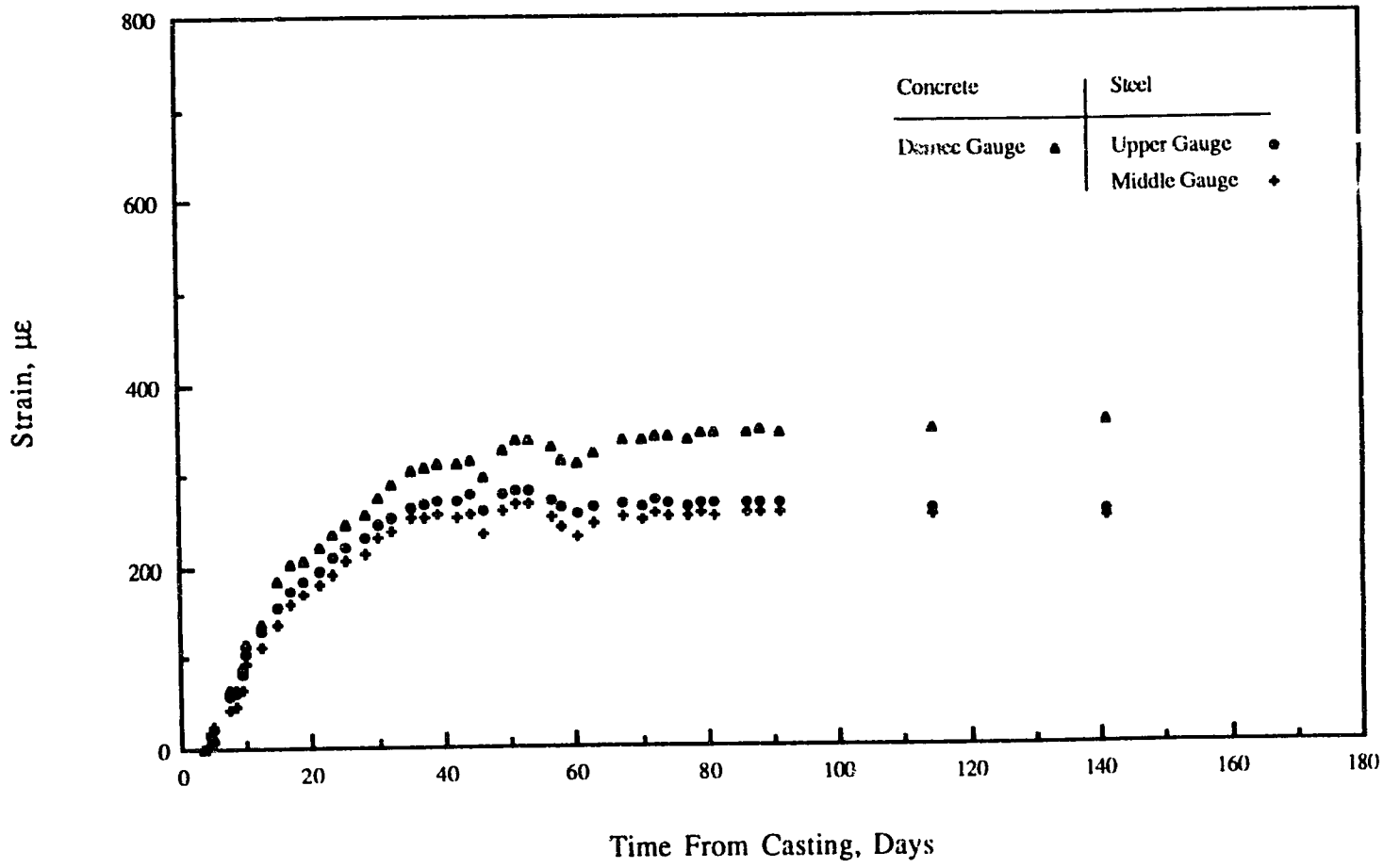

Fig. 5.23 Development of Shrinkage Strains at Mid Length with Time, Specimen 2251

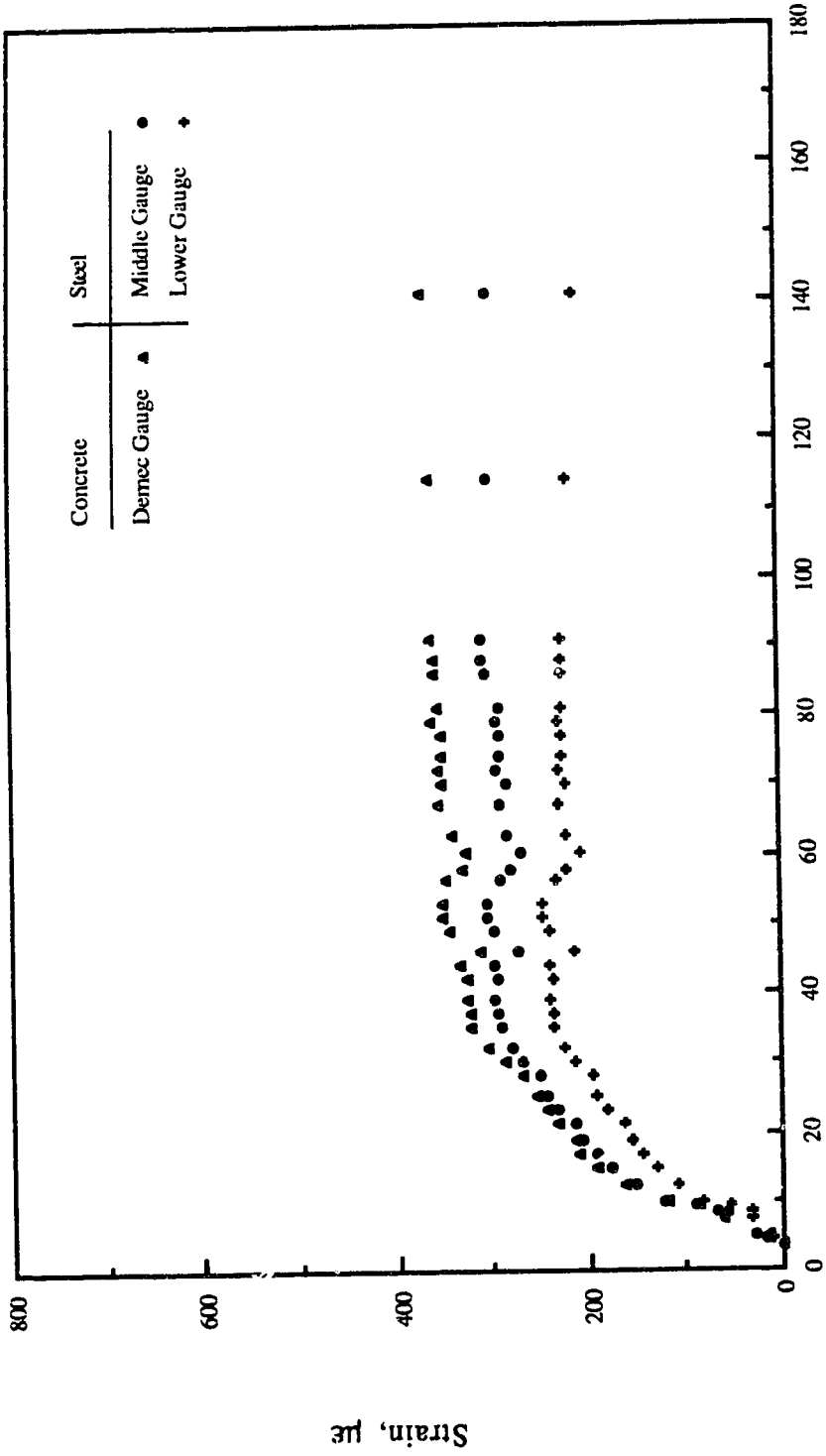

Fig. 5.24 Development of Shrinkage Strains at Mid Length with Time, Specimen 2252

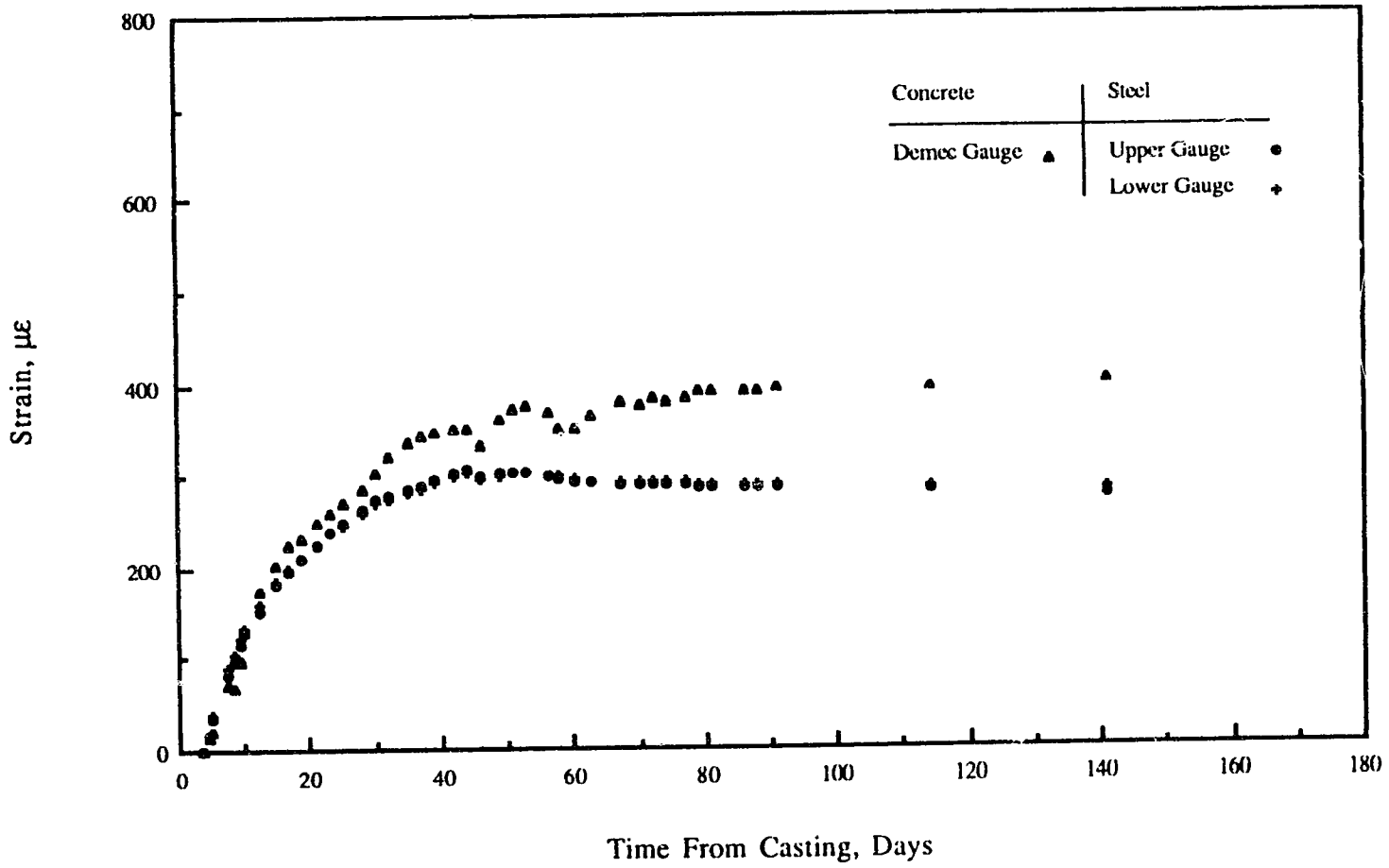

Fig. 5.25 Development of Shrinkage Strains at Mid Length with Time, Specimen 2253

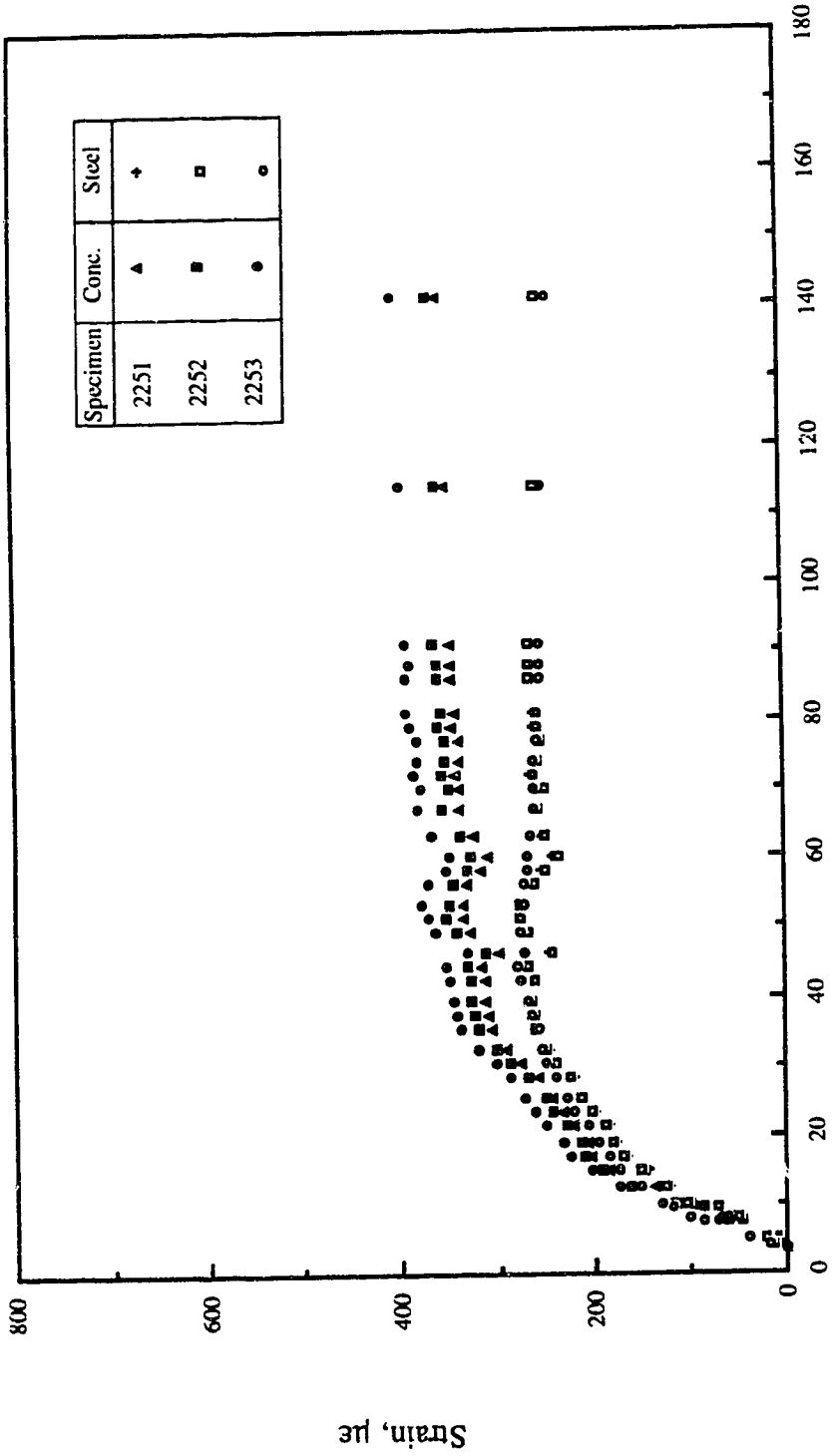

Fig. 5.26 Development of Average Shrinkage Strains at Mid Length with Time, Specimens 2251 to 2253

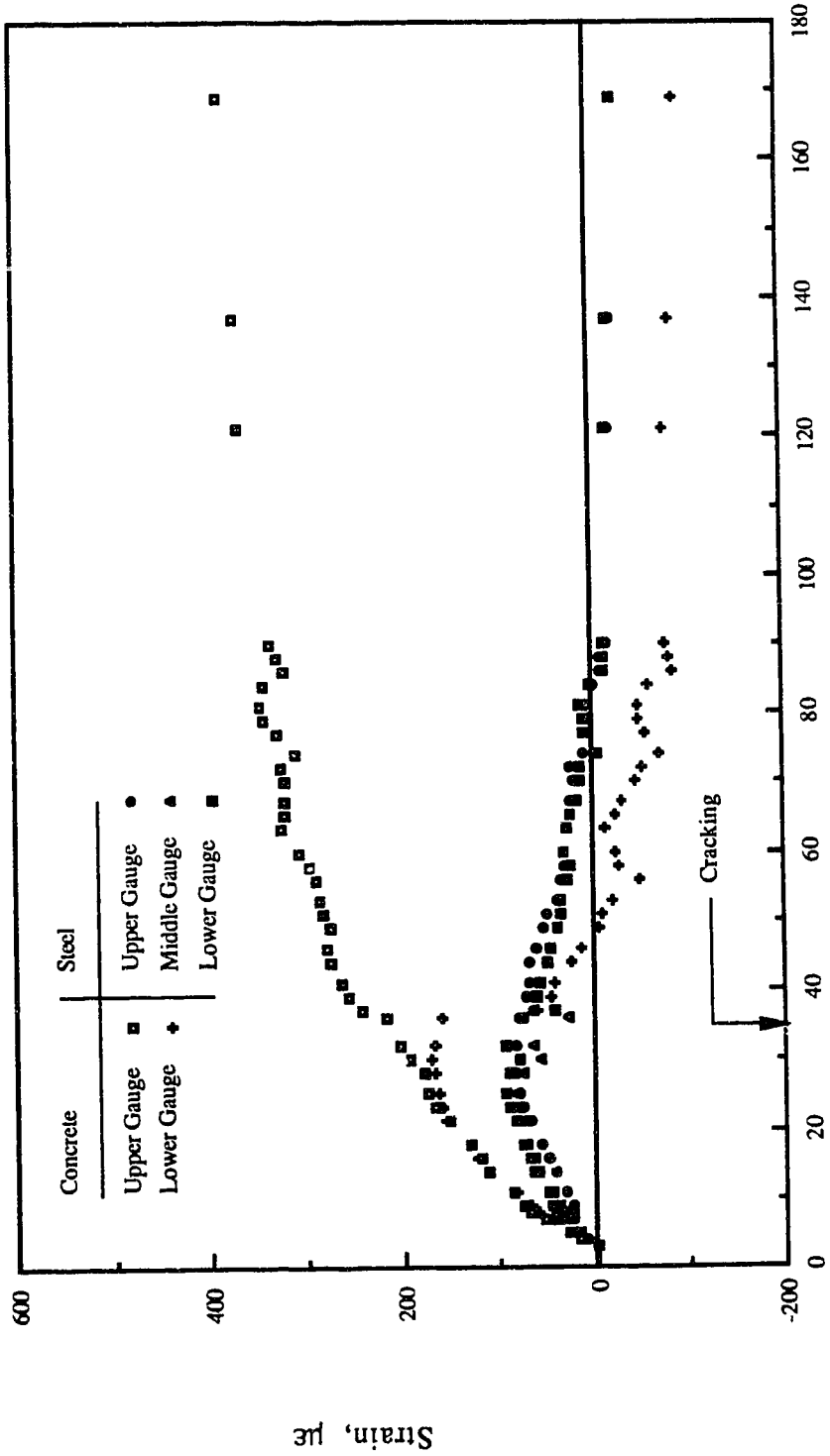

Fig. 5.27 Development of Shrinkage Strains at Mid Length with Time, Specimen 1351

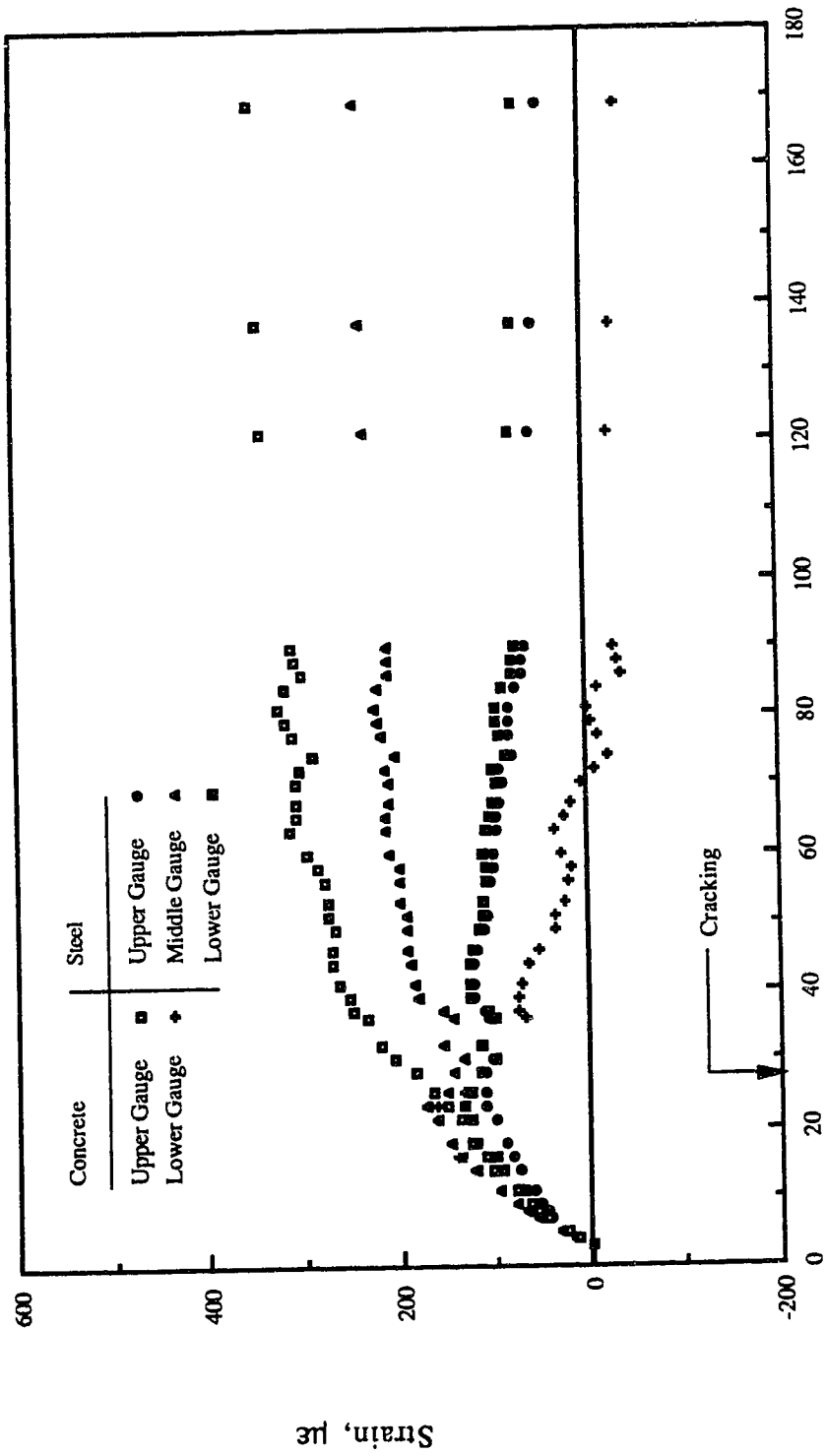

Fig. 5.28 Development of Shrinkage Strains at Mid Length with Time, Specimen 1352

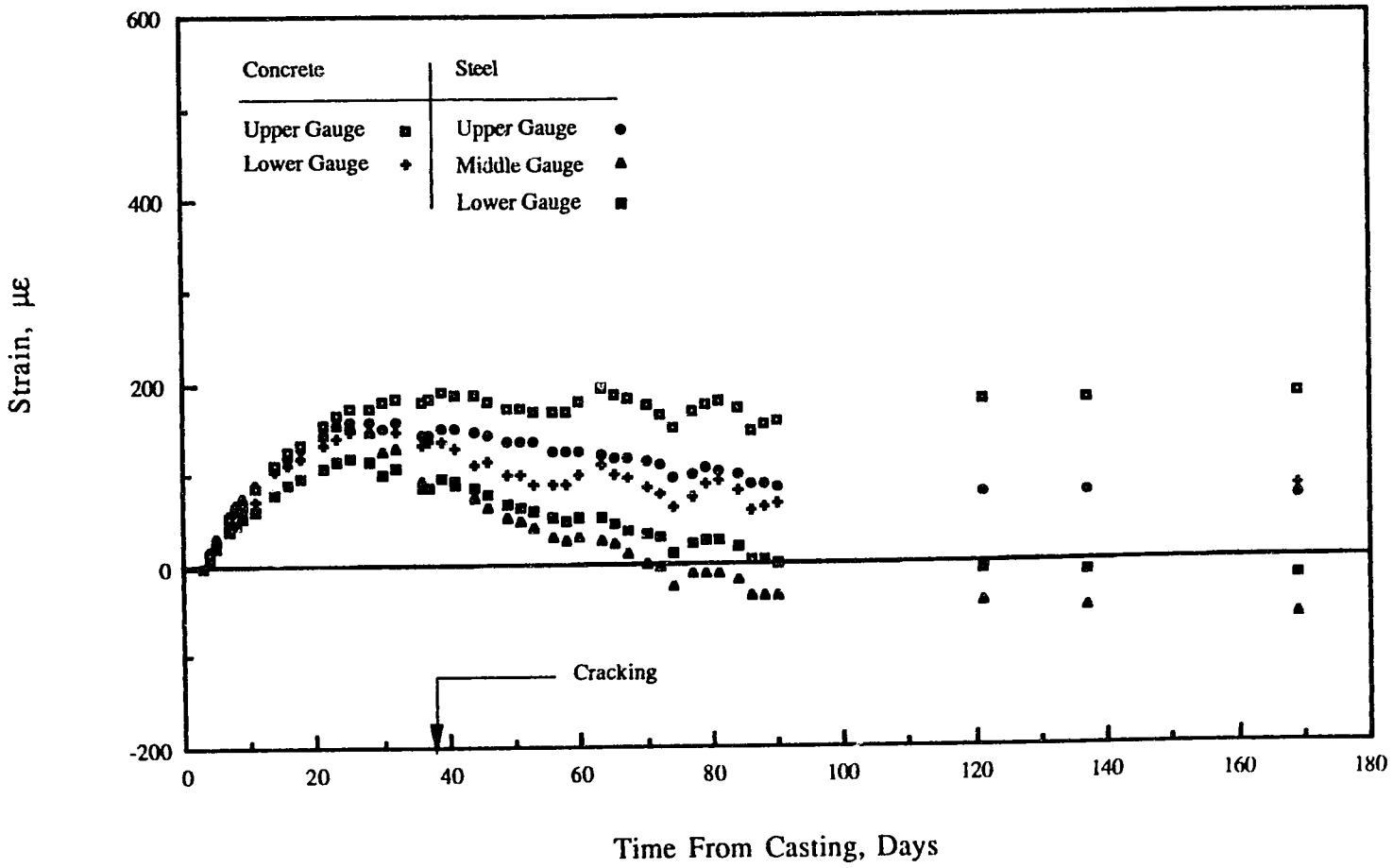

Fig. 5.29 Development of Shrinkage Strains at Mid Length with Time, Specimen 1353

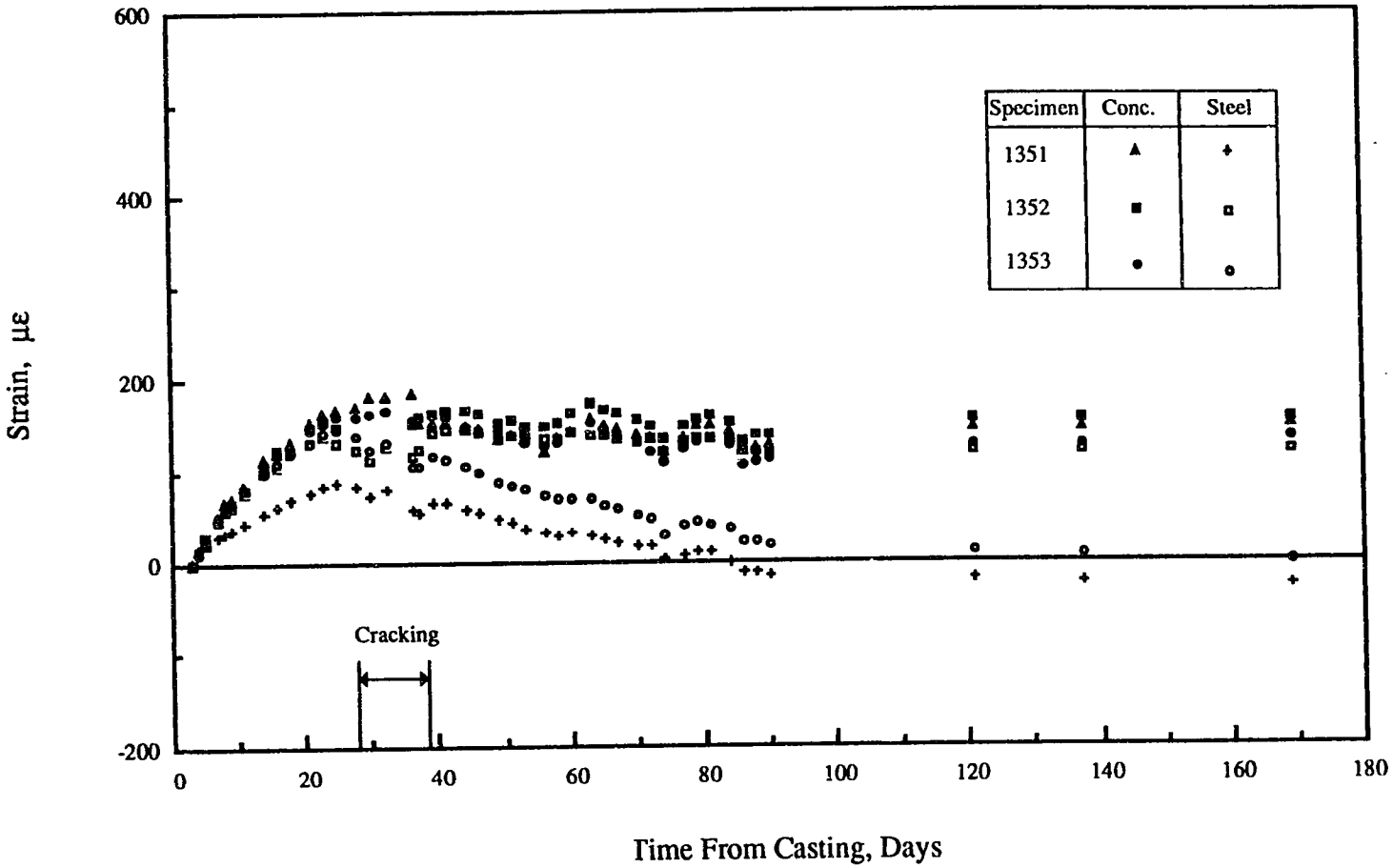

Fig. 5.30 Development of Average Shrinkage Strains at Mid Length with Time, Specimens 1351 to 1353

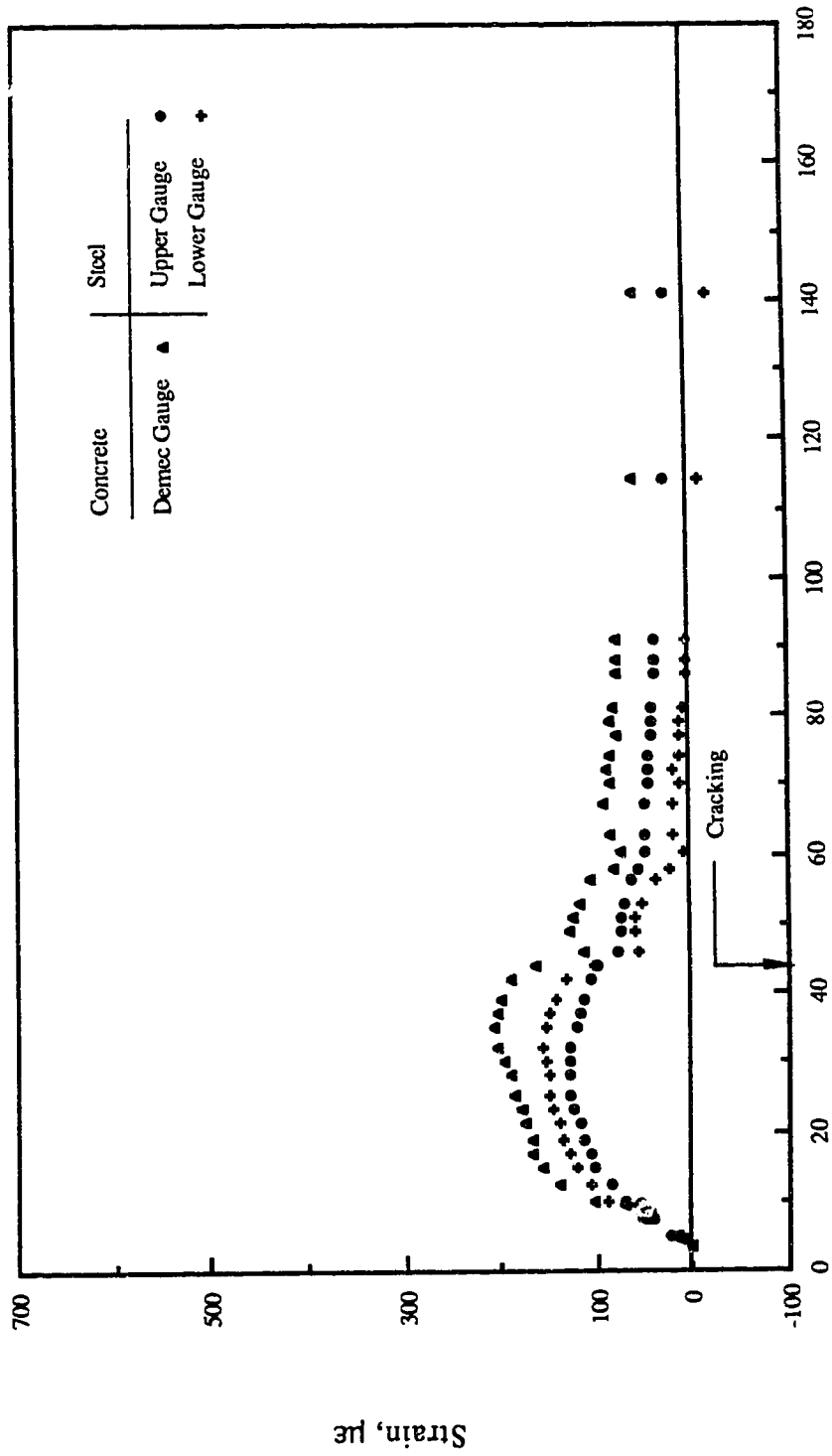

Fig. 5.31 Development of Shrinkage Strains at Mid Length with Time, Specimen 2351

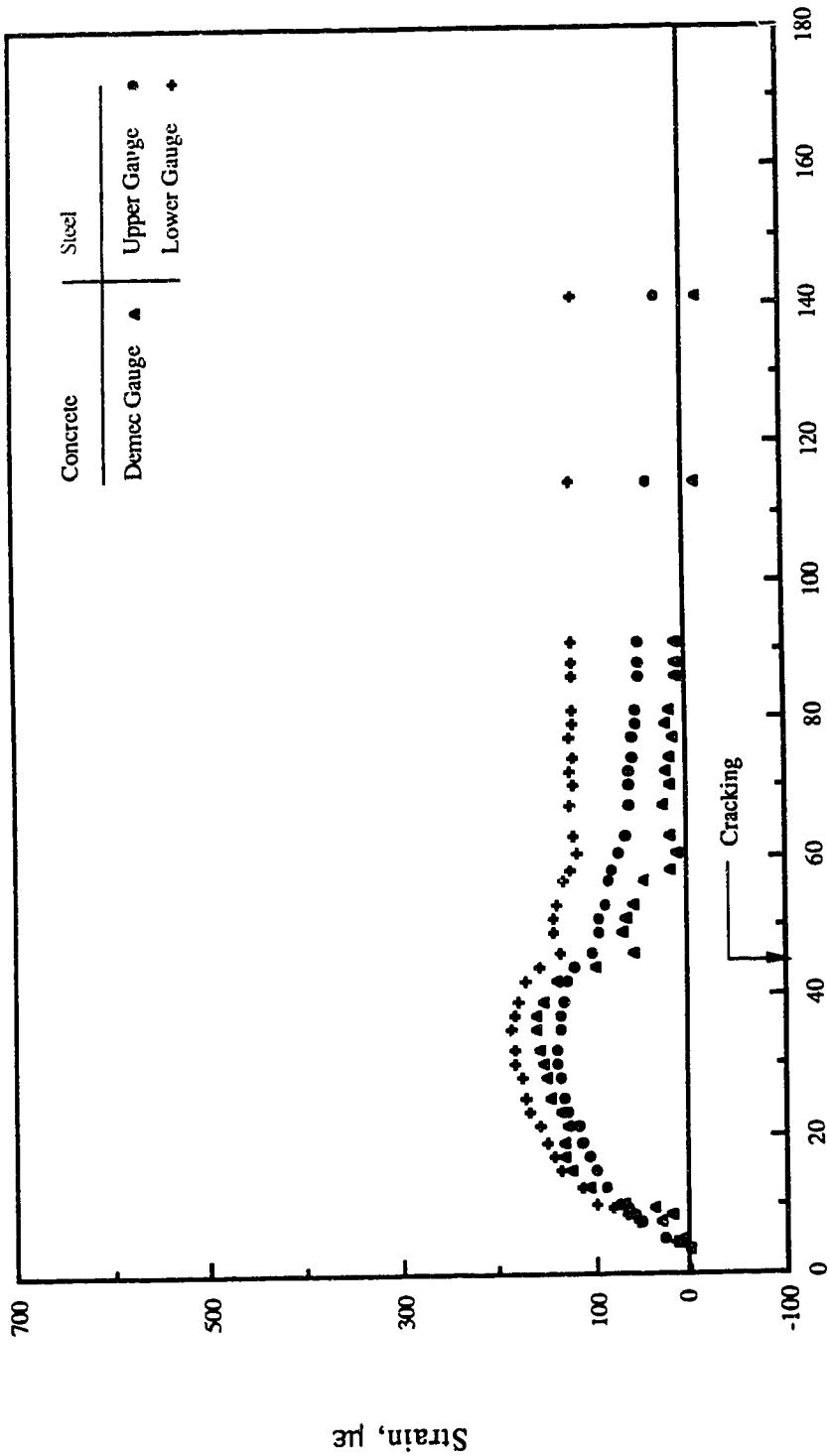

Fig. 5.32 Development of Shrinkage Strains at Mid Length with Time, Specimen 2352

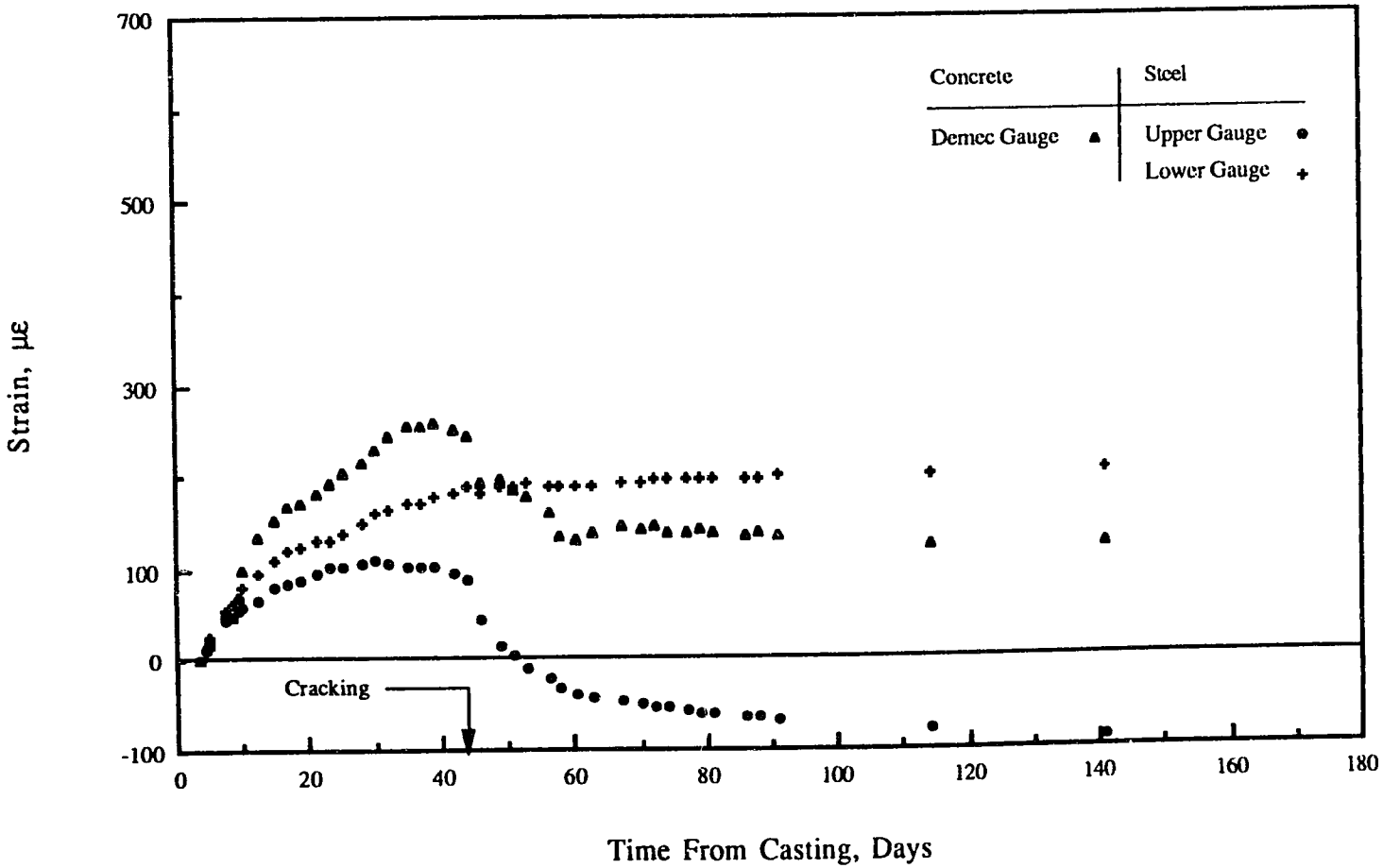

Fig. 5.33 Development of Shrinkage Strains at Mid Length with Time, Specimen 2353

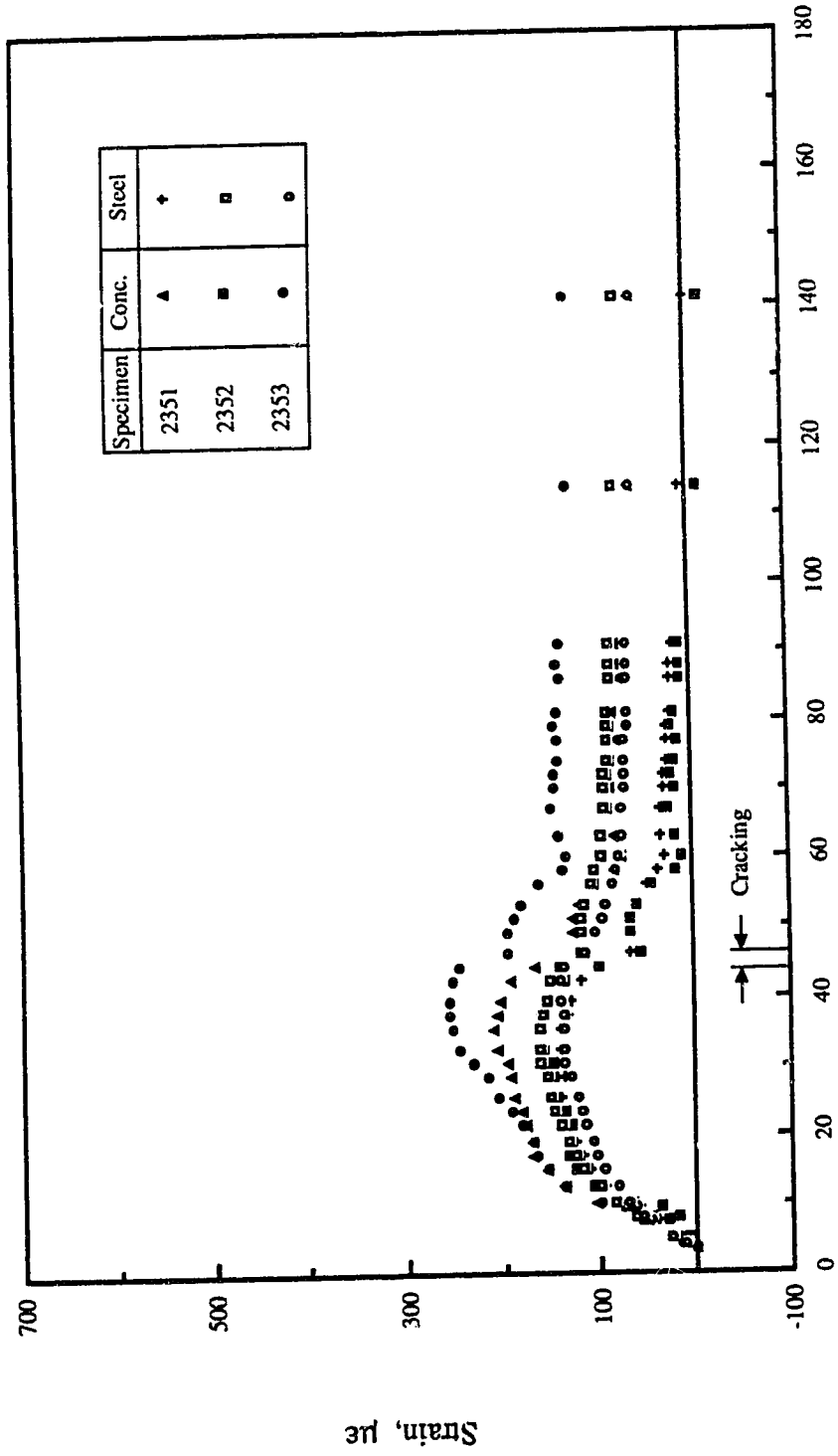

Fig. 5.34 Development of Average Shrinkage Strains at Mid Length with Time, Specimens 2351 to 2353

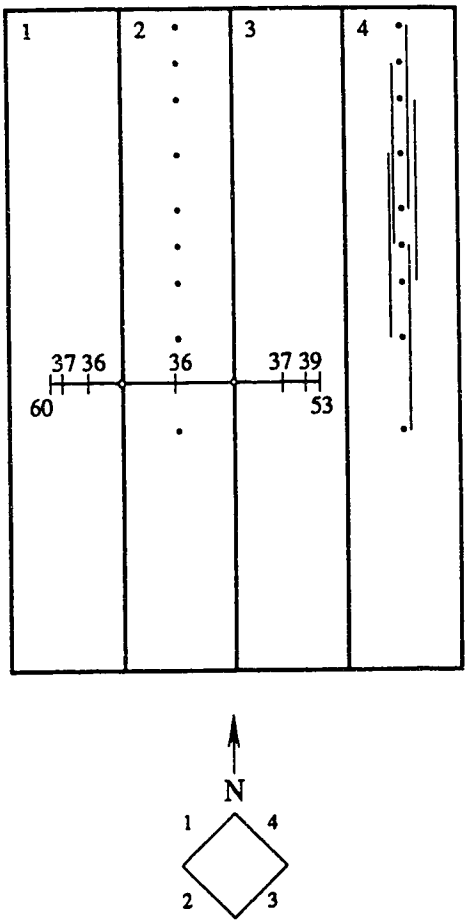

Fig. 5.35 Crack Development on Specimen 1351

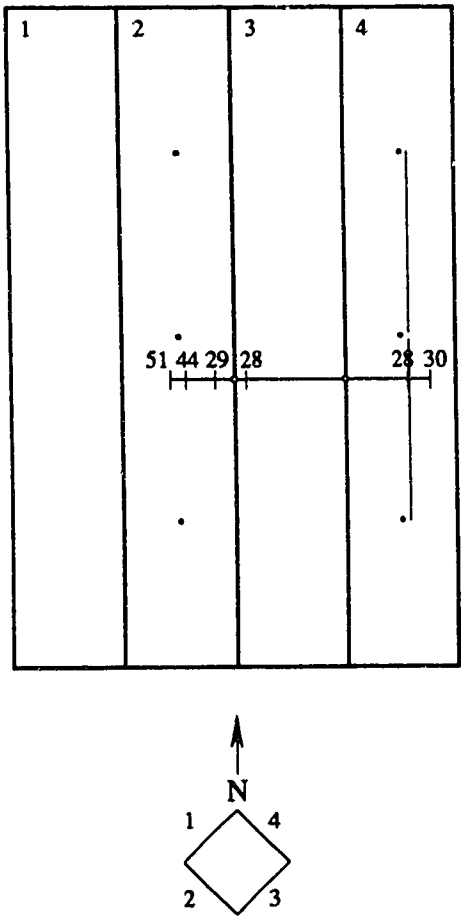

Fig. 5.36 Crack Development on Specimen 1352

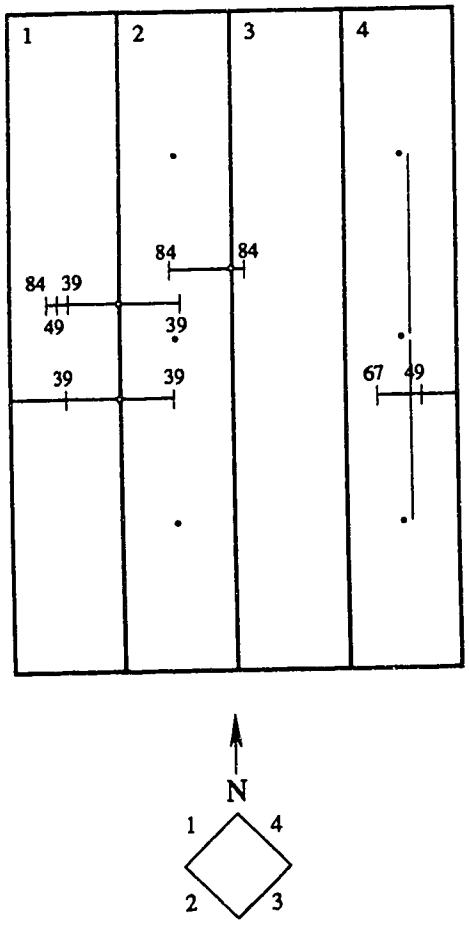

Fig. 5.37 Crack Development on Specimen 1353

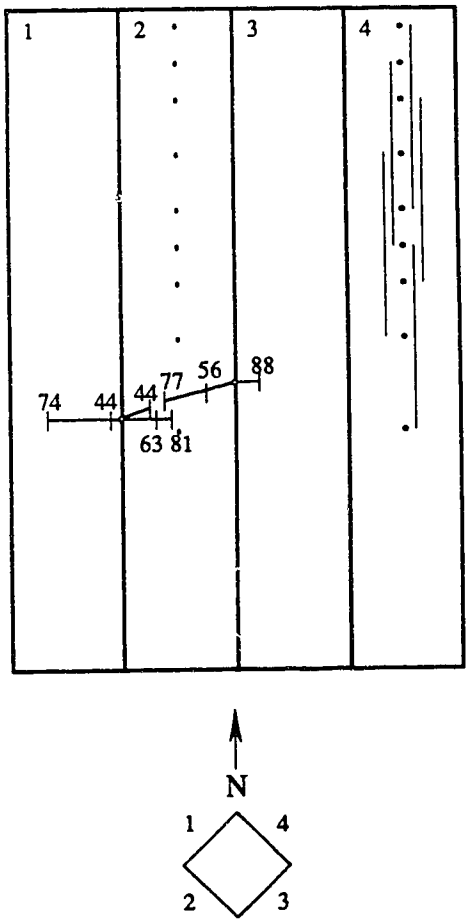

Fig. 5.38 Crack Development on Specimen 2351

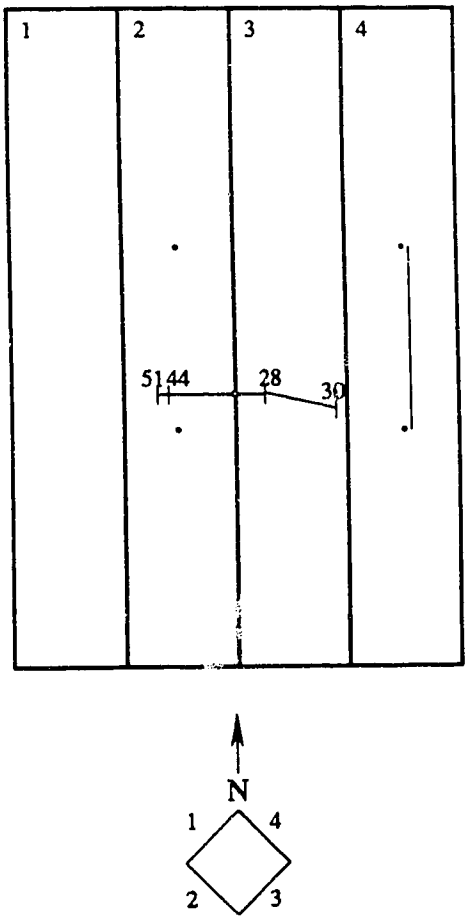

Fig. 5.39 Crack Development on Specimen 2352

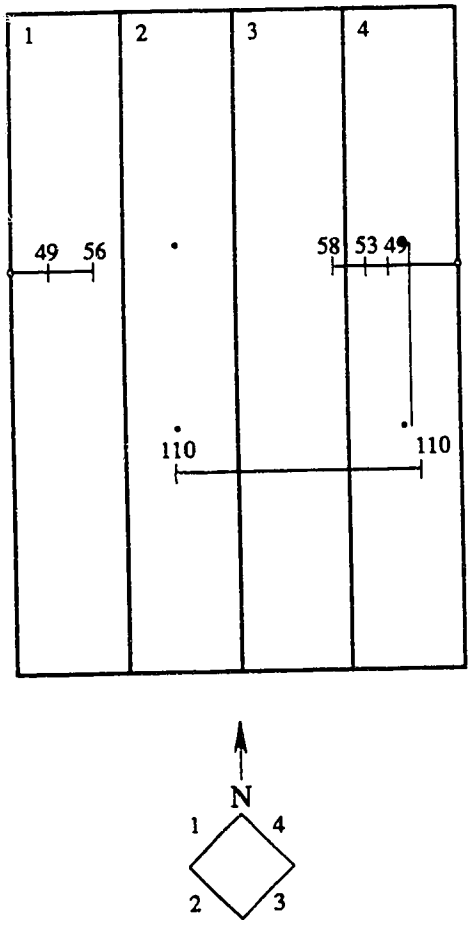

Fig. 5.40 Crack Development on Specimen 2353

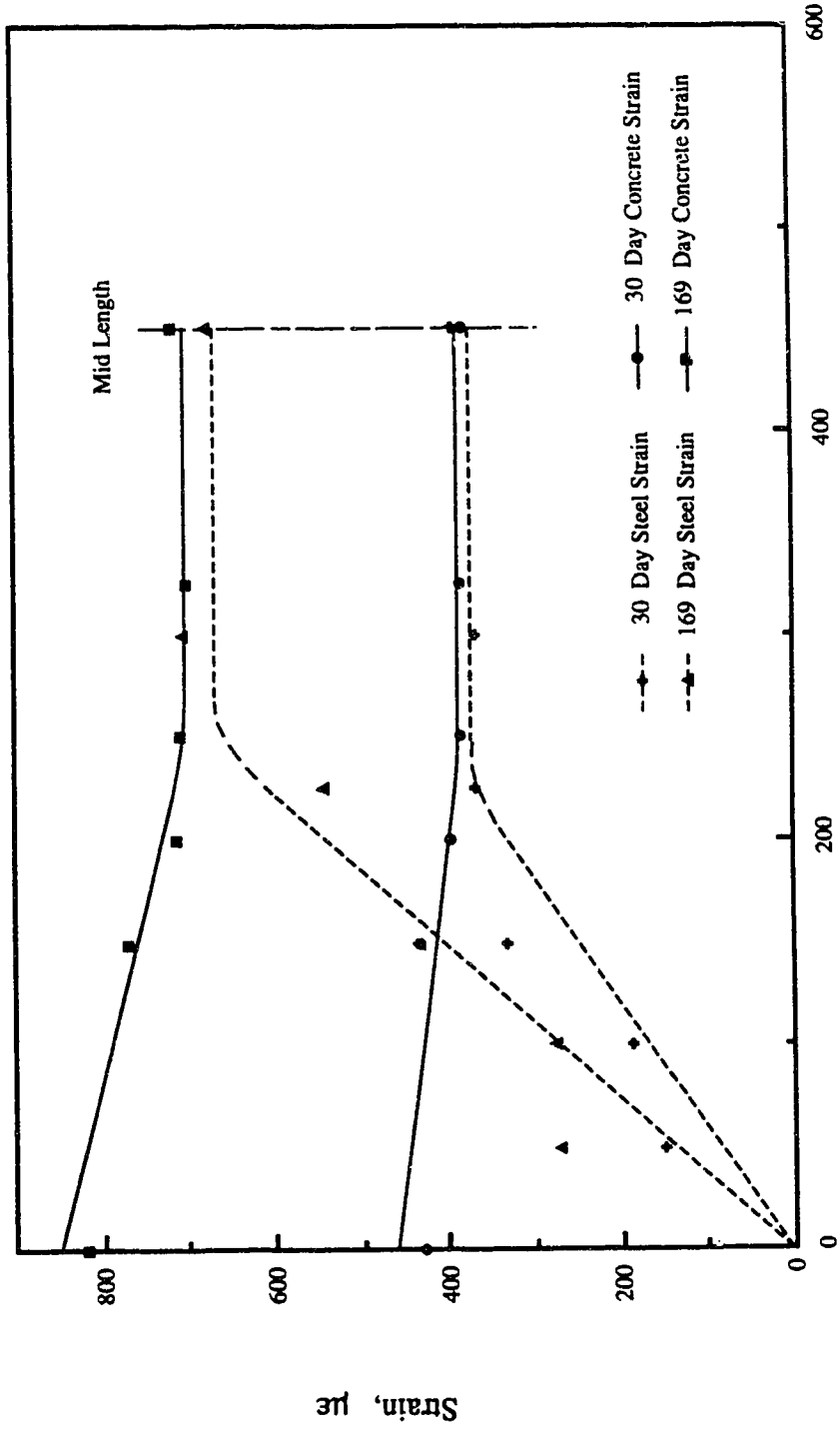

Fig. 5.41 Development of Shrinkage Strains Along Length, Specimen 1101

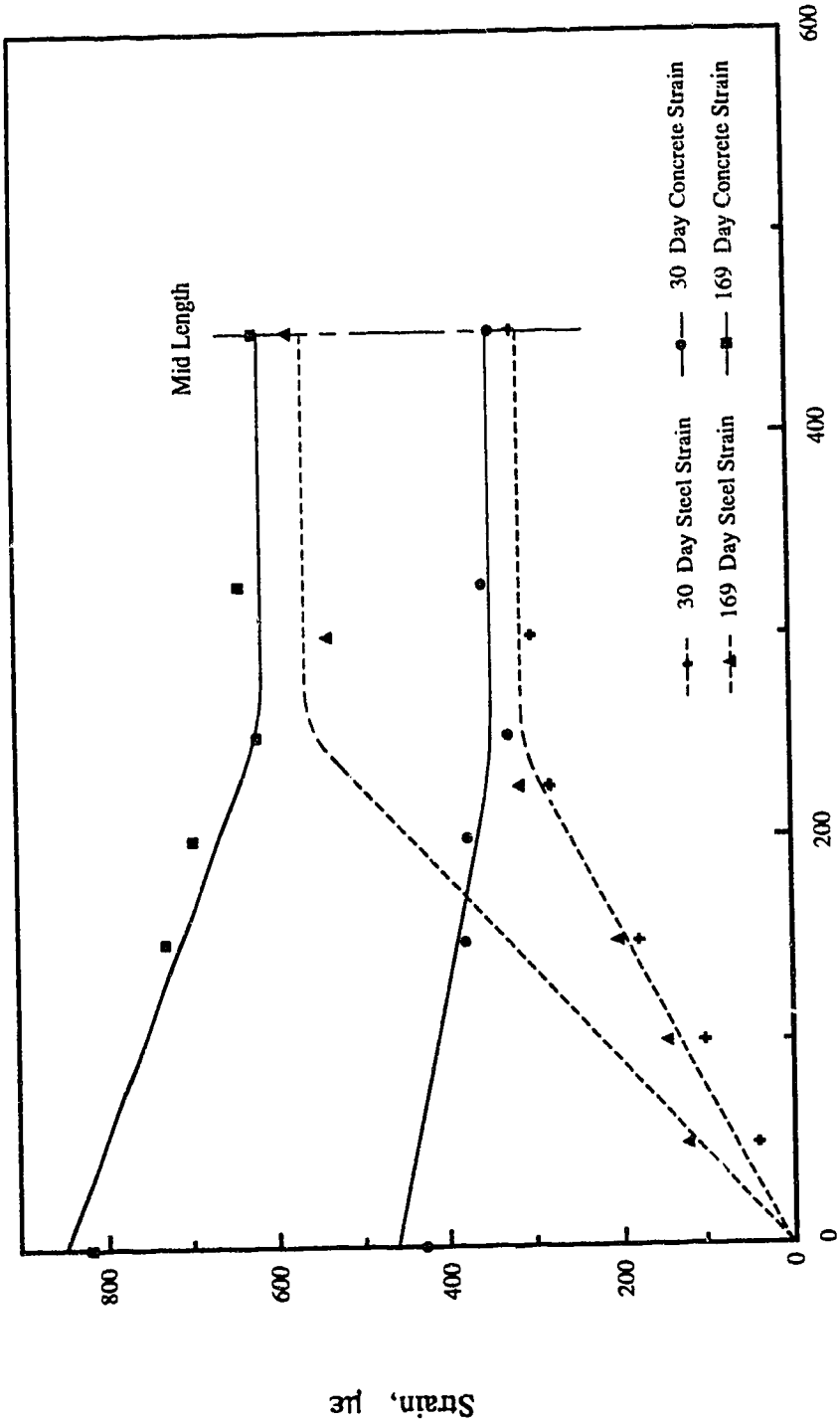

Fig. 5.42 Development of Shrinkage Strains Along Length, Specimen 1151

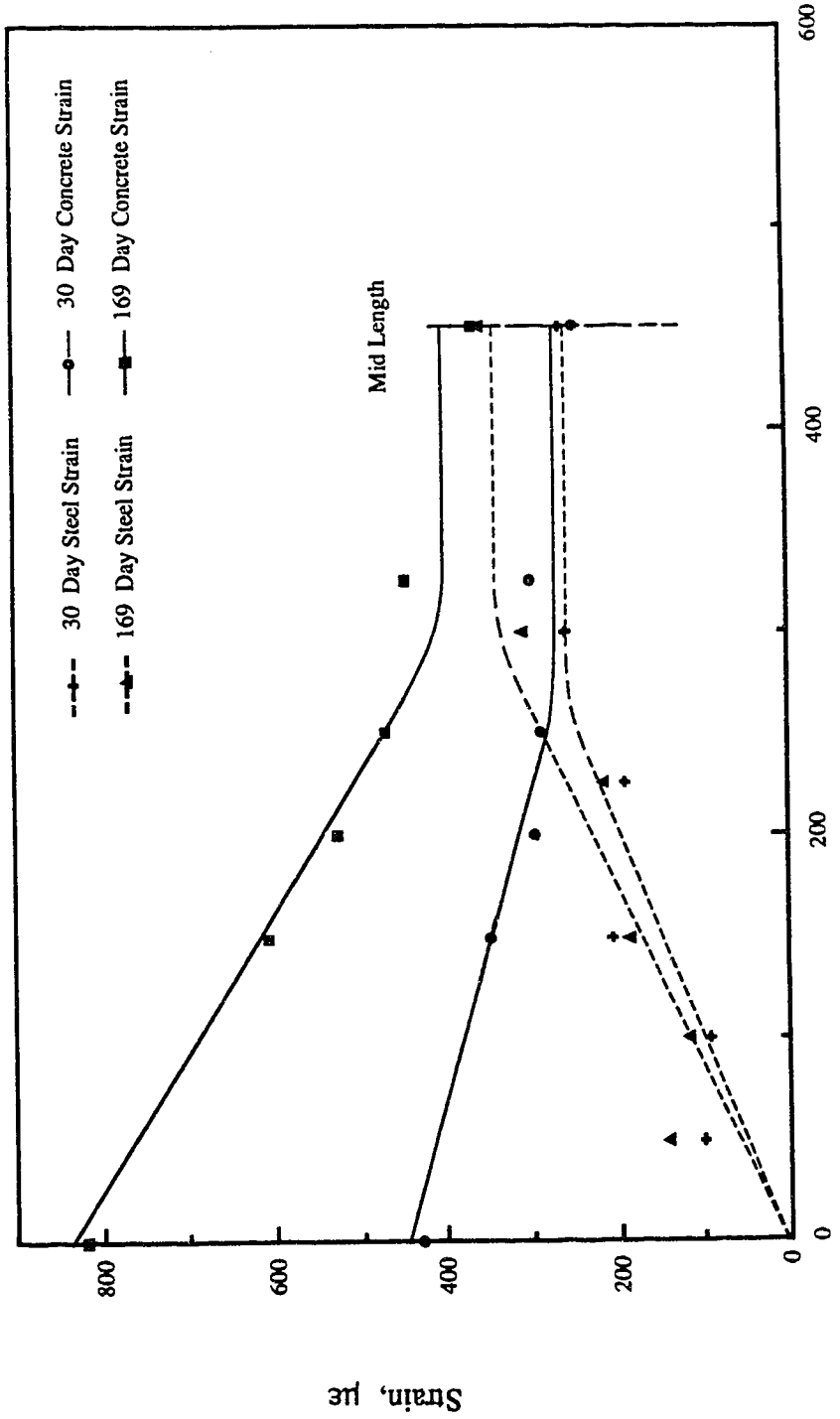

Fig. 5.43 Development of Shrinkage Strains Along Length, Specimen 1251

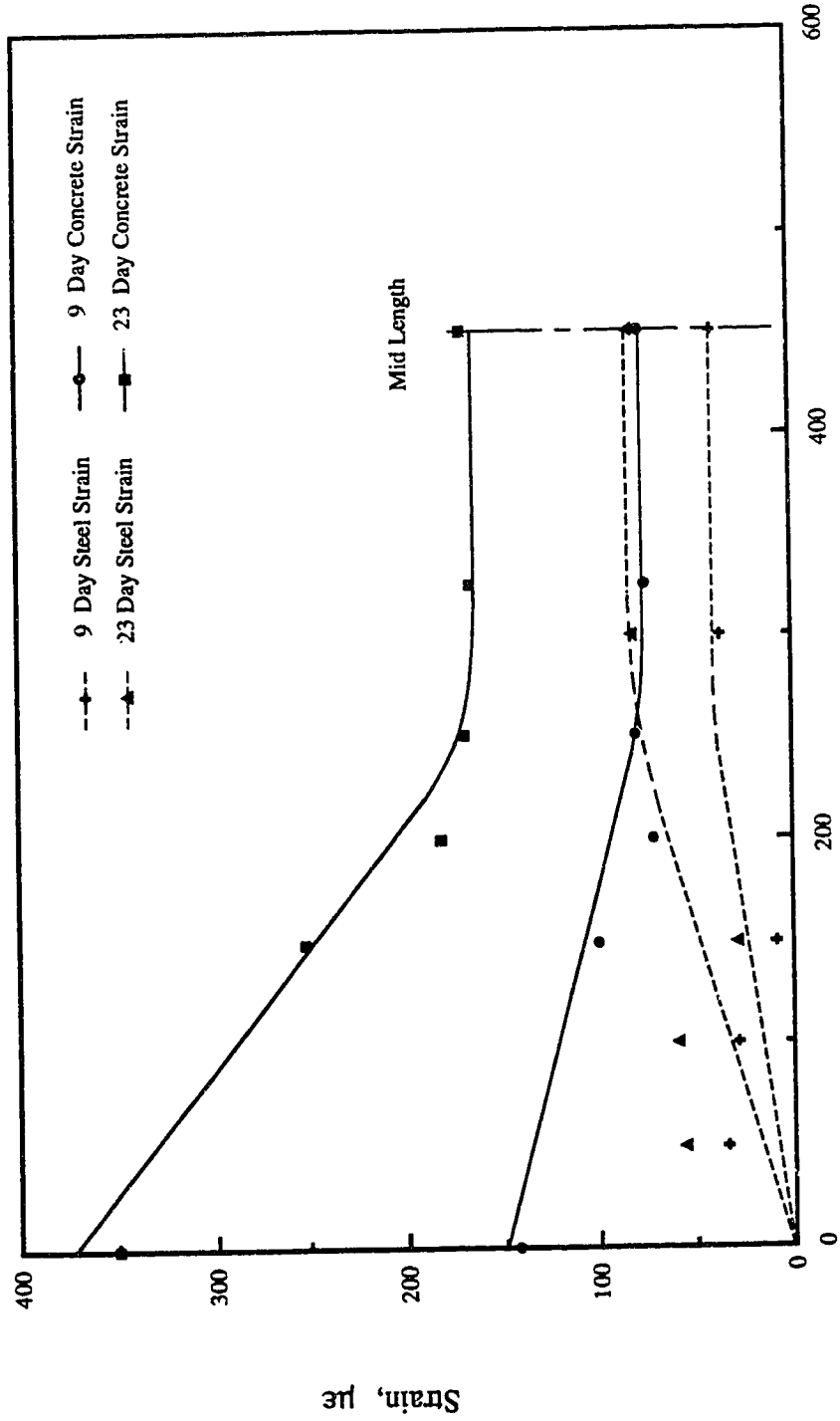

Fig. 5.44 Development of Shrinkage Strains Along Length, Specimen 1351

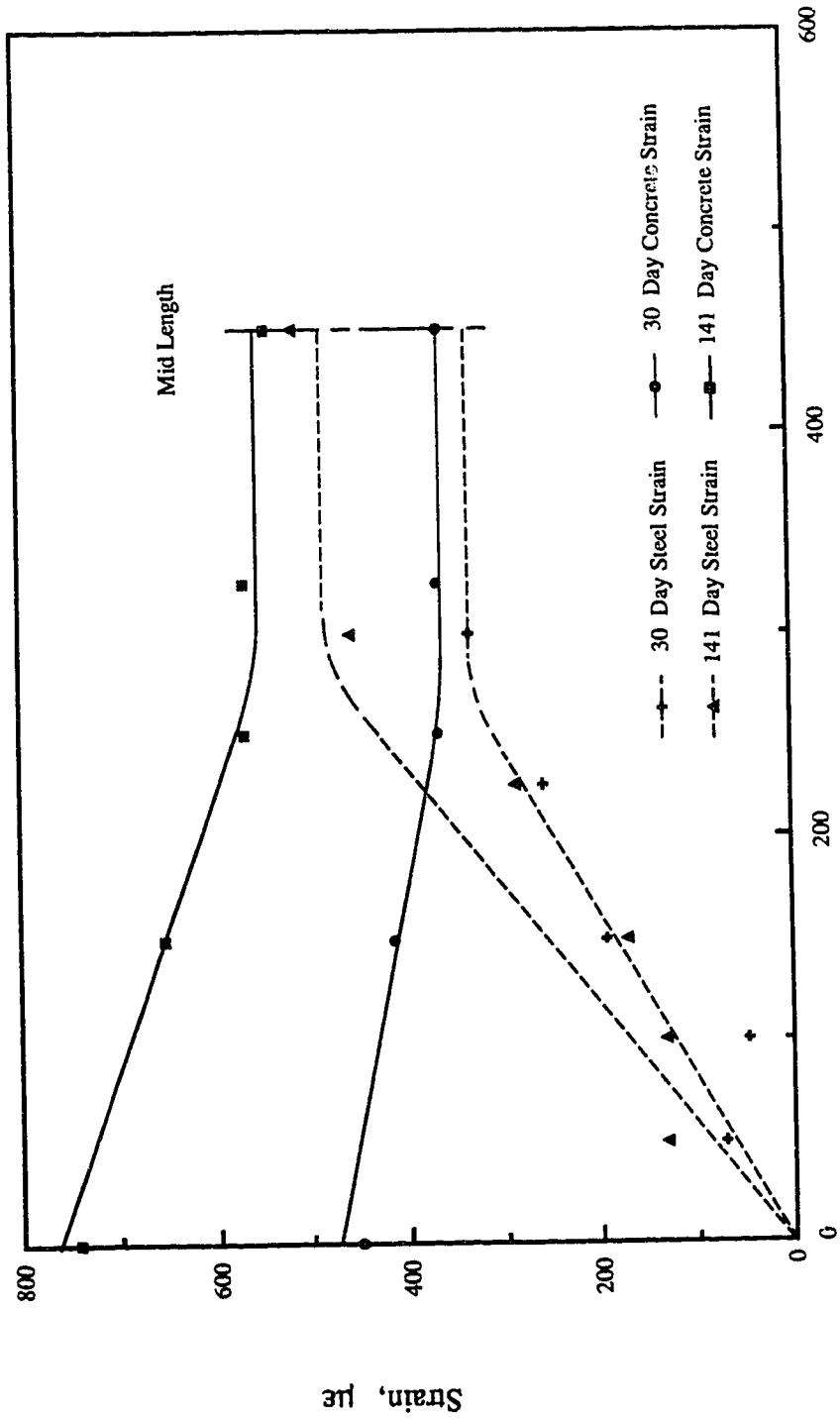

Fig. 5.45 Development of Shrinkage Strains Along Length, Specimen 2151

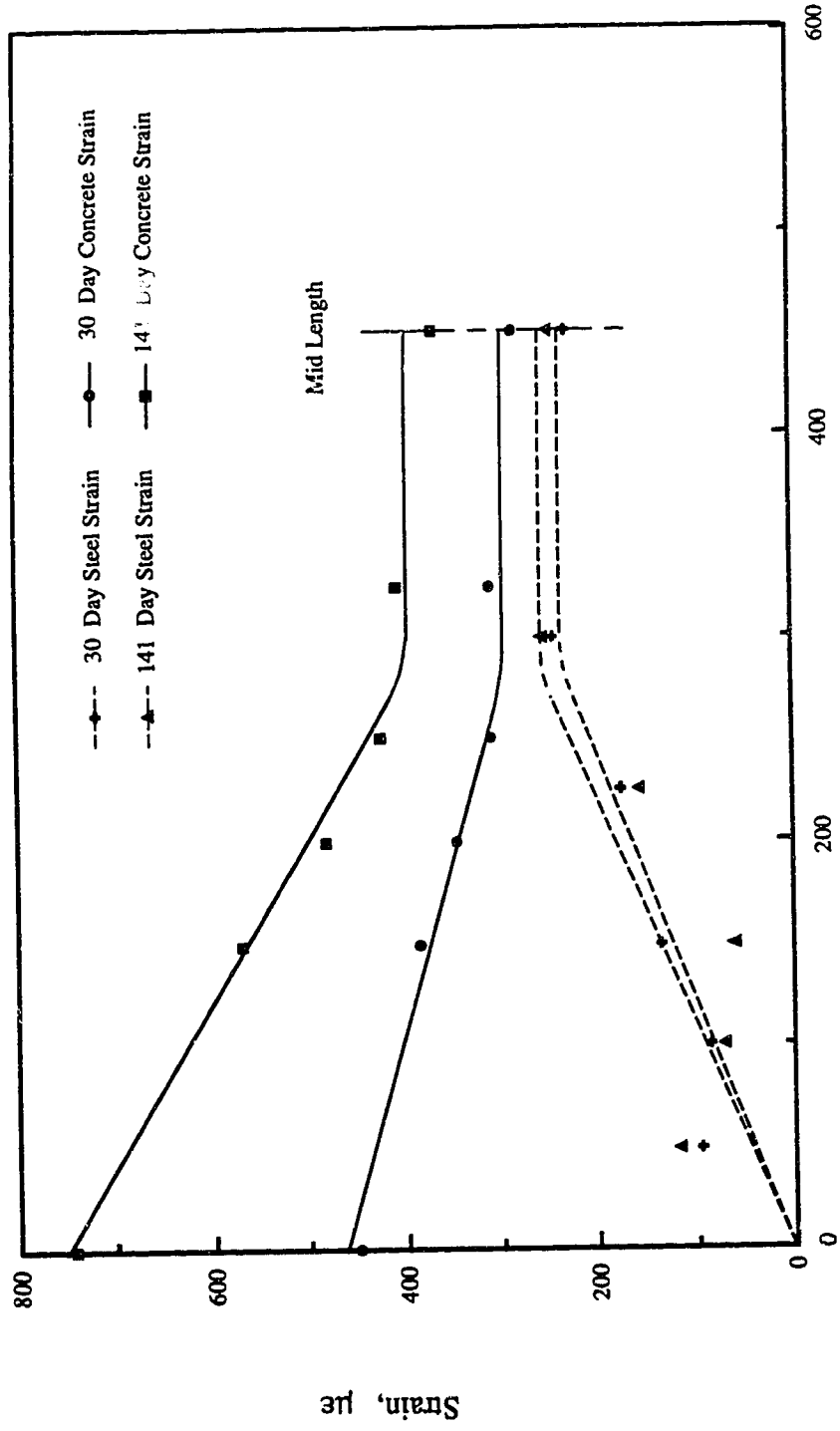

Fig. 5.46 Development of Shrinkage Strains Along Length, Specimen 2251

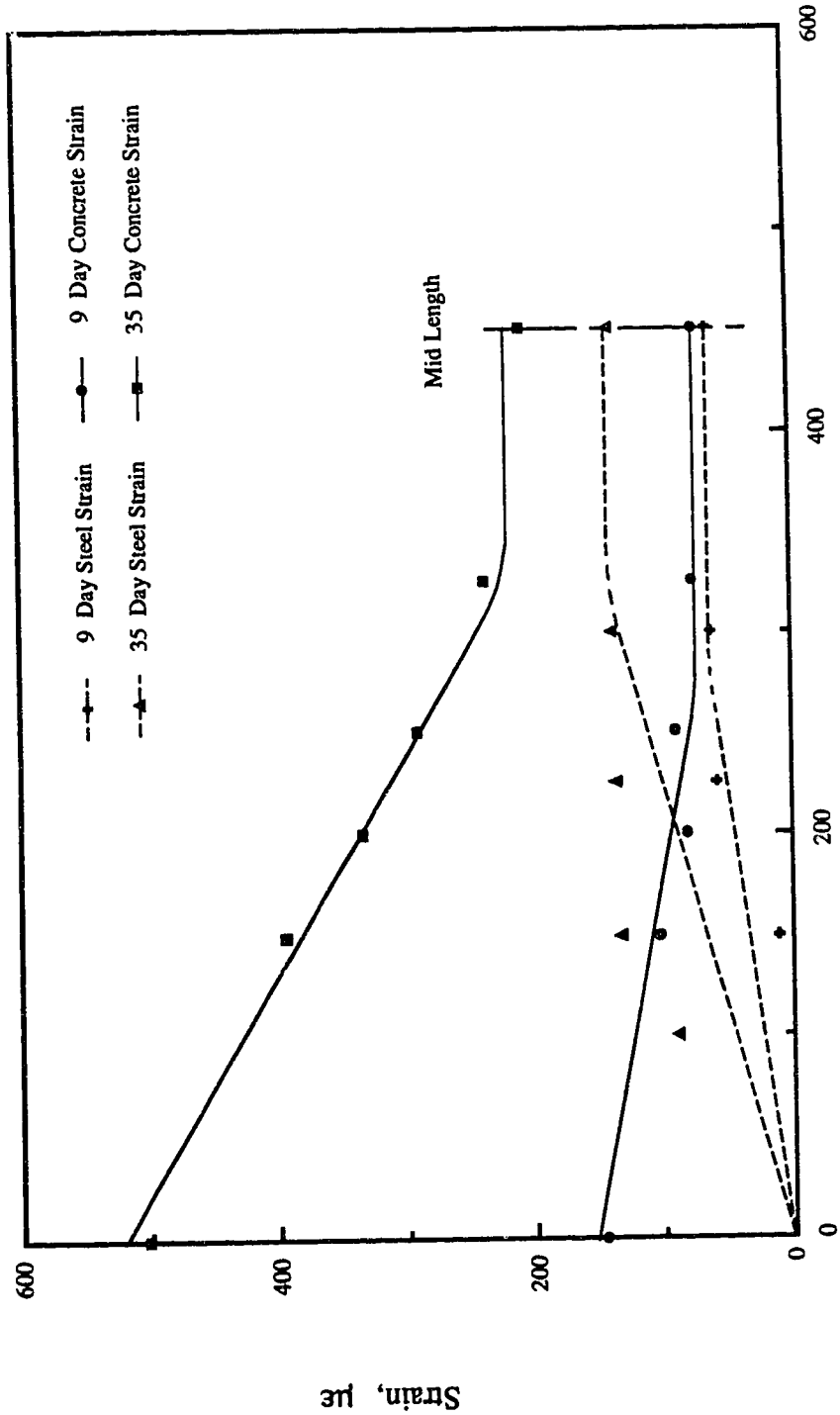

Fig. 5.47 Development of Shrinkage Strains Along Length, Specimen 2351

Chapter 6

ANALYSIS OF TEST RESULTS

6.1 Shrinkage Strains in Plain Concrete Specimens

Consider a plain or unreinforced concrete specimen in a drying atmosphere. The surfaces of the specimen dry first and a moisture gradient develops in the specimen. The dashed line in the strain diagram of Fig. 6.1(a), drawn for a unit length of the specimen where conditions are uniform, shows the resulting strains, assumed to vary linearly, that would occur if the adjacent elemental layers of concrete were free to shrink independently. Because the adjacent layers of concrete are conjoined one with another, the inner layers restrain the outer layers. Consequently, tensile strains develop in the outer layers and compressive strains develop in the inner layers. The accompanying self equilibrating stresses would be expected to vary in a manner consistent with the strains developed as shown in Fig. 6.1(b). In small specimens the moisture gradient will eventually dissipate leading to uniform shrinkage across the specimen and the disappearance of the shrinkage stresses. Thus in early stages of shrinkage, a plain concrete specimen actually restrains itself. As concrete shrinkage strains can conveniently only be measured on the surface, the recorded strains, ε_f, may therefore, in effect, be considered restrained shrinkage strains.

In Figs. 6.2 and 6.3 are plotted the average values of the free shrinkage strains obtained from the 3 unreinforced specimens of each of mixes 1 and 2 respectively versus time.

An exponential equation of the form

[6.1] $$\varepsilon_f = \varepsilon_u (1 - e^{-\alpha t})$$

was attributed to Ulitskii (1962) by Neville (1970) to describe the development of the unrestrained shrinkage with time.

Equation [6.1] was rectified and regression analyses were carried out to determine the best values of α and ε_u for both mixes. The calculated values of α and ε_u based on the entire observation period give,

[6.1a] $$\varepsilon_f = 855 (1 - e^{-0.0245 t}) \quad \text{and}$$

[6.1b] $$\varepsilon_f = 748 (1 - e^{-0.0323 t})$$

for mixes 1 and 2 respectively. These equations are plotted on the corresponding figures.

Using the test results and [2.2] as suggested by Branson, ε_u was calculated at different times and its average value was taken as the ultimate unrestrained shrinkage strain. The calculated values of ε_u were 1000 $\mu\varepsilon$ for mix 1 and 995 $\mu\varepsilon$ for mix 2. These values were used in [2.2] and are plotted for both mixes in Figs. 6.1 and 6.2 as is [2.2] using the value of 800 $\mu\varepsilon$ for the ultimate unrestrained shrinkage strain as suggested by the ACI (1982) when no test data are available.

These figures show that the exponential functions fit the test data closely, that using [2.2] with values of ε_u calculated according

to Branson would tend to overestimate the shrinkage strains for extended time periods and that using 800 $\mu\varepsilon$ for ε_u underestimates them, at least during the observation period.

However, in many cases shrinkage data cannot be collected over long time periods and reasonable values of the ultimate shrinkage strain are needed to be predicted from shrinkage measurements over relatively short time periods of about 28 days. Using [6.1] and the same procedure described previously, values of α and ε_u were calculated using shrinkage measurements taken over different time periods from casting. The results are shown in Table 6.1 for both mixes. These data show that the predicted ultimate shrinkage, ε_u, increases and the value of α decreases as the observation period increases. In other words it becomes increasingly difficult to predict the ultimate shrinkage as the observation period decreases. Based on the tabulated data, the ultimate shrinkage predicted from 28 days of data should be increased by about 1/3.

6.2 Effect of Variables of Concrete Mix on Shrinkage

As only 2 mixes were investigated, with different 28 day compressive strengths and water contents, it is difficult to assess the effects of these variables on the measured shrinkage strains. Measured restrained and unrestrained shrinkage strains for both concrete mixes were of the same order of magnitude for corresponding specimens and the development of shrinkage strains followed the same pattern. The greater shrinkage of mix 1

could be attributed to its higher water content. The free shrinkage strain of mix 1 concrete at 140 days was 825 με, about 77 με higher than that of mix 2 concrete of 748 με.

6.3 Shrinkage Strains in Reinforced Concrete Specimens

Development of restrained shrinkage strains measured at the central portion of reinforced concrete specimens with time was similar to that of the free shrinkage strains. The free ends of a concrete prism reinforced by a central steel bar are unrestrained and undergo the free shrinkage strain. If the specimen is sufficiently long, a central portion of the specimen will be fully restrained. The length required to develop full restraint is called the development length. In this length, shear stresses must exist between the bar and the concrete and between adjacent elemental layers of concrete in order to develop the restraint.

Fig. 6.4 shows diagrammatically the variation of strains in the steel and concrete over a half length of the specimen. The steel strains increase from zero at the free end and, attaining a maximum value at the end of the development length, are constant over the remainder. Concrete strains start from the free shrinkage strain at the ends and reduce to the completely restrained shrinkage strain at the end of the development length. The difference between the concrete and the steel strain in the central portion is due to the moisture gradient across the specimen. At any point along the specimen, the vertical distance, $\varepsilon_f - \varepsilon_c$, represents the total tensile strain in the concrete including creep.

[6.2] $$\varepsilon_{ct} = \varepsilon_f - \varepsilon_c$$

The integration of the area between the steel and the concrete strain curves over the development length represents the relative displacement between the concrete surfaces and the steel bar at the end of the specimen. It was noted that the ends of the specimens, reinforced with a No. 25 bar in particular, were convex. This relative displacement at the ends is a manifestation of the shear lag that exists within the development length (Lay, 1982).

Fig. 6.5(a) shows a unit length of a reinforced concrete specimen taken from the central portion of the specimen where full restraint has been developed and where there is no longitudinal strain gradient. The free shrinkage strains have the same distribution as shown in Fig. 6.1(a) for an unreinforced specimen (greater at the perimeter than in the center of the specimen). From [6.2], the tensile strains that develop in the concrete as it attempts to shrink and is restrained by the steel bar result in a reduced concrete shrinkage strain ε_c. For compatibility of strains, the steel strain, ε_s, is as shown in the figure. Figs. 6.5(b) and 6.5(c) show the resulting stress and force diagrams and the equilibrium equation is

[6.3] $$C_s = T_c$$

6.3.1 Effect of the Amount of Restraint on Measured Shrinkage Strains

In Figs. 6.6 and 6.7 are plotted the normalized restrained shrinkage strains versus the percentage of reinforcement, ρ, for

mixes 1 and 2 respectively at specific times after casting. The restrained shrinkage has been normalized by dividing it by the free shrinkage strain for the corresponding number of days. The normalized strain at any time decreases with increased ratios of reinforcement; with no reinforcement, the restrained strain would equal the free shrinkage strain, and with a large percentage of reinforcement the restrained strain would approach zero. The normalized strain for any value of ρ starts from its maximum at the end of the curing period and decreases with time to reach a minimum value because the free shrinkage strain increases more rapidly with time than the restrained strain.

Anticipating that an exponential equation might fit the data, one can write

$$\varepsilon_r = \varepsilon_f e^{-\rho c t^s} \qquad [6.4]$$

Regression analyses of [6.4] gave values of c of 0.10 and 0.11 for mixes 1 and 2 respectively and a value of s of 0.28 for both mixes. The data for specimens with a No. 35 bar (ρ = 4.44%) for 60 days and more were not included in the regression analysis because these specimens cracked between 28 and 44 days. It is noted that the data for these cracked specimens fall below the curves indicating that cracking reduces the degree of restraint.

Also plotted in Figs. 6.6 and 6.7 are the normalized strains computed from [2.22] based on Ghali's work and using the age adjusted modulus of elasticity as proposed by the CEB. In computing the age adjusted modulus, it was assumed that the

concrete was cured for 3 days thus resulting in a maximum value of the creep coefficient. This in turn means that the minimum value of the age adjusted modulus was used and from [2.22], a minimum value of the normalized strain. Although these curves therefore represent the minimum normalized strains following this procedure, they are seen to overestimate the normalized strains. The discrepancy between [2.22] and the test results is due to the use of an age adjusted modulus based on the 28 day modulus of elasticity of concrete in compression.

Equation [2.10], based on equilibrium conditions and strain compatibility is hyperbolic in form provided that all the terms for a given time are constant. However, as shown subsequently, the modulus of elasticity of concrete is a function of the ratio of reinforcement and time.

6.4 Effective Modulus of Elasticity of Concrete in Tension

The effective modulus of elasticity of concrete in tension as it sets, drys, shrinks, creeps, and is gradually loaded from the green condition is an important constitutive property of the concrete. It includes the effect of the creep of concrete under the sustained tensile stresses induced by concrete shrinkage and the presence of the steel reinforcement. As established in Section 6.3, using [6.2] and [6.3], one can write

$$[6.5] \qquad C_s = \varepsilon_s A_s E_s = \varepsilon_{ct} A_c E_e = T_c$$

The tensile stress, σ_{ct}, is

$$[6.6] \qquad \sigma_{ct} = \frac{\varepsilon_s A_s E_s}{A_c}$$

and therefore, the effective modulus of elasticity, E_e, is

$$[6.7] \qquad E_e = \frac{\sigma_{ct}}{\varepsilon_{ct}}$$

Using the strains obtained from the reinforced specimens of both mixes 1 and 2 in [6.6] and [6.7], the effective modulus of elasticity of concrete in tension was calculated at different times.

6.4.1 Development of the Effective Modulus

In Figs. 6.8 and 6.9 the effective modulus is plotted versus time for mixes 1 and 2 respectively. Data are presented with different symbols for specimens reinforced with different sizes of bars and therefore with different degrees of restraint. For each bar size, an exponential equation of the form

$$[6.8] \qquad E_e = E_\infty + (E_i - E_\infty)^{-\gamma t}$$

has been fitted to the test data using non-linear regression analysis. Tables 6.3 and 6.4 give the values of the parameters for the different bar sizes for the two mixes. The correlation coefficients, R^2, are generally high although somewhat low for specimens with a No. 35 bar as discussed subsequently.

Initially, the modulus is high. As shrinkage begins at the end of the curing period, the initial restrained shrinkage strains are very low and little creep occurs in the concrete. With time, the increasing tensile stresses in the concrete (see Figs. 6.10 and 6.11), lead to increasing creep and therefore a decreased effective modulus of elasticity. The curves in Figs. 6.8 and 6.9 approach horizontal asymptotes and the asymptotic values decrease with increasing restraint or bar size. With increased restraint, greater tensile stresses are developed in the concrete as shown in Figs. 6.10 and 6.11. These greater tensile stresses result in more creep and therefore a reduced effective modulus.

In both Figs. 6.8 and 6.9, the exponential curves for specimens reinforced with a No. 35 bar have been fitted to the experimental data up to the time that these specimens cracked. The apparent moduli of elasticity calculated for times after cracking, assuming the specimens to be uncracked, lie below the exponential curves. This is due to the fact that cracking reduces the restraint. The apparent restrained shrinkage strain in the concrete measured over a crack decreases and from [6.2] and [6.7], the effective modulus is reduced. An analysis taking cracking into account is presented subsequently. It is also evident from Figs. 6.10 and 6.11 that cracking of the concrete occurred only in the specimens with a No. 35 bar. Only for these specimens does the average tensile stress decrease rapidly from its peak value. (The tensile stresses calculated after cracking are really fictitious as they are obtained assuming that the concrete is uncracked.) For

all the other specimens, relatively high tensile stresses are maintained with time. The lesser values of the correlation coefficients of the data with respect to [6.8] for the specimens with a No. 35 bar arise from two sources. First, the data for these specimens have a limited time base and second, for all specimens, the initial data are based on strains that are relatively small as compared to the sensitivity of the measuring devices.

From [6.8], when $t = 0$, it is seen that E_i represents the initial value of the effective modulus, and when $t = \infty$, E_∞ is the asymptotic value of the effective modulus. A unique value of the initial modulus should exist for a given mix because, at the beginning of drying, as the induced stresses approach zero, creep approaches zero. The mean value of the initial effective modulus for mix 1 is 9,570 MPa with a coefficient of variation of 0.143 and 9,490 MPa with a coefficient of variation of 0.126 for mix 2. Even these initial values are only about 50% of the initial static moduli in compression of 17,800 MPa and 20,400 MPa obtained from mixes 1 and 2 respectively at 3 days. When comparison is made to the initial modulus in compression at 28 days, the ratio reduces to about 40%. When the long term values of the effective moduli of elasticity are compared to the 28 day values of the initial moduli in compression, the ratios fall between 21% to 5% as the degree of restraint increases.

Modular ratios are obtained by dividing the modulus of elasticity of steel, taken as 200,000 MPa, by the effective modulus of concrete in tension. The modular ratio increases from an initial

value of 21 to long term values ranging from 43 to 200 with the latter values increasing with the degree of restraint.

6.4.2 Inferred Stress-Strain Characteristics in Tension

Each point plotted in Figs. 6.12 and 6.13 for mixes 1 and 2 represents the average tensile stress and strain in the concrete as these values developed with time. The points for a given percentage of steel therefore represent the entire loading history from the end of curing to the maximum time of observation. The tensile stresses and strains have been calculated from [6.2] and [6.6]. Fictitious values after cracking are not shown.

Curve A in Fig. 6.12 has been drawn through the stress-strain data points at 169 days for the three percentages of steel of 0.44, 0.89 and 2.22. It therefore represents the stress strain curve in tension of the concrete as it is gradually loaded through the shrinkage process over a period of 169 days. For any stress level, the corresponding tensile strain can be determined at 169 days and therefore the secant modulus of elasticity as well. Such values would be consistent with the data plotted in Fig. 6.8. Curve B in Fig. 6.12, drawn as was curve A, is for 28 days and obviously curves can be drawn in this manner for any number of days. A tangent drawn to the data at the origin would represent the initial modulus of elasticity at zero days. Also drawn on Figs. 6.12 and 6.13 are lines representing the average value of the initial modulus of elasticity at 0 days as given in Tables 6.3 and 6.4 for the two mixes. These lines, as would be expected, are about

tangent to the data close to the origin. Curve C, similar to curves A and B on Fig. 6.12, has been drawn on Fig. 6.13 for mix 2 at 141 days.

The above procedure therefore allows the stress strain curves for the concrete to be drawn over any specific time period as it is gradually loaded in tension (from the green condition) and creeps. From such a curve, provided that the stress developed gradually over a known time period, the modulus of elasticity of concrete in tension can be determined at any stress level.

It is also of interest to examine the data for one particular percentage of steel, say for example curve D in Fig. 6.13 of mix 2 concrete for a reinforcement ratio of 0.89%. The curve, as do others, consists of two parts: an initial gradually curving portion that lies within the bulk of the data, rising rather steeply, and a final portion branching from it at a lesser slope. The initial portion results from the rapid development of both free and restrained shrinkage strains (and stresses) at the beginning of drying and therefore a low rate of creep. The second portion portrays significant creep behaviour but at increasing stress levels due to the continued shrinkage. With greater restraint, the second portion of the curve is essentially flat indicative of a much higher rate of creep than the first portion.

All the stress-strain data for mixes 1 and 2, up to cracking, are plotted in Fig. 6.14. The data, even grouping that for the 2 mixes, are not broadly dispersed suggesting that a mean curve, E,

could be used to represent the stress-strain relationship in tension for these two concretes. It is noted that while the curve models the creep behaviour well at high stress levels and that creep is insignificant at low stress levels, at intermediate stress levels the second branch of the stress-strain curve for a particular percentage of steel (curve D in Fig. 6.13) is not modelled. This omission may not be that significant. A single curve allows the secant modulus to be estimated as a function of the stress level only. From curve E, the modulus is calculated to vary from an initial value of 9,650 MPa to a minimum long term value of 2,540 MPa at a tensile stress level of 1.07 MPa

6.4.3 Variation of the Effective Modulus With the Induced Tensile Stress

In Fig. 6.15, the effective modulus of elasticity of concrete in tension is plotted against the induced average tensile stress in the concrete at 180 days. For any data point, representing a specific percentage of steel, the tensile stress was obtained from Figs 6.10 or 6.11 for mixes 1 and 2 respectively and the corresponding value of the effective modulus was obtained from [6.8]. A curve has been fitted to the test data and begins at the average initial value of the tensile modulus for the two mixes because the initial values represent a state of zero stress. The curve extends to the point representing the maximum calculated tensile stress at 180 days.

For any problem involving the determination of shrinkage induced stains, stresses and deflections, the curve could be used to

establish, by trial and error, values of the modulus of elasticity consistent with the conditions of equilibrium and strain compatibility.

6.5 Shrinkage-Induced Cracking of Concrete

Transverse shrinkage cracks developed nonsymmetrically, as discussed in Section 5.4, in each of the specimens reinforced with a No. 35 bar starting at 28 to 44 days. Average tensile stresses of 1.1 and 1.3 MPa were developed just before cracking in the specimens of mixes 1 and 2 respectively. These stresses are in the range of 0.50 to 0.44 of the tensile strength obtained from the split cylinder test. It appears the reason for this difference is that shrinkage-induced tensile stresses at the surface of the concrete were higher than the calculated average tensile stress when cracking occurred.

Fig. 6.16(a) shows the assumed linear strain distribution across the cracked cross section. It is recognized that the strain distribution is likely invalid in the vicinity of the crack. Furthermore, of the strain measurements taken on the four surfaces of the concrete using Demec gauges, those averaged over the crack will likely be in error and therefore were not used in the analysis. As well, although the steel bars were placed in the forms with the electrical resistance strain gauges on top, the bar may have rotated about its longitudinal axis during casting therefore putting the exact position of the gauge in doubt. It is also assumed that the crack leaves an uncracked rectangular cross section even

though cracking generally started in one corner and may have caused biaxial bending. Thus the crack tip may not actually lie on a straight line joining the observed crack tips on the surface as shown in Fig. 6.17. Under the assumed simplified conditions, the equilibrium equations (Fig. 6.16) are

$$M = M_c + M_s = C_s e = T_c e \qquad [6.9]$$

$$C_s = A_c E_e \varepsilon_{ct} = A_s E_s \varepsilon_s = T_c \qquad [6.10]$$

$$M_c = S_c E_e \varepsilon_{cb} \qquad [6.11]$$

$$M_s = S_s E_s \varepsilon_{sb} \qquad [6.12]$$

With the assumptions of strain compatibility as shown in Fig. 6.16(a), the effective modulus of the concrete in tension at any time, assuming it does not vary across the section, can be computed iteratively as follows:

(i) From the measured steel and concrete strains at a certain time, the strain gradient across the cross section is established and therefore the compressive force in the steel, C_s, and the moment in the steel, M_s, are determined from [6.10] and [6.12],

(ii) when the total moment in the concrete, M_c, is assumed, the total moment, M, and the eccentricity, e, are obtained using [6.9],

(iii) values of the effective modulus, E_e, can now be computed from both [6.10] and [6.11], and

(iv) iterations are performed until the desired convergence is obtained.

Values of E_e, calculated in this manner for specimen 1353 which had almost identical cracks on the lateral surfaces, are plotted in Fig. 6.8. It is seen that these values fit the curve obtained by the regression analysis for data prior to cracking reasonably well.

Considering Fig. 6.16(a) when a steep strain gradient exists in the steel due to bending of the specimen and when there is a relatively low compression strain because of the reduced restraint at cracking, tensile stresses can develop on one side of the steel bar as were documented. Though reinforcement is generally considered to be axially loaded, the flexural stiffness of a No. 35 bar is about 9% of that of uncracked concrete with a modulus of elasticity of say 4,000 MPa and when the concrete is cracked to 1/3 of the depth and has a modulus of say 1,300 MPa, the stiffness of the bar increases to 90% of that of the uncracked concrete.

6.6 A Design Application

Shrinkage deflections were calculated at 180 days for a composite concrete-steel beam 10,000 mm long consisting of a W460 x 74 grade 300 W steel beam with a 2,270 mm wide by 130 mm deep solid 30 MPa concrete cover slab. The concrete is assumed to have the same properties of mix 1 and the curing conditions are the same as in the test. The equilibrium method as described here, and the restrained shrinkage method and the

unrestrained shrinkage method, both as given in Appendix L of CSA Standard S16.1-M89 (CSA, 1989), were used.

6.6.1 The Equilibrium Method

This method is based on the equilibrium of the shrinkage induced forces and compatibility of strains in the cross section (Kennedy and Brattland, 1991). As shown in Fig. 6.18, an axial tensile force, T_c, is induced in the concrete slab due to shrinkage and an equal axial compressive force, C_s, exists in the steel. The moment $M = C_s e = T_c e$ is required for rotational equilibrium. It is assumed that moment in the concrete is zero.

6.6.1.1 General Procedure

From the strain diagram in Fig. 6.18

[6.12] $$\varepsilon_r = \varepsilon_f - \varepsilon_{ct}$$

where ε_{ct} , the tensile strain in the concrete, is

[6.13] $$\varepsilon_{ct} = \frac{T_c}{A_c E_e}$$

substituting [6.12] in [6.13] gives

[6.14] $$T_c = (\varepsilon_f - \varepsilon_r) A_c E_e = C_s$$

therefore, the moment, M, is

[6.15] $$M = (\varepsilon_f - \varepsilon_r) A_c E_e (t_c + d)/2$$

The stress in the steel at any distance y from the centroid, is

[6.16] $$\sigma = \frac{C_s}{A_s} + \frac{M}{I_s} y$$

thus, the strain is

[6.17] $$\varepsilon = \frac{1}{E_s}\left[\frac{C_s}{A_s} + \frac{M}{I_s} y\right]$$

Substituting [6.14] and [6.15] in [6.17], the strain at the centroid of the concrete slab, at $y = (t_c + d)/2$, is

[6.18] $$\varepsilon_r = \varepsilon_f \frac{1}{1 + \frac{A_s E_s}{A_c E_e}\left[\frac{1}{1 + y^2 A_s / I_s}\right]}$$

The shrinkage deflection of the beam at midspan, Δ_{sh}, is

[6.19] $$\Delta_{sh} = \frac{(\varepsilon_f - \varepsilon_r) A_c E_e L^2 y}{8 E_s I_s}$$

The shrinkage deflection is calculated as follows;

(i) Using [6.1a], ε_f is calculated at 180 days,

(ii) a value is assumed for the effective modulus, E_e, and the restrained strain, ε_r, is calculated from [6.18], and therefore the tensile strain in the concrete, ε_{ct}, is determined from [6.12],

(iii) using the assumed value of E_e and the calculated value of ε_{ct}, the tensile stress in the concrete, σ_{ct}, is calculated from [6.13], and

(iv) Fig. 6.15 is used to compare E_e and σ_{ct}. The procedure is repeated until the required convergence is achieved. The deflection, Δ_{sh}, is then calculated using [6.19].

Table 6.4 gives values of the parameters used in this procedure. The calculated shrinkage deflection is found to be 16.7 mm.

6.6.1.2 Approximate Procedure

An alternative approximate procedure is to use an assumed free shrinkage strain (say 800 $\mu\varepsilon$) and stress-strain curve E of Fig. 6.14 to get a pair of values of the modulus of elasticity and the tensile strain consistent with [6.18]. Using this procedure iteratively, a value of E_e of 5,190 MPa corresponding to a tensile strain, $(\varepsilon_f - \varepsilon_r)$, of 211 $\mu\varepsilon$ is established. The product of these two values, $(\varepsilon_f - \varepsilon_r)\, E_e$, appearing in [6.19], is a tensile stress of 1.095 MPa. The same product, corresponding to the calculated shrinkage deflection at 180 days of 16.7 mm, from the data for the equilibrium method in Table 6.4, is 3,500 MPa times 293 $\mu\varepsilon$ or 1.03 MPa. The approximate value is only 6% greater than the value taking into account the time dependence of the shrinkage deflection. The deflection parameters are given in Table 6.4.

6.6.2 The Restrained Shrinkage Method

In this method proposed by Chien and Ritchie (1984), a compressive force equal to that required to shorten the concrete cover slab an amount equal to the restrained shrinkage strain is

applied at the centroid of the cover slab. The composite section is then assumed to be subjected to a constant moment equal to the compressive force multiplied by the distance from its line of action to the centroid of the transformed section. The resulting deflection is

$$[6.20] \qquad \Delta_{sh} = \frac{\varepsilon A_c E_c L^2 y}{8 E_s I_t}$$

where E_c is the 28 day modulus of elasticity of concrete in compression and ε is an assumed restrained shrinkage strain. Note also that I_t is a transformed moment of inertia and y is the distance from the compressive force in the slab to the elastic neutral axis of the transformed section. The restrained shrinkage strain is generally taken as 200 to 350 $\mu\varepsilon$ (Chien and Ritchie, 1984) but for this example the calculated value of 550 $\mu\varepsilon$, as given in Table 6.4, is used. Table 6.4 lists the values of the other parameters used and the shrinkage deflection is calculated to be 15.3 mm. Obviously, had the restrained shrinkage strain been taken as 200 $\mu\varepsilon$, a shrinkage deflection of only 5.6 mm would have been calculated.

6.6.3 The Unrestrained Shrinkage Method

In this method, proposed by Montgomery et al. (1983), the concrete slab is assumed to undergo the free shrinkage strain. To satisfy compatibility, the concrete section is then subjected to an axial tensile force to elongate it to its original length. Equilibrium is then achieved by applying an equal opposite and collinear

compressive force. The shrinkage deflection therefore results from the constant moment, caused by the eccentricity of the compressive force, acting on the composite section. The deflection is found from [6.20] with E_c being the age adjusted modulus of elasticity of concrete calculated from [2.16] using the CEB values for the creep coefficient, $\phi(t, t_o)$, and the relaxation coefficient, χ. The strain, ε, is the free shrinkage strain as could be calculated using [6.1a]. Values of the parameters used are given in Table 6.4 where the shrinkage deflection is calculated to be 19.7 mm.

6.6.4 Discussion

The equilibrium method recognizes the fundamental action that shrinkage of the restrained concrete places it in tension and therefore that the modulus of elasticity of the concrete in tension governs the magnitude of the equilibrating forces that result.

By using both the time dependent modulus of elasticity and the free shrinkage strain, the development of the shrinkage deflection with time can be established. The approximate method using the tensile stress-strain curve of Fig. 6.14 together with an assumed free shrinkage strain (say 800 $\mu\varepsilon$) gives one value for the shrinkage deflection which, at least, recognizes that the concrete is in tension due to shrinkage.

Although the unrestrained shrinkage method is based on the correct unrestrained shrinkage strain, the age adjusted modulus used is too large and therefore the calculated shrinkage forces and moments are too great. These forces and moments are then

applied to a section which is too stiff since the transformed concrete area is based on the same excessive value of the modulus. The two factors compensate one another substantially as evident by the fact that the calculated shrinkage deflection is not appreciably different from that calculated using the equilibrium method.

That methods using the restrained shrinkage strain may give reasonable answers is seen to be simply fortuitous, on two grounds: the restrained shrinkage strain is a function of the degree of restraint, and again, it is the effective modulus of elasticity of concrete in tension that should be used to calculate the restraining forces, not the 28 day compression modulus.

6.6.7 Comparison with a Measured Deflection

Brattland and Kennedy (1991) report a measured shrinkage deflection at 65 days of 8.9 mm for a composite truss with a 28 MPa concrete slab cast on fluted deck. To establish a calculated deflection to compare to this measured value, the properties of concrete mix 1 with a 28 day strength of 30 MPa are used. Using the equilibrium method, a shrinkage deflection at 65 days, allowing for the increased flexibility of the open web system, of 12.7 mm is calculated. This is in reasonable agreement with the measured value of 8.9 mm. The difference could be attributed to the differences of the two concretes and the curing conditions.

Table 6.1 Values of ε_u and α at Different Times, Mixes 1 and 2

	Mix 1		Mix 2	
Time, (Days)	ε_u, με	α	ε_u, με	α
28	618	0.0425	575	0.0539
36	664	0.0387	638	0.0460
44	730	0.0340	654	0.0450
56	745	0.0330	695	0.0399
80	803	0.0291	716	0.0373
90	809	0.0287	727	0.0359
114			735	0.0348
121	840	0.0261		
137	844	0.0257		
141			748	0.0323
169	855	0.0246		

Table 6.2 Values of E_i, E_∞ and γ, Mix 1

Bar No.	E_i, MPa	E_∞, MPa	γ	R^2,%
10	10 793	4 645	0.022	94
15	11 009	4 417	0.022	95
25	8 708	2 600	0.020	98
35	7 777	1 000	0.029	83
	μ = 9 571			
	σ = 1 372			

Table 6.3 Values of E_i, E_∞ and γ, Mix 2

Bar No.	E_i, MPa	E_∞, MPa	γ	R^2,%
15	11 053	3 853	0.024	96
25	9 276	2 531	0.024	97
35	8 150	1 150	0.030	82
	μ = 9 493			
	σ = 1 195			

Table 6.4 Shrinkage Deflection Parameter Values

Parameter	Equilibrium Method	Approximate Procedure	Restrained Shrinkage Method	Unrestrained Shrinkage Method
ε, $\mu\varepsilon$	293	211	551	844
E_c, MPa	3 500	5 190	21 800	6 374
A_c, mm^2	295 100	295 100	295 100	295 100
L, mm	10 000	10 000	10 000	10 000
E_s, MPa	200 000	200 000	200 000	200 000
I_s or I_t, mm^4	333×10^6	333×10^6	962×10^6	739×10^6
y, mm	293.5	293.5	66.65	147.1
Δ_{sh}, mm	16.7	17.8	15.3	19.7

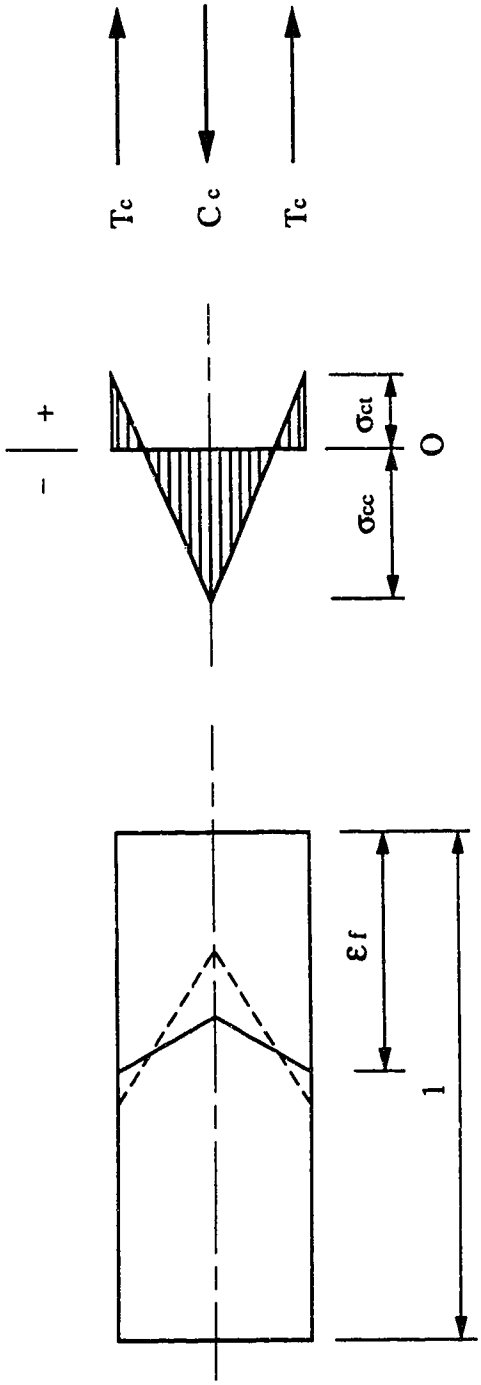

Fig. 6.1 Strain, Stress and Force Diagrams for an Unreinforced Concrete Specimen at Mid-Length

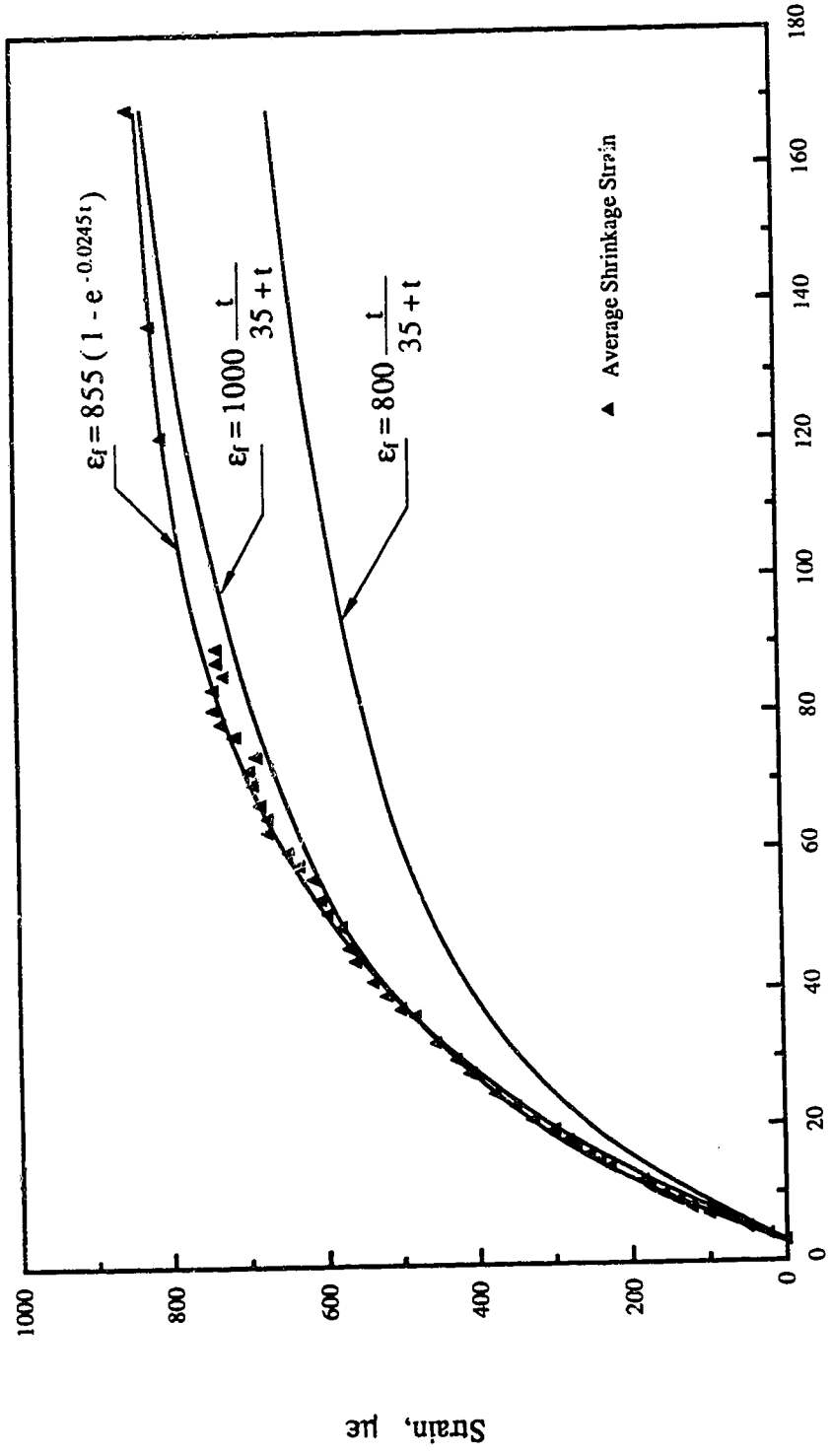

Fig. 6.2 Measured and Predicted Unrestrained Shrinkage Strains versus Time, Mix 1

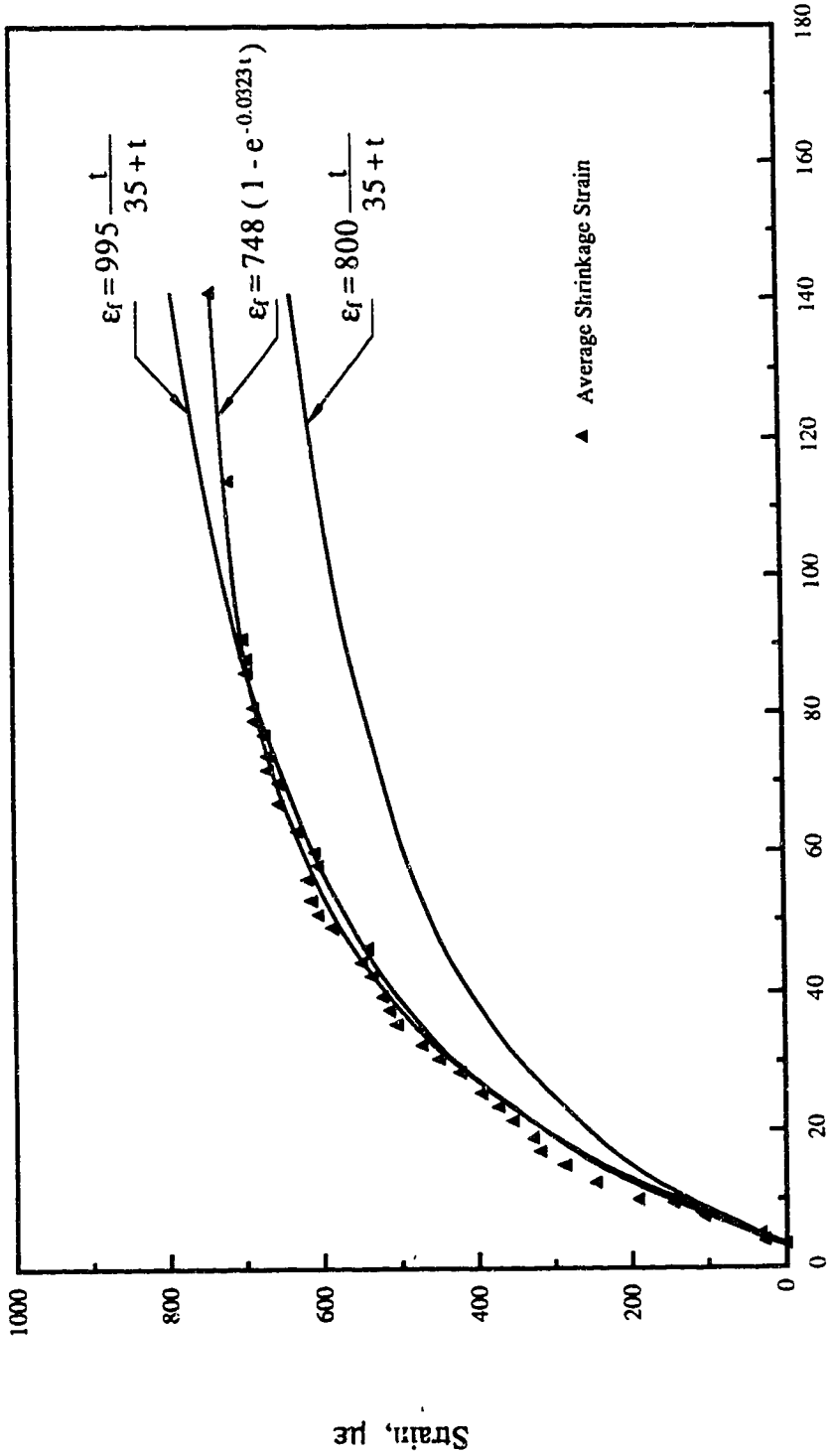

Fig. 6.3 Measured and Predicted Unrestrained Shrinkage Strains versus Time, Mix 2

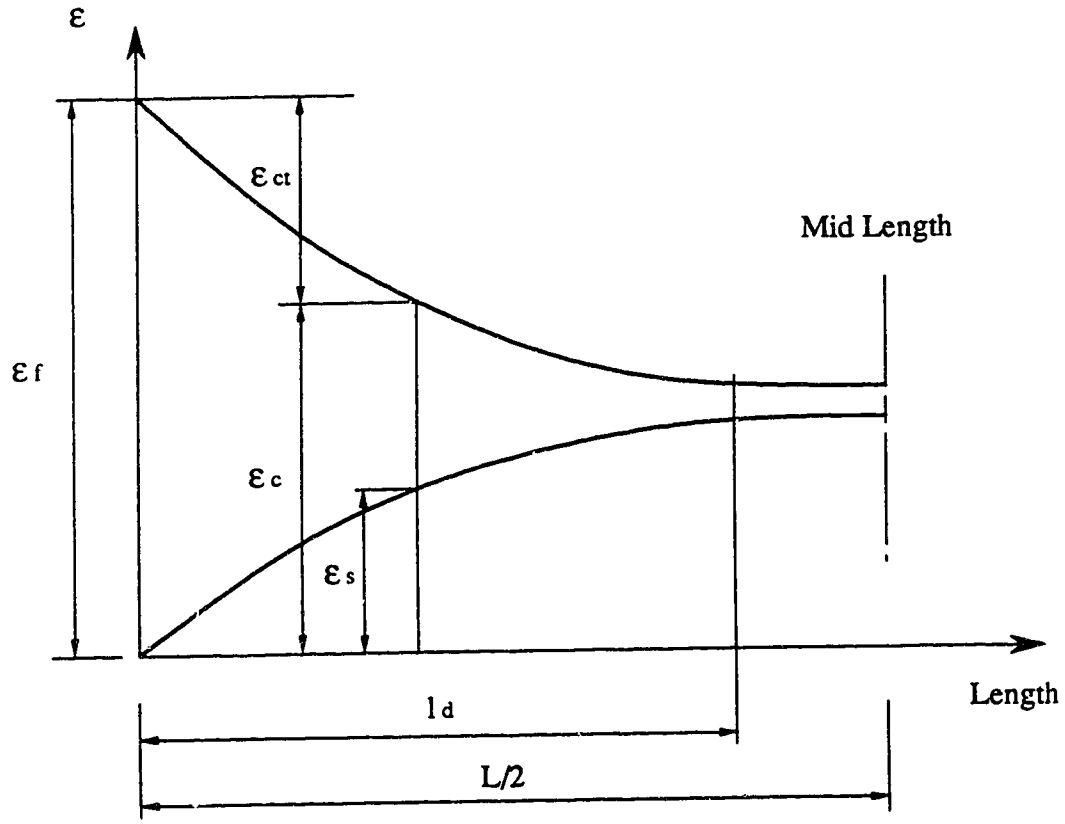

Fig. 6.4 Variation of Steel and Concrete Strains Over Half Length of a Reinforced Specimen

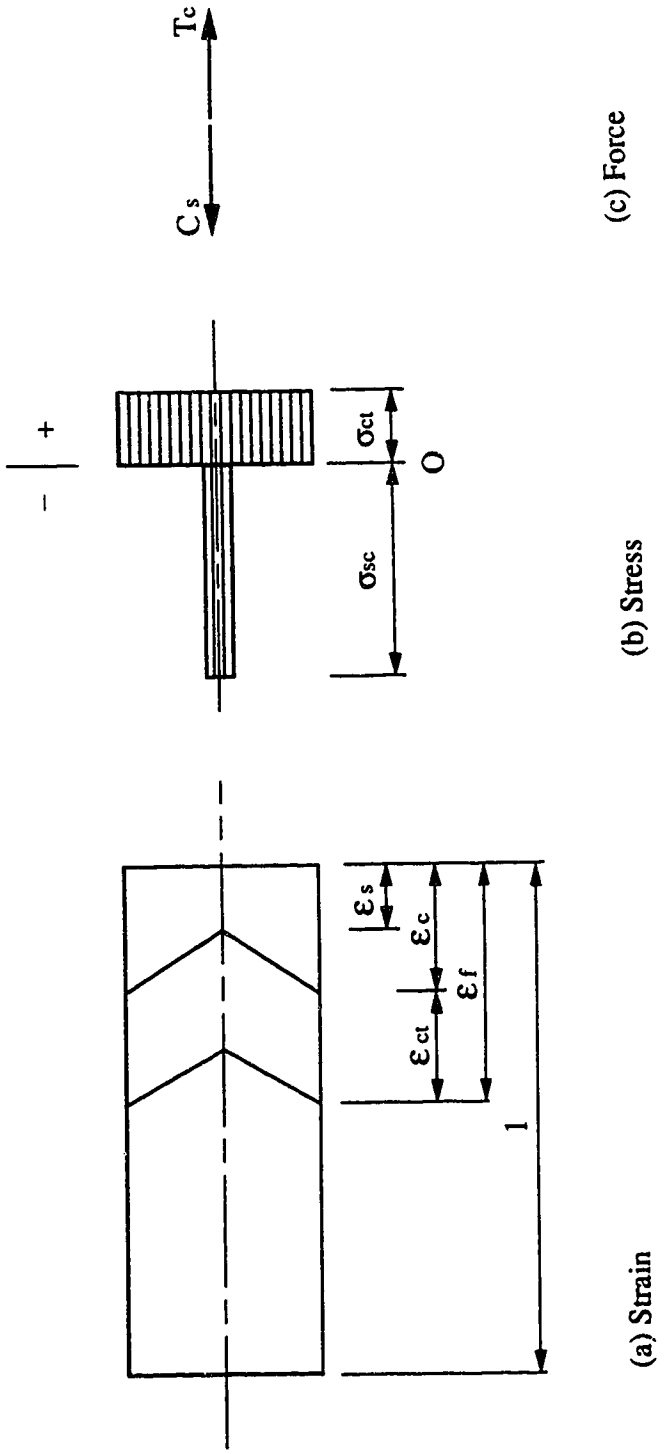

Fig. 6.5 Strain, Stress and Force Diagrams for a Reinforced Concrete Specimen at Mid-Length

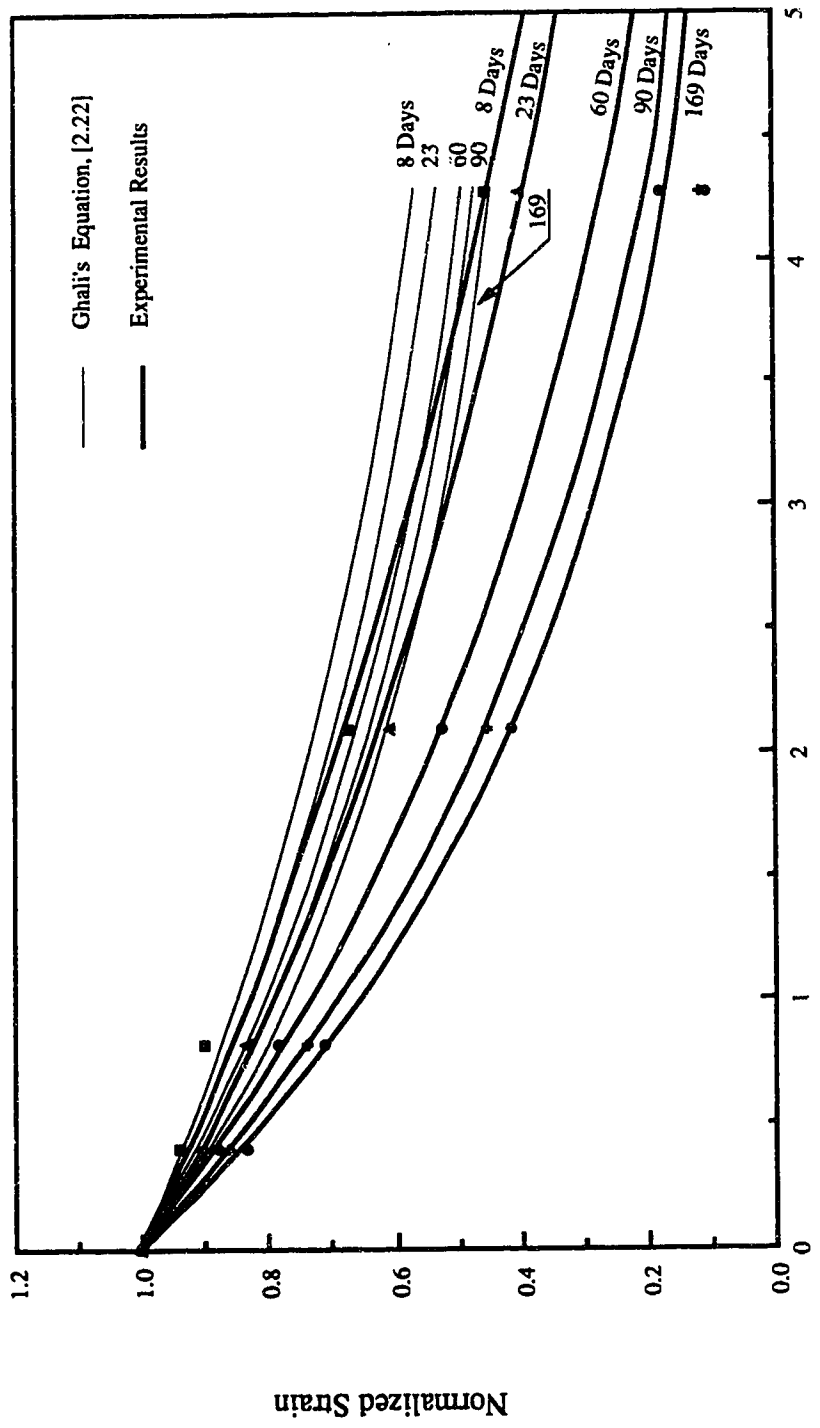

Fig. 6.6 Normalized Restrained Strain Versus the Percentage of Steel, Mix 1

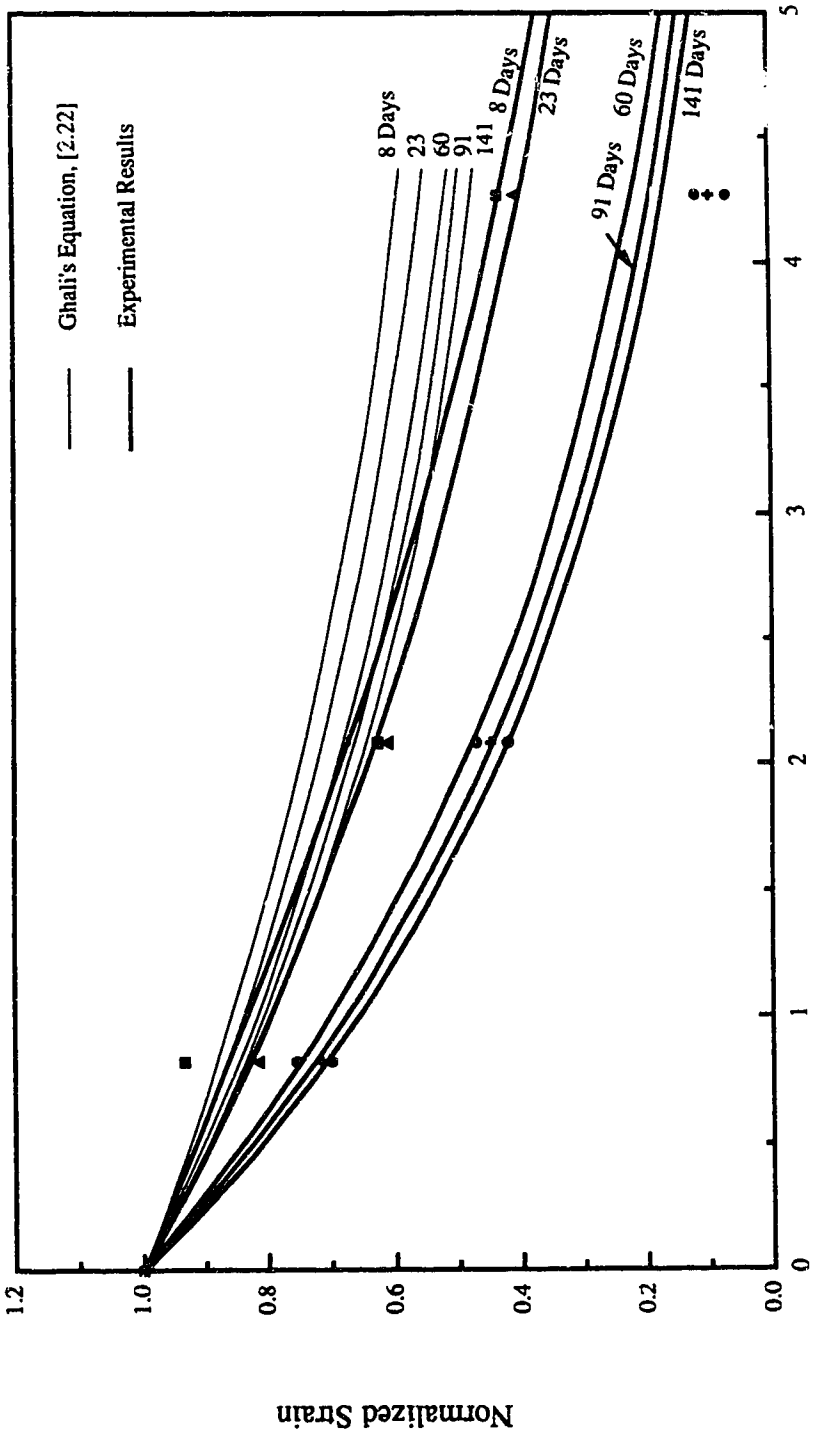

Fig. 6.7 Normalized Restrained Strain Versus the Percentage of Steel, Mix 2

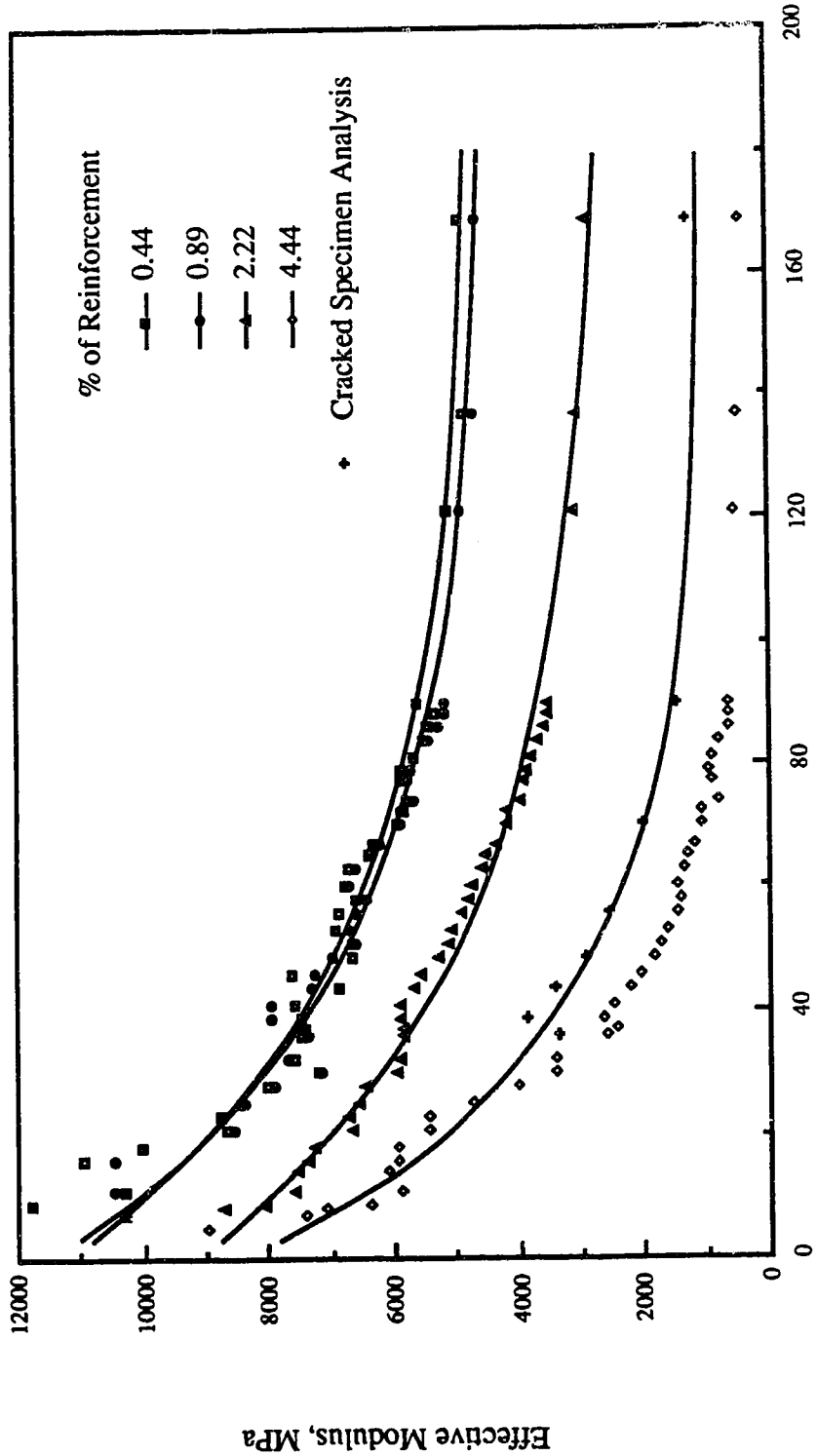

Fig. 6.8 Effective Modulus of Elasticity of Concrete in Tension versus Time, Mix 1

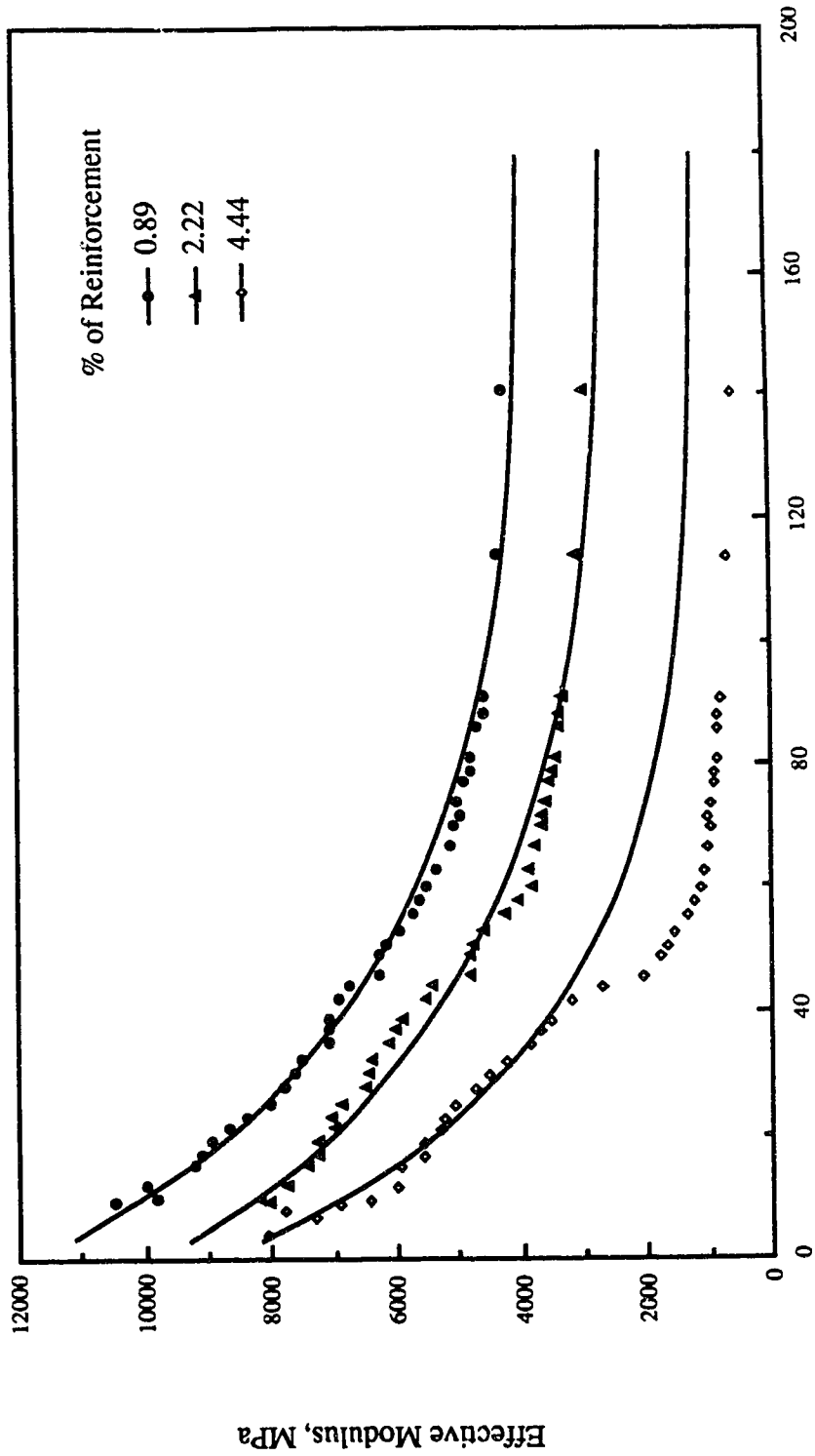

Fig. 6.9 Effective Modulus of Elasticity of Concrete in Tension versus Time, Mix 2

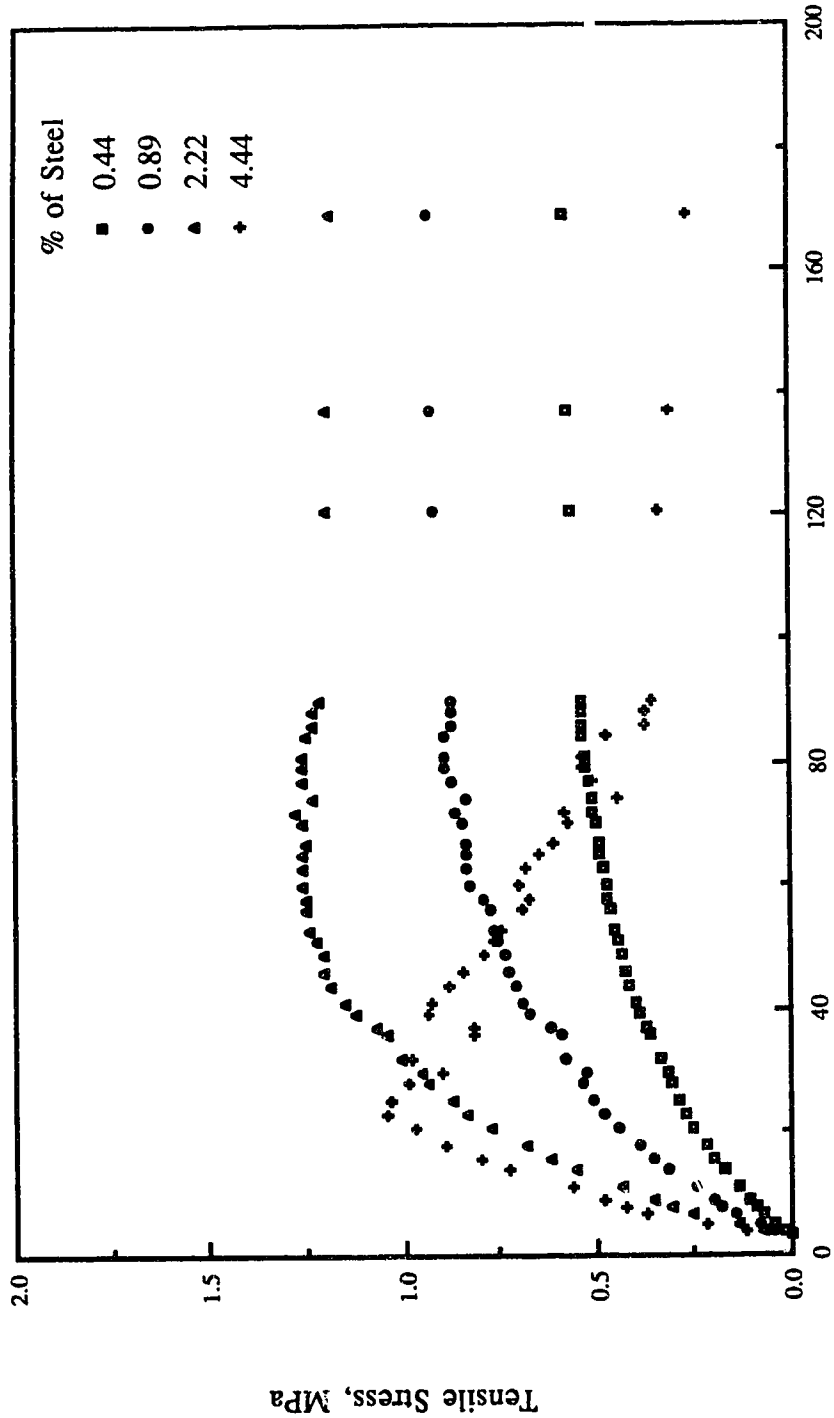

Fig. 6.10 Development of Tensile Stress in Concrete With Time, Mix 1

Fig. 6.11 Development of Tensile Stress in Concrete With Time, Mix 2

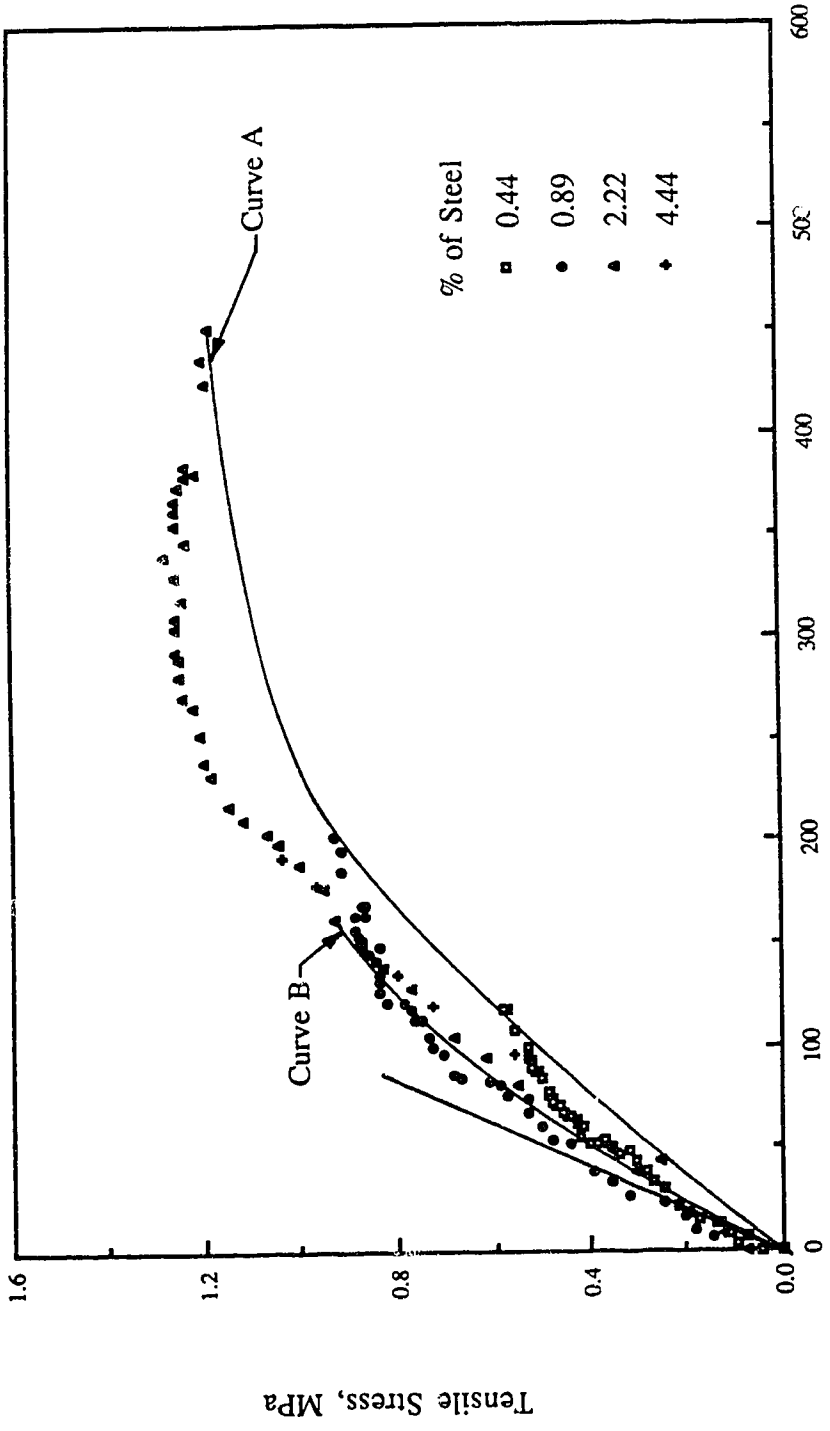

Fig. 6.12 Inferred Stress-Strain Curve of Concrete in Tension, Mix 1

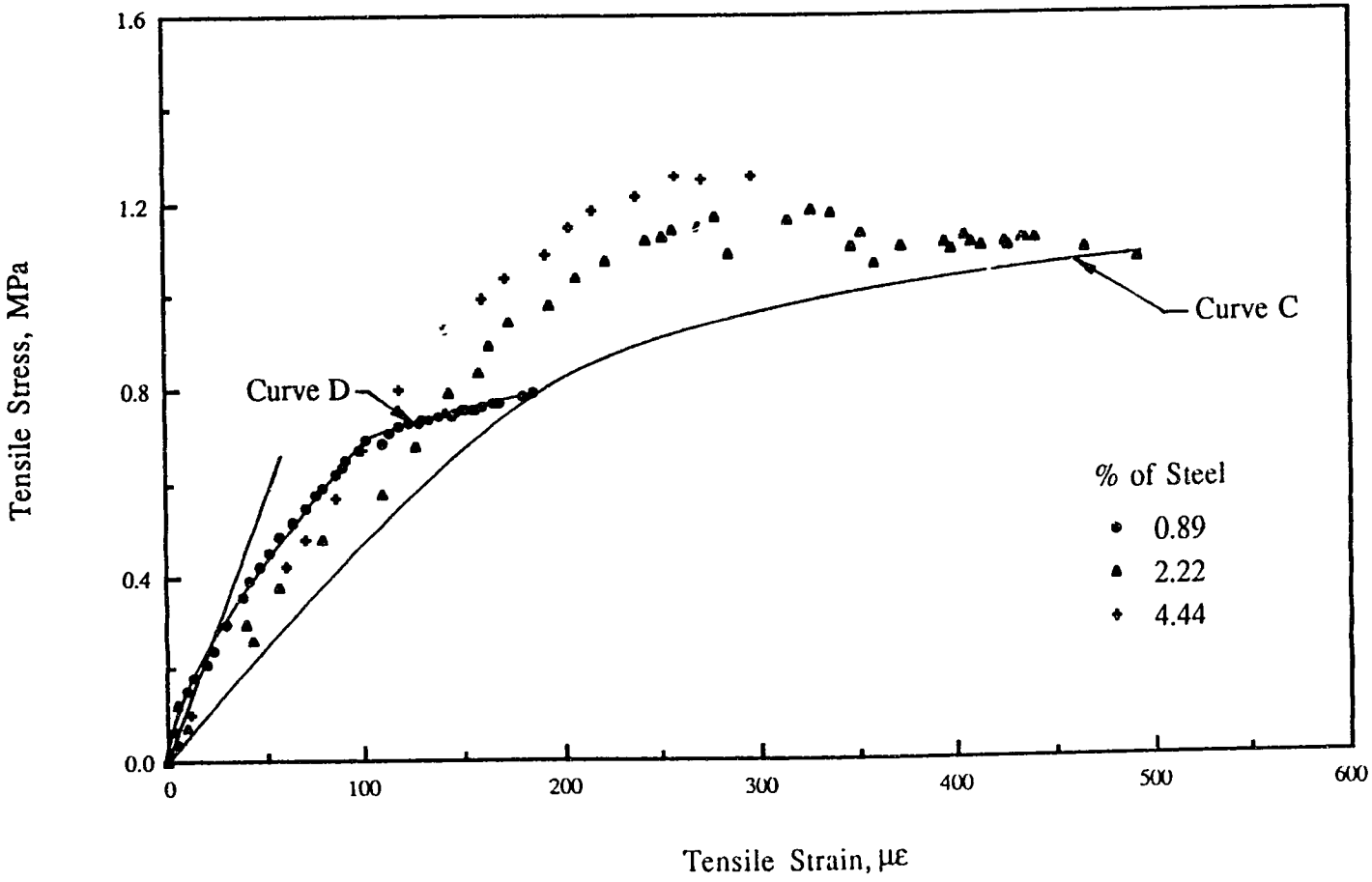

Fig. 6.13 Inferred Stress-Strain Curve of Concrete in Tension, Mix 2

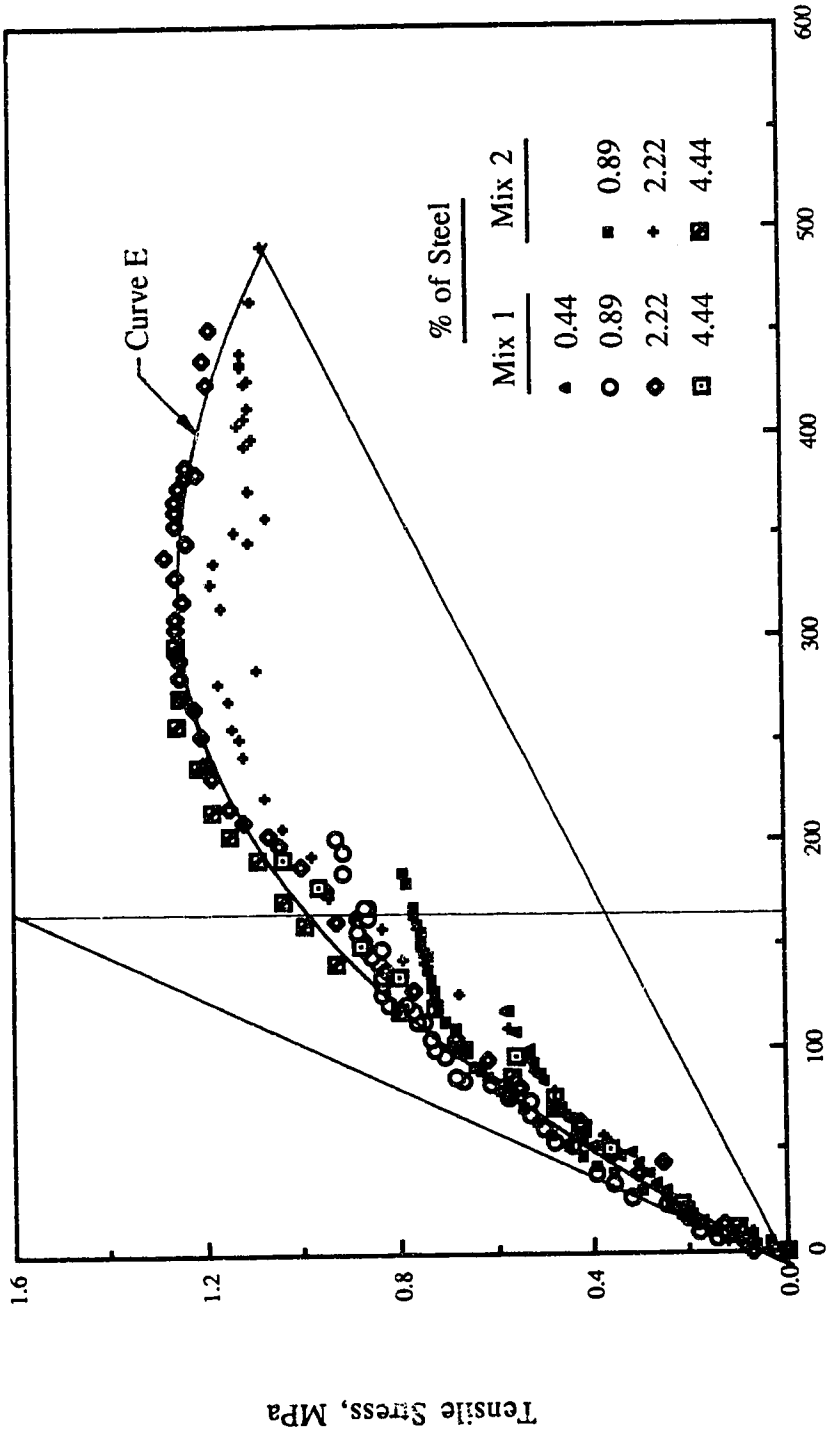

Fig. 6.14 Inferred Stress-Strain Curve of Concrete in Tension, Mixes 1 and 2

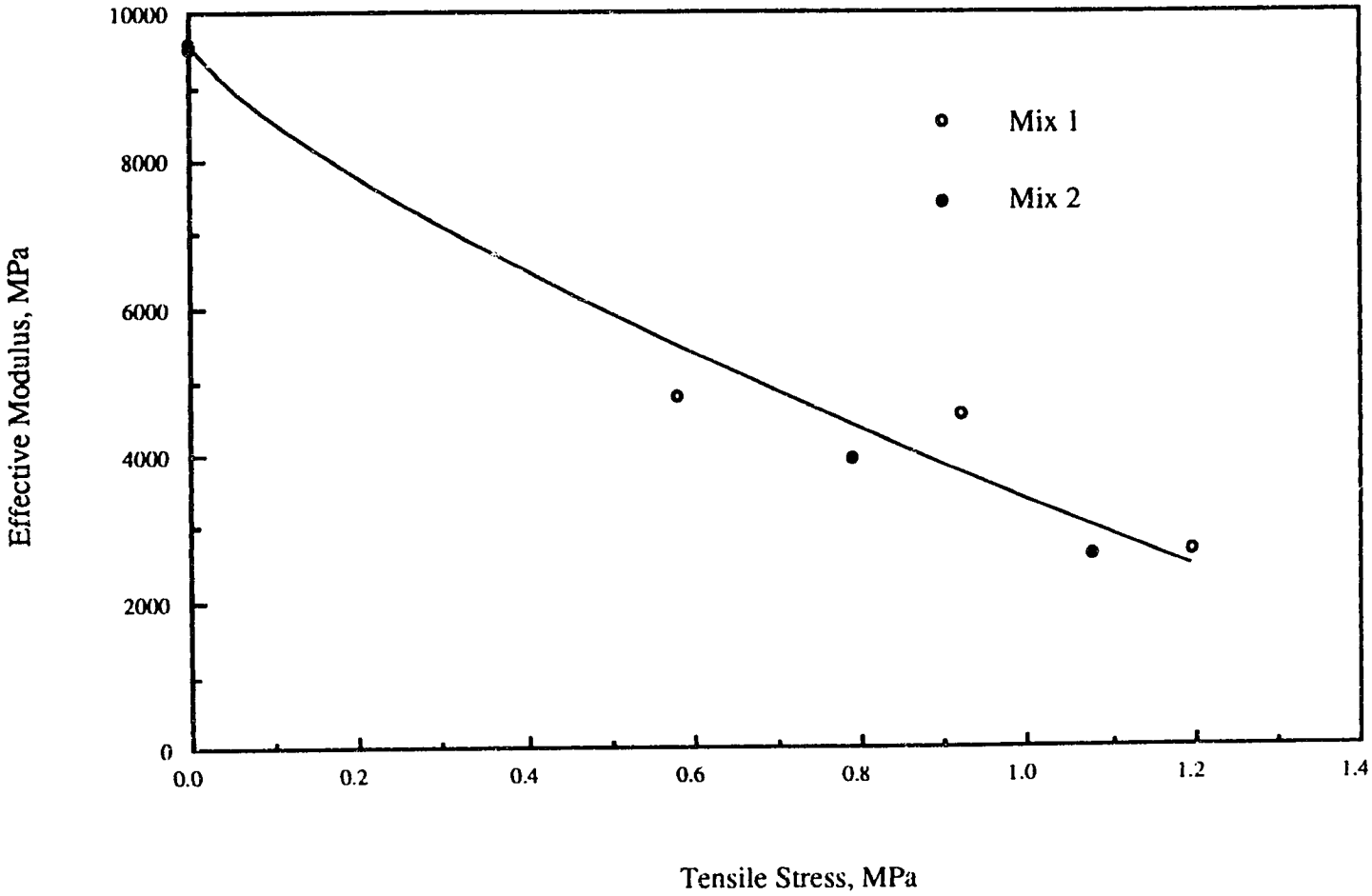

Fig. 6.15 Effective Modulus of Concrete in Tension versus the Tensile Stress at 180 days

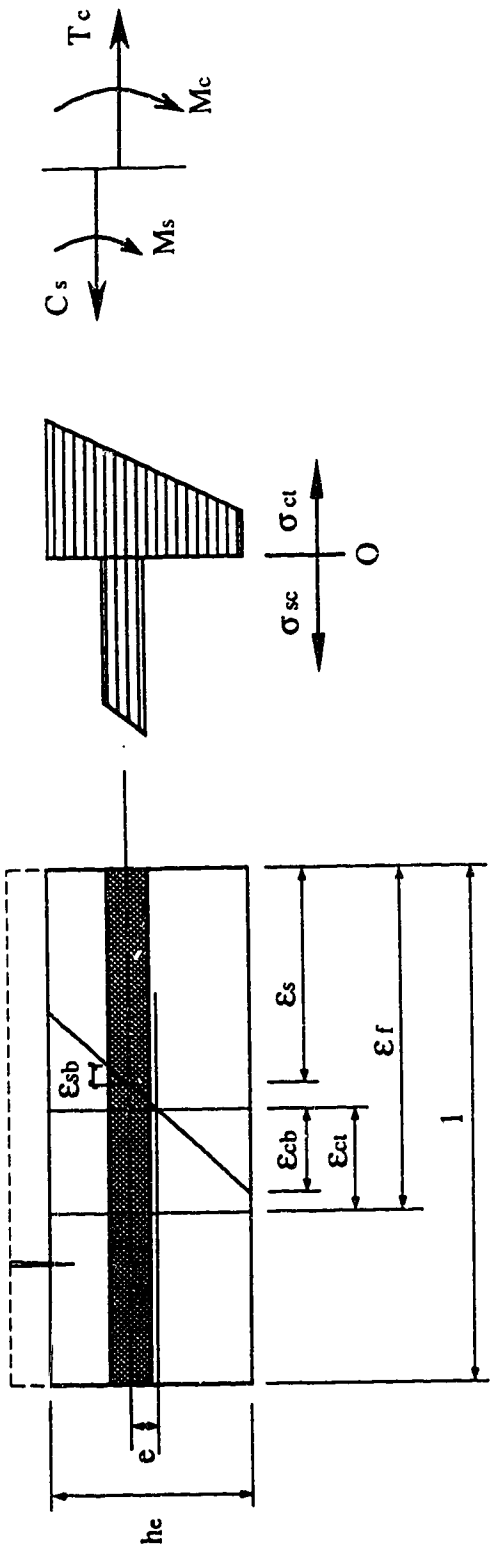

Fig. 6.16 Strain, Stress, and Force Diagrams in a Cracked Reinforced Concrete Specimen

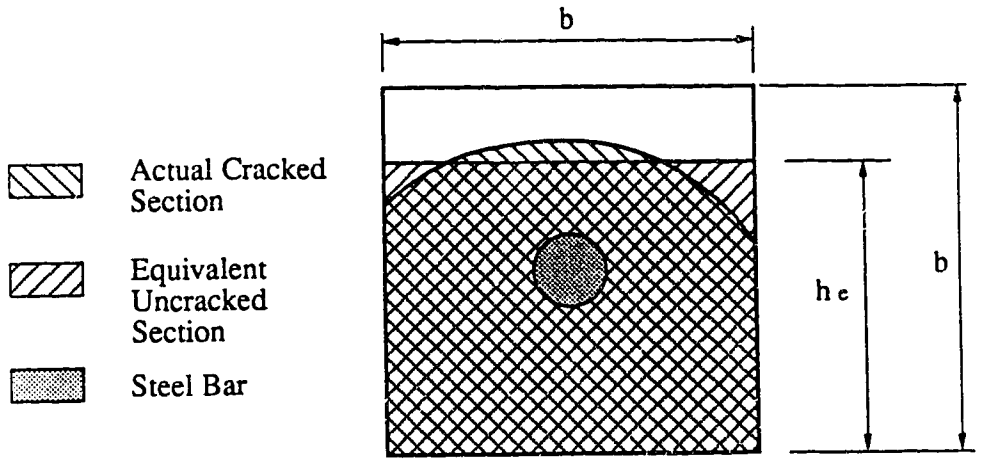

Fig. 6.17 A Cross-Section at the Crack

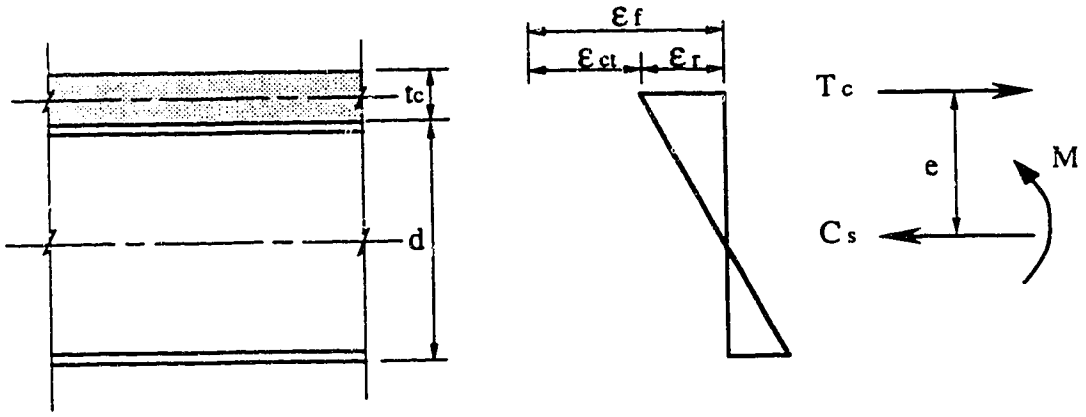

Fig. 6.18 Shrinkage Strain and Force Distribution in a Composite Beam at Midspan

Chapter 7

SUMMARY AND CONCLUSIONS

7.1 Summary

1. A total of 27 concrete prisms 152 x 152 mm by 900 mm long of two concrete mixes were prepared to measure shrinkage strains. Three of the specimens of each mix were unreinforced while the remainder of the specimens were reinforced longitudinally with a single steel bar placed along the longitudinal axis of the specimen. The percentages of reinforcement investigated were 0.44, 0.89, 2.22 and 4.44% corresponding to single No. 10, 15, 25 and 35 bars.

2. Concrete strains, steel strains, relative humidity, and ambient temperature were monitored over a period of up to 170 days for mix 1 and 140 days for mix 2.

3. Ancillary tests were performed to determine the compressive strength, tensile strength, and the modulus of elasticity of the concrete in compression as a function of time. Steel specimens were tested in tension to determine the yield strength and modulus of elasticity of the steel reinforcement.

4. Exponential equations are proposed to relate the shrinkage strains and the long term unrestrained shrinkage strains with time.

5. From the restrained shrinkage strains obtained from the reinforced concrete specimens and the free shrinkage strains obtained from the unreinforced specimens, the effective

modulus of elasticity of concrete in tension was calculated as a function of time and the amount of restraint.

6. Cracking of the specimens reinforced with a No. 35 bar was monitored and an equilibrium model was used to analyze the shrinkage strains and stresses after cracking. Based on this, an iterative procedure was used to calculate the effective modulus of elasticity of concrete in tension after cracking.

7. A design application to compute the deflection of a composite truss using the equilibrium method, with the effective modulus of elasticity of concrete in tension and its free shrinkage strain, as well as the restrained shrinkage and the unrestrained shrinkage methods, as given in the S16.1, is presented.

7.2 Observations and Conclusions

1. Both the free (unrestrained) and restrained shrinkage strains increased at a gradually decreasing rate over the test period. About 90% of the maximum measured unrestrained shrinkage strain occurred within the first 90 days of drying. An exponential formula was found to fit the test data better than the hyperbolic formula used in the ACI and the CEB/FIP standards.

2. The maximum unrestrained shrinkage strain at the end of the measurement period was 855 $\mu\varepsilon$ for mix 1 and 748 $\mu\varepsilon$ for mix 2.

3. Restrained shrinkage strains developed with time at similar rates for both concrete mixes but were less than the unrestrained strains. The restrained shrinkage strain decreased with increasing percentages of steel. Regression analyses were performed and exponential expressions are proposed to relate the normalized restrained strain to the percentage of steel and time.

4. By the end of the test period the restrained shrinkage strains measured from the reinforced specimens had reached a constant value or even decreased slightly due to creep. Restrained shrinkage strains reduced sharply upon cracking for all the specimens reinforced with a No. 35 bar.

5. Only the specimens with a No. 35 bar developed transverse cracks that were observed near midlength between 28 and 44 days from casting. Cracks initiated at one or two corners at the same time and developed with time on the adjacent surfaces.

6. Crack development was accompanied by a sharp decrease in the shrinkage strain measured across the crack and a simultaneous increase in the shrinkage strain measured at the same section but on the opposite side. The average shrinkage strains and the accompanying shrinkage stresses also decreased. In all cases, the average tensile stress at cracking was lower than the measured tensile strength of concrete.

7. Restrained concrete shrinkage strains decreased along the specimen from the unrestrained shrinkage strain at the ends to their minimum value near mid length, while the compressive strains in the steel bar increased from zero at the ends to their maximum value near mid length.

8. At mid length of the specimen, the concrete and steel strains were virtually constant indicating that complete restraint has been developed. The length required to develop complete restraint increased with the percentage of steel.

9. The effective modulus of elasticity of concrete in tension was calculated at mid length of the specimen for all the reinforced specimens of both mixes. In using the equilibrium method developed by Kennedy and Brattland to calculate the effective modulus of elasticity of the cracked specimens, the bending stiffness of the reinforcement had to be considered.

10. The effective modulus of elasticity of concrete in tension is maximum at the beginning of drying and decreases exponentially as drying continues. The value of the effective modulus at a given time decreases with the increase of the percentage of steel because of the increase in shrinkage induced tensile stresses. At 150 days, the effective modulus ranged from 10 to 20% of the modulus of elasticity of concrete in compression. The modular ratios relative to the elastic modulus of steel were in the range of 45 to 200.

11. Within the scope of this investigation, neither the shrinkage of concrete nor its effective modulus of elasticity in tension is significantly affected by its compressive strength.

12. By using the time dependent effective modulus of elasticity of concrete in tension and free shrinkage strain, the development of shrinkage deflections of composite flexural members with time can be established using the equilibrium method.

13. The approximate procedure, using a tensile stress-strain curve and a fixed value for the free shrinkage strain, allows the shrinkage deflection to be estimated with reasonable accuracy.

14. The unrestrained shrinkage method is based on a modulus of elasticity of concrete that is too large. However, because this modulus also makes the section stiffer, the resultant deflection that is computed may not be significantly in error.

15. The restrained shrinkage method does not really recognize the true behaviour of the shrinkage mechanism.

7.3 Areas of Further Research

Areas that need further research are:

1. Experimental studies are needed to examine the distribution of shrinkage strains inside a reinforced concrete member and the effect of different member sizes, drying conditions and

concrete mixes on that distribution and on the effective modulus of elasticity of concrete in tension.

2. Shrinkage cracking should be investigated more thoroughly to determine the strain distribution in concrete after cracking.

3. Experimental and analytical studies should be conducted to relate the long time behaviour of concrete in tension to that in compression.

REFERENCES

American Concrete Institute (ACI), Committe 209, 1971, Prediction of Creep, Shrinkage, and Temperature Effects in Concrete Structures, in Designing for the Effects of Creep, Shrinkage, and Temperature in Concrete Structures, SP 27, American Concrete Institute, Detroit, Michigan, pp. 51-93.

American Concrete Institute (ACI), Committee 209, 1982, Prediction of Creep, Shrinkage, and Temperature Effects in Concrete Structures, in Designing for the Effects of Creep, Shrinkage, and Temperature in Concrete Structures, SP 76, American Concrete Institute, Detroit, Michigan, pp. 193-300.

American Concrete Institute (ACI), Committee 318, 1983, Commentary on Building Code Requirements for Reinforced Concrete (ACI-318-83), ACI Publication 318R-83, American Concrete Institute, Detroit, Michigan, 155 pages.

American Society for Testing and Material (ASTM), 1977, Standard Methods and Definitions for Material Testing of Steel Products (ASTM A370-77), Philadelphia, Pennsylvania.

Arnaouti, C., and Sangakkara, S.R., 1984, Creep and Shrinkage in a Lightweight-aggregate Concrete, Magazine of Concrete Research, Vol. 36, No. 128, September, pp. 165-173.

Base, G. D., 1982, Bond and Control of Cracking in Reinforced Concrete, Proceedings, International Conference on Bond in Concrete, Paisley College of Technology, Scotland, June, pp. 446-457.

Birkeland, H.W., 1960, Differential Shrinkage in Composite Beams, American Concrete Institute, Vol. 34, No. 11, May, pp. 1123-1136.

Branson, D.E., and Christiason, M.L., 1971, Time Dependent Concrete Properties Related to Design-Strength and Elastic Properties, Creep, and Shrinkage, in ACI, SP-27, Creep Shrinkage, and Temperature Effects in Concrete Structures, American Concrete Institute, Detroit, Michigan, pp. 257-277.

Branson, D.E., Meyers, B.L., and Shumann, C.G., 1972, Prediction of Creep and Shrinkage Behaviour for Design from Short-Term Tests, Portland Cement Institute Journal, May-June, pp. 29-43.

Brattland, A., and Kennedy, D.J.L., 1986, Shrinkage and Flexural Tests of Two Full-Scale Composite Trusses, Structural Engineering Report 143, Department of Civil Engineering, University of Alberta, Edmonton, Alberta, December, 210 pages.

Bryant, H. A., and Vadhanavikkit, C. , 1987, Creep, Shrinkage - Size and Age at Loading Effects, American Concrete Institute Materials Journal, Vol.84, No. 2, March-April, pp. 117-123.

Canadian Standards Association (CSA), 1984, Design of Concrete Structures for Buildings CAN3-A23.3-M84, Canadian Standards Association, Rexdale, Ontario.

Canadian Standards Association (CSA), 1989, Limit States Design of Steel Structures CAN/CSA-S16.1-M89, Canadian Standards Association, Rexdale, Ontario.

Canadian Standards Association (CSA), 1990, Methods of Tests for Concrete, National Standards of Canada CAN3-A23.2-M90, Canadian Standards Association, Rexdale, Ontario.

Carlson, R.W., 1940, Attempts to Measure the Cracking Tendency of Concrete, American Concrete Institute Journal, Vol. 11, June, pp. 533-537.

Chien, E.Y.L. and Ritchie, J.K., 1984, Design and Construction of Composite Floor Systems, Canadian Institute of Steel Construction, Willowdale, Ontario, 323 pages.

Comite Euro-International du Beton - Federation International de la Precontrainte (CEB/FIP), 1978, International System of Unified Standard Codes of Practice for Structures (English Translation), Comite Euro-International du Beton, April.

Comite Euro-International du Beton - Federation International de la Precontrainte (CEB/FIP), 1990, CEB/FIP Model Code - First Draft, Bulletin D'Information, No. 195, Paris, March.

Ferguson, M. P., 1958, Discussion of Miller, L. A., Warping of Reinforced Concrete Due to Shrinkage, American Concrete Institute Journal, Vol. 30, No. 6, Part 2, December, PP. 939-950.

Gamble, B.R., and Parott, L.J., 1978, Creep of Concrete in Compression During Drying and Wetting, Magazine of Concrete Research, Vol. 30, No. 104, September, pp. 129-138.

Ghali, A., and Favre, R., 1986, Concrete Structures - Stresses and Deformations, Chapman & Hall, London, 352 pages.

Glanville, W.H., 1930, Studies in Reinforced Concrete, Part II-Shrinkage Stresses, Department of Scientific and Industrial Research, Building Research, Technical Paper No. 11, London, 49 pages.

Hobbs, D.W., and Parrott, L.J., 1979, Prediction of Drying Shrinkage, Concrete, London, Vol. 13, No. 2, February, pp. 19-24.

Hansen, C. T., and Mattock, H. A., 1966, Influence of Size and Shape of Member on the Shrinkage and Creep of Concrete, American Concrete Institute Journal, Proceedings, Vol. 63, Part 1, pp. 267-290.

Kawamura, M., 1978, Internal Stresses and Microcrack Formation Caused by Drying in Hardened Cement Pastes, American Ceramic Society Journal, Vol. 61, pp. 281-283.

Keeton, J.R., 1965, Study of Creep in Concrete, U.S. Naval Civil Engineering Laboratory, Technical Reports No. R 333-I, R 333-II, January, February, and May.

Keeton, J.R., and Roll, F., et al., 1970, Effects of Concrete Constituents, Environment, and Stress on Creep and Shrinkage of Concrete, American Concrete Institute Committee 209, Subcommittee 1, Special Publication SP-27, April, pp. 1-23.

Kennedy, D.J.L. and Brattland, A., 1991, Shrinkage tests of two full-scale composite trusses, Canadian Journal of Civil Engineering, Submitted March.

Lay, M.G., 1982, Structural Steel Fundamentals - an Engineering and Metallurgical Primer, Australian Research Board, Victoria, Australia, 241 pages.

MacGregor, J.G., 1988, Reinforced Concrete Mechanics and Design, Prentice Hall, 799 pages.

Miller, L. A., 1958, Warping of Reinforced Concrete Due to Shrinkage, American Concrete Institute Journal, Vol. 29, No. 11, May, pp. 939-950.

Mills, R.H., 1969, Collapse of Structure and Creep in Concrete, Proceedings, International Conference on Structure, Solid Mechanics, and Engineering Design in Civil Engineering Materials, Southampton, April.

Montgomery, C.J., Kulak, G.L., and Shwartsburd, G., 1983, Deflection of a Composite Floor System, Canadian Journal of Civil Engineering, Vol. 10, No. 2, June, pp. 192-204.

Neville, A.M., 1970, Creep of Concrete: Plain, Reinforced, and Prestressed, Elsevier, New York, 622 pages.

Neville, A.M., 1981, Properties of Concrete, Pitman, Bath, 779 pages.

Nilson, A.H., Slate, F.O., and Smadi, M.M., 1987, Shrinkage and Creep of High-, Medium-, and Low-Strength Concretes, Including Overloads, American Concrete Institute Materials Journal, Technical Paper No. 84-M 25, Vol. 84, No. 3, May-June, pp. 224-234.

Park, R., and Paulay, T., 1975, Reinforced Concrete Structures, John Wiley & Sons, New York, 769 pages.

Pickett, G., 1946, Shrinkage Stresses in Concrete, Part 1, and Part 2: Shrinkage Stresses in Concrete - Application of the Theory Presented in Part 1 to Experimental Results, American Concrete Institute Proceedings, Vol. 17, No. 3, January, pp. 165-204, and Vol. 17, No. 4, February, pp. 361-398.

Powers, T.C., 1968, Mechanisms of Shrinkage and Reversible Creep of Hardened Cement Paste, Proceedings, International Conference on the Structure of Concrete (London, 1965), Cement and Concrete Assosiation, London, pp. 87-104.

Ross, A.M., 1937, Concrete Creep Data, The Structural Engineer, London, Vol. 15, No. 8, August, pp. 314-326.

Rush, H., Jungwirth, D., and Hilsdorf, K. H., 1983, Creep and Shrinkage - Their Effect on the Behaviour of Concrete Structures, Springer-Verlag, New York, Heidelberg, Berlin, 284 pages.

Troxell, G.E., Raphael, J.M., and Davis, R.E., 1958, Long-Time Creep and Shrinkage Tests of Plain and Reinforced Concrete, Proceedings, American Society for Testing and Materials, Vol. 58, pp. 1101-1120.

Wittmann, F.H., 1982, Creep and Shrinkage Mechanisms, in Creep and Shrinkage in Concrete Structures, Editor: Bazant, Z.P., John Wiley & Sons, Chichester, pp. 129-161.

Young, J.F., 1988, Physical Mechanisms and their Mathematical Descriptions, in Mathematical Modelling of Creep and Shrinkage of Concrete. Editor: Bazant, Z.P., John Wiley & Sons, Chichester, pp. 63-98.